

## ASSESSMENT OF HIP FRACTURE RISK IN OLDER ADULTS

ASSESSMENT OF HIP FRACTURE RISK  
IN OLDER ADULTS BY CONSIDERING THE EFFECT OF GEOMETRY AND  
BONE MINERAL DENSITY DISTRIBUTION IN THE FEMUR USING SINGLE  
DUAL-ENERGY X-RAY ABSORPTIOMETRY SCANS

By

FATEMEH JAZINIZADEH, B.Sc., M.Sc.

A Thesis Submitted to the School of Graduate Studies in Partial Fulfilment of the  
Requirements for the Degree of Doctor of Philosophy

McMaster University © Copyright by Fatemeh Jazinizadeh, August 2020

McMaster University DOCTOR OF PHILOSOPHY (2020) Hamilton, Ontario

(Mechanical Engineering)

TITLE: Assessment of Hip Fracture Risk in Older Adults by Considering the Effect of  
Geometry and Bone Mineral Density Distribution in the Femur Using Single Dual-energy  
X-ray Absorptiometry Scans

AUTHOR: Fatemeh Jazinizadeh, B.Sc., M.Sc.

SUPERVISOR: Cheryl E. Quenneville, B.Sc., M.E.Sc., Ph.D.

NUMBER OF PAGES: xix, 114

## **Lay Abstract**

---

Diagnosis of osteoporosis and consequently hip fracture risk is based on the measurement of bone mineral density in clinical imaging called DXA scanning. However, studies have shown that this method is not sufficient in identifying all patients at high risk of sustaining a hip fracture.

The purpose of this work was to incorporate the geometry and bone mineral density distribution of the proximal femur in hip fracture risk prediction through image processing of DXA scans. Two algorithms of 2D and 3D statistical shape and appearance modeling were implemented and evaluated in a cadaveric study (comparing the predicted fracture load to measured ones) as well as a clinical study (comparing the fracture predictions to the fracture history of patients).

The results indicated that new techniques can enhance hip fracture risk estimation compared to the clinical standard method, and hence the devastating injury can be prevented through applying protective measures.

## Abstract

---

Hip fractures in older adults have severe effects on patients' morbidity as well as mortality, so it is crucial to avoid this injury through the early identification of patients at high risk. Currently, the diagnosis of osteoporosis and consequently hip fracture risk is done through the measurement of bone mineral density by a dual-energy X-ray absorptiometry (DXA) scan. However, studies show that this method is not accurate enough, and a high percentage of patients who sustain a hip fracture had non-osteoporotic DXA scans less than a year before the incidence.

In this research, to enhance the hip fracture risk prediction, the effect of a femur's geometry and bone mineral density distribution was considered in the hip fracture risk estimation. This was done through 2D and 3D statistical shape and appearance modeling of the proximal femur using standard clinical DXA scans. To assess the proposed techniques, destructive mechanical tests were performed on 16 isolated cadaveric femurs. Also, through collaboration with the Canadian Osteoporosis Study (CaMos), the proposed statistical techniques to predict the hip fracture risk were evaluated in a clinical population as well.

The results of this study showed that new techniques can enhance hip fracture risk estimation; in the clinical study, 2D and 3D statistical modeling were able to improve identifying patients at high risk by 40% and 44% over the clinical standard method. Also, the percentage of correct predictions using 2D statistical models did not differ significantly from the 3D predictions. Therefore, by applying these techniques in clinical practice it

could be possible to identify patients at high risk of sustaining a hip fracture more accurately and eventually reduce the incidence of hip fractures and the pain and social and economic burden that comes with it.

## **Acknowledgments**

---

I would like to begin by thanking my supervisor, Dr. Cheryl Quenneville. Thank you for your continued support and nurturing mentorship. It has been a long journey with many ups and downs, thank you for welcoming my new ideas, trusting me when facing the challenges and encouraging me to keep taking steps forward. I have learned a lot from you and enjoyed every second of working with you.

Thank you to everyone who contributed to the success of this project: To the members of my supervisory committee: Dr. Wohl, thank you for your meticulous feedback and always sharing a laugh; Dr. Stolle, thank you for encouraging me to look beyond; and Dr. Adachi, thank you for opening the door to the clinical studies to me. Thank you to the people at the Canadian Multicentre Osteoporosis study (CaMos): Design, Analysis, and Publication (DAP) committee for granting me the collaboration with CaMos, Silvia and Claudie, for their help in choosing the data, and Martin for his help in acquiring the data. A big thanks to Chantal for her help in DXA scanning and Sandra for her help in CT scanning. Thank you to the guys in the machine shop for teaching me how use the machines and their help in designing and creating the parts: Dan, Michael, Mark, John and Justin.

Thanks to the members of my research group at the Injury Biomechanics Lab for all the laughs, help though frustration, and distracting me from the challenges: Avery, Alberto, Cooper, Marisa, Julia, Noah, Julian and Ariana.

I'd also like to thank McMaster University and Labarge Optimal Aging Initiative for providing me with the funding to conduct this research.

Finally, to my mother who always inspired me to pursue my passion for learning, and to my father who always encouraged me and gave me the strength – Thank you, I would not have been here if it wasn't for your support. To Diana – Thank you for being the kindest, and the most understanding angel on the earth for me. To Mohammadreza – Thank you for traveling half the world for me to support me to achieve my dreams, I love you and I owe this to you.

## Table of Contents

---

<b>CHAPTER 1 – Introduction .....</b>	<b>1</b>
1.1 Motivation .....	1
1.2 Hip and Femur Anatomy.....	4
1.3 Factors Affecting the Hip Fracture Risk and Current Evaluation Methods .....	6
1.4 Mathematical and Statistical Analysis .....	8
1.4.1 Principal Component Analysis .....	8
1.4.2 Logistic Regression Analysis .....	9
1.4.3 Leave-one-out Cross-validation .....	10
1.4.4 Receiver Operating Characteristic Curve .....	12
1.5 Texture Analysis .....	12
1.6 Direct Measurement of Geometry and BMD Distribution .....	14
1.6.1 Direct Measure of Geometry .....	14
1.6.2 Hip Structural Analysis .....	16
1.7 Model Reconstruction .....	16
1.7.1 Recreating the 2D Model .....	17
1.7.2 Recreating the 3D Model Based on a Template Model .....	18
1.7.3 Recreating the 3D Model Based on Geometrical Parameters .....	21
1.7.4 Recreating the 3D Model Based on SSAM .....	23
1.8 Evaluation Techniques .....	25
1.8.1 Cadaveric Studies .....	26
1.8.2 Clinical Studies .....	27

1.9	Study Objectives .....	28
1.9.1	Objectives .....	28
1.10	Structure of the Thesis .....	30
1.11	References .....	31
<b>CHAPTER 2 - Comparing the Fracture Limits of The Proximal Femur Under Impact and Quasi-static Conditions in Simulation of a Sideways Fall .....</b>		<b>41</b>
2.1	Abstract .....	42
2.2	Introduction .....	42
2.3	Materials and Methods .....	43
2.3.1	Specimen Preparation .....	43
2.3.2	Mechanical Testing .....	43
2.4	Results .....	44
2.5	Discussion .....	45
2.6	References .....	49
<b>CHAPTER 3 - Enhancing Hip Fracture Risk Prediction by Statistical Modeling and Texture Analysis on DXA Images .....</b>		<b>50</b>
3.1	Abstract .....	51
3.2	Introduction .....	51
3.3	Materials and Methods .....	52
3.3.1	Making the SSAM .....	52
3.3.2	Method Evaluation .....	52
3.4	Results .....	54

3.5	Discussion .....	54
3.6	References .....	56
<b>CHAPTER 4 - Advanced 2D Image Processing Technique to Predict Hip Fracture Risk in an Older Population Based on Single DXA Scans .....58</b>		
4.1	Abstract .....	59
4.2	Introduction .....	59
4.3	Materials and Methods .....	60
4.3.1	Study Population .....	60
4.3.2	Image Processing .....	61
4.3.3	Fracture Risk Estimation .....	61
4.4	Results .....	61
4.5	Discussion .....	62
4.6	References .....	66
<b>CHAPTER 5 - Predicting Hip Fracture Risk Based on the 3D Reconstruction of Proximal Femur’s Geometry and Material Distribution from a Single DXA Scan in a Clinical Population and Comparing the Results with 2D Model Reconstruction .....68</b>		
5.1	Abstract .....	70
5.2	Introduction .....	72
5.3	Materials and Methods .....	74
5.3.1	3D Model Reconstruction .....	74
5.3.1.1	Creating the BMD and Geometry Template Models .....	75
5.3.1.2	Assessing a New Scan .....	77

5.3.2	Evaluation of the 3D Model Reconstruction .....	77
5.3.3	Clinical Data .....	79
5.3.3.1	Predicting the Fracture Risk Based on 3D Model Reconstruction .....	79
5.3.3.2	Predicting the Fracture Risk based on 2D Model Reconstruction	81
5.3.4	Evaluation of the Fracture Risk Predictions .....	82
5.4	Results .....	82
5.5	Discussion .....	89
5.6	References .....	95
<b>CHAPTER 6 – General Discussion and Conclusion .....</b>		<b>101</b>
6.1	Summary .....	101
6.2	Strength and Limitation .....	104
6.3	Future Directions .....	107
6.4	Clinical Significance .....	111
6.5	References .....	112
<b>APPENDIX A – Glossary of the Medical Terms .....</b>		<b>113</b>

## List of Figures

---

Figure 1.1: The Anterior View of the Proximal Femur .....	5
Figure 1.2: Diagram of Leave-one-out Cross-Validation .....	11
Figure 2.1: Illustration of Geometrical Landmarks That Were Used to Pot the Specimens Vertically.....	44
Figure 2.2: Location of the Strain Gauges .....	44
Figure 2.3: QS Testing Setup .....	45
Figure 2.4: Impact Setup .....	45
Figure 2.5: A Typical Force-time Graph from the Impact Testing .....	46
Figure 2.6: A Typical Force-displacement Graph from the QS Testing .....	46
Figure 2.7: The Relationship Between IM and QS Fracture Loads for the Seven Pairs of Specimens .....	46
Figure 2.8: Fracture Load vs. BMD for the Two Test Configurations .....	47
Figure 2.9: Fracture Patterns in the QS and IM Groups .....	47
Figure 3.1: The Location of the Landmarks and Region of Interest .....	52
Figure 3.2: Flowchart of Creating the Template Model from the Training Set and Adjusting It to Describe a New Shape in the Test Group .....	53
Figure 3.3: Flowchart showing training set and test group selection .....	53
Figure 3.4: The Relationship Between BMD and Predicted Fracture Loads with the Measured Ones from the Experimental Test for a Representative Test Group .....	54
Figure 3.5: Demonstration of the First Geometry Modes and BMD Distribution .....	54

Figure 3.6: Comparison of the New Method and Currently Used Method in Clinical Practice .....	55
Figure 4.1: The Percentage of the Variances Explained by the Number of SSAM Modes Used in the Analysis .....	62
Figure 4.2: Graphical Illustration of Some of the Modes That Were Significantly Different Between the Fractured and Non-Fractured Subjects .....	63
Figure 4.3: The Average BMD Distribution in the Fractured and Non-Fractured Groups for All Subjects .....	63
Figure 4.4: Receiver Operating Characteristic (ROC) Curve for the Various Fracture Risk Predictors .....	64
Figure 5.1: Flowchart of Creating The 3D Statistical Shape and Appearance Models ....	76
Figure 5.2: The Flowchart of Finding the Modes for a New DXA Scan .....	78
Figure 5.3: Illustration of the Error in Reconstruction of the Geometry .....	83
Figure 5.4: Illustration of the Volumetric BMD in the Average Model from the CT Scans and the Average Model from the BMD Reconstruction in Two Views .....	85
Figure 5.5: Receiver Operating Characteristic Curves for Various Hip Fracture Risk Predictors .....	87
Figure 5.6: Surface Geometry Variation Between the Mean Fractured and Non-Fractured Subjects .....	88
Figure 5.7: Volumetric BMD Variation in the Mid-Frontal Plane Between the Mean Fractured and Non-Fractured Subjects .....	90

## List of Tables

---

Table 1.1: Summary of Research Studies of Hip Geometry in Fx vs. Control Groups ....	15
Table 2.1: Summary of Specimens' Characteristics .....	43
Table 2.2: Summary of the Results .....	46
Table 2.3: Maximum principal strain and strain rate measured in the QS and IM tests ..	47
Table 2.4: Comparison of the Relevant Studies .....	48
Table 3.1: Specimen Characteristics .....	54
Table 4.1: Comparing the First Ten Modes by Student t-test Between the Two Groups of Fractured and Non-Fractured When Using SSM, SAM, SSAM .....	62
Table 4.2: Summary of the Results When Using Various Predictors for Hip Fracture Risk .....	64
Table 5.1: The Summary of Patients' Characteristics .....	80
Table 5.2: A Summary of the Hip Fracture Risk Prediction Results for Various Classifiers .....	86
Table 6.1: Inter-user Reproducibility of Fracture Risk Based on 2D SSAM .....	109
Table 6.2: Inter-user Reproducibility of Fracture Risk Based on 3D SSAM .....	109
Table 6.3: Intra-user Reproducibility of Fracture Risk Based on 2D SSAM .....	110
Table 6.4: Intra-user Reproducibility of Fracture Risk Based on 3D SSAM .....	110

## List of all Abbreviations and Symbols

---

”	inch
°	degree
%	percent
±	plus/minus
<b>2D</b>	two-dimensional
<b>3D</b>	three-dimensional
<b><math>\alpha</math></b>	level of significance
<b><math>\varepsilon</math></b>	strain
<b><math>\mu\varepsilon</math></b>	micro strain
<b>aBMD</b>	areal Bone Mineral Density
<b>Ant</b>	Anterior
<b>BMD</b>	Bone Mineral Density
<b>CaMos</b>	Canadian Multicentre Osteoporosis Study
<b>cm</b>	centimeter
<b>CT</b>	Computed Tomography
<b>DXA</b>	Dual-energy X-ray Absorptiometry
<b>FEA</b>	Finite Element Analysis
<b>FNW</b>	Femoral Neck Width
<b>Fx</b>	fracture
<b>GLCM</b>	Gray-Level Co-occurrence Matrices
<b>GPA</b>	General Procrustes Analysis

<b>g</b>	gram
<b>HAL</b>	Hip Axis Length
<b>HI</b>	Homogeneity Index
<b>HSA</b>	Hip Structural Analysis
<b>HU</b>	Hounsfield units
<b>Hz</b>	Hertz
<b>IM</b>	Impact
<b>ISCD</b>	International Society of Clinical Densitometry
<b>kHz</b>	kiloHertz
<b>kg</b>	kilogram
<b>kN</b>	kilonewton
<b>mg</b>	milligram
<b>mm</b>	millimetre
<b>ms</b>	milisecond
<b>N</b>	Newton
<b>N/A</b>	Not Applicable
<b>NSA</b>	Neck-Shaft Angle
<b>PCA</b>	Principal Component Analysis
<b>PCS</b>	Principal Compressive System
<b>Post</b>	Posterior
<b>PTS</b>	Principal Tensile System
<b>QS</b>	Quasi-Static

<b>ROC</b>	Receiver Operating Characteristic
<b>s</b>	second
<b>SAM</b>	Statistical Appearance Modeling
<b>SSAM</b>	Statistical Shape and Appearance Modeling
<b>SSM</b>	Statistical Shape Modeling
<b>STL</b>	Stereolithography file format
<b>TBS</b>	Trabecular Bone Score
<b>TPS</b>	Thin-Plate Spline
<b>vBMD</b>	volumetric BMD
<b>WHO</b>	World Health Organization

## **Declaration of the Academic Achievement**

---

The following is a declaration that I, Fatemeh Jazinizadeh acknowledge that the studies conducted in this thesis were a result of collaborative efforts. The contribution that each individual made are detailed below.

Chapter 1: Fatemeh Jazinizadeh – wrote the manuscript; Cheryl Quenneville – reviewed the manuscript.

Chapter 2: Fatemeh Jazinizadeh – responsible for study design, data collection, and data analysis, wrote the manuscript; Hojjat Mohammadi – contributed to data collection; Cheryl Quenneville – contributed to study design, reviewed the manuscript.

Chapter 3: Fatemeh Jazinizadeh – responsible for study design, data collection, and data analysis, wrote manuscript; Cheryl Quenneville – contributed to study design, reviewed manuscript.

Chapter 4: Fatemeh Jazinizadeh – responsible for study design, data collection, and data analysis, wrote the manuscript; Jonathan Adachi – contributed to study design, reviewed the manuscript: Cheryl Quenneville – contributed to study design, reviewed the manuscript.

Chapter 5: Fatemeh Jazinizadeh – responsible for study design, data collection, and data analysis, wrote the manuscript; Cheryl Quenneville – contributed to study design, reviewed the manuscript.

Chapter 6: Fatemeh Jazinizadeh – wrote the manuscript; Cheryl Quenneville – reviewed the manuscript.

## CHAPTER 1- Introduction

---

*Overview: Hip fractures in older adults with osteoporosis are a significant cause of morbidity and mortality, and due to the associated complications, it is crucial to identify people at high risk so that these injuries can be prevented through protective measures. Currently, diagnosis of osteoporosis and consequently hip fracture risk is done through the measurement of bone mineral density (BMD) in the proximal femur; however, studies have shown that this method is not effective enough. Therefore, more accurate methods with higher sensitivity are required to correctly identify patients at high risk. This chapter outlines the anatomy of the proximal femur and hip, a summary of statistical analyses used in this thesis, a review of the factors that have an effect of the femur's structural integrity, and evaluation techniques. It concludes with the study's overall goal, objectives, the corresponding hypotheses, and a thesis overview<sup>1</sup>.*

### 1.1 Motivation

---

Osteoporosis is a generalized skeletal disorder in which a reduction in Bone Mineral Density (BMD) decreases the bone's strength, which may result in an increased risk of fracture. This disease is most common in older adults and is the main reason for a broken bone among them [1]. A previous study has shown that osteoporotic fractures occur more

---

<sup>1</sup> Due to the interdisciplinary nature of this work, a glossary of anatomical terms is included as Appendix A.

frequently than heart attacks and strokes combined in the United States [2], and with the global aging population, these numbers are expected to rise in the coming years.

The hip is one of the most common sites affected by osteoporosis, the fracture of which has a severe effect on the patient's morbidity and mortality. A study in 2009 [3] showed that there is an 8% to 36% excess mortality rate for patients one year after hip fracture, compared to adults without one. Hip fractures are not only associated with pain and reduced quality of life for the patients but also are responsible for high health care costs for society [4]. A large percentage of patients who suffer from hip fractures never regain the same level of functional independence as before and need to live in assisted living facilities [5]. In addition, many hip fracture patients have also multiple health issues that negatively affect recovery time [6]. Economically speaking, the acute cost for treating hip fractures in Canada annually is about \$620 million in comparison with \$553 million for all other fragility fractures combined. Adding indirect expenses, the cost associated with osteoporosis can go as high as \$3.2 billion each year, only in Canada [7]. Therefore, it is crucial to prevent fractures from happening through early identification of people at greatest risk of sustaining the injury, who may then use protective measures such as hip protectors [8], energy attenuating floors [9], targeted exercise [10], and pharmacological interventions [11].

Currently, the primary diagnosis of osteoporosis relies on the measurement of the Bone Mineral Density (BMD) derived from a Dual-energy X-ray Absorptiometry (DXA) scan [12]. The measured BMD is normalized to the mean and standard deviation of the

BMD of a young adult reference population to calculate the T-score (which represents the number of standard deviations below or above the average). According to the World Health Organization (WHO), a patient with a T-score of -2.5 at the hip or spine is considered to suffer from osteoporosis [13]. Some studies have shown that using the BMD measurement from the DXA scans alone is not sufficient in identifying all patients at risk of a hip fracture, and a large proportion of hip fractures occur in women with a non-osteoporotic diagnosis based on a DXA scan [14,15]. The urgent need to improve the assessment of fracture risk in older adults has led researchers toward using numerical analyses such as finite element analysis (FEA) and image processing techniques.

Finite element analysis has great potential for predicting the strength of bones since it gives information about the complete state of strain and stress throughout an object [16]. It can provide 3D information about the structure of the bone as well as its BMD distribution, yielding potentially the most accurate method to predict the bone's behavior under mechanical loading [17–22]. However, the implementation of FEA in clinical practice is disputed due to the substantial computation time, accessibility, and high level of radiation exposure (*e.g.* Computed Tomography (CT)- based FEA). There are also a fair number of challenges in validating the results of these models. Therefore, it is anticipated that DXA scans will remain for the foreseeable future the primary means of osteoporosis diagnosis and subsequently hip fracture risk [23].

Femur structural strength depends on its geometry, spatial BMD distribution, and the structure of the trabecula [24]. The clinician's gold standard for predicting fracture risk

is only based on the average areal BMD (aBMD) in certain regions, so there is potential to develop better methods for predicting fracture risk based on the factors mentioned above. Therefore, the overall purpose of this research was to apply various image processing techniques to DXA scans to investigate their potential as tools to identify patients at high risk of sustaining a hip fracture in comparison to the standard method. To examine the accuracy of the techniques the results were evaluated through both an isolated cadaveric femur study and a clinical population study.

## **1.2 Hip and Femur Anatomy**

---

The femur is the bone of the upper leg (thigh) and is the strongest and longest bone in the human body. The round head of the femur forms a ball-and-socket joint with the concave part of the pelvis known as the acetabulum [25]. This joint is called the hip and is held together by strong surrounding ligaments. The upper part of the femur (close to the pelvis) is called the proximal femur, and can be classified into four regions: the femoral head, neck, trochanteric, and subtrochanteric areas (Figure 1.1).

The femoral head is roughly a hemispherical structure that sits in the hip joint, and also is adjacent to the femoral neck. Its main purpose is to provide a smooth articulation with the acetabulum with a large range of motion, and accept load from the pelvis and transfer it to the diaphysis by way of the neck. The femoral neck offsets the head from the long axis of the femur and is the bridge between the head and the trochanteric area [26]. The trochanteric area is located between the femoral neck and femoral shaft (also known as diaphysis), and has two major protrusions. The lateral (further from the mid-line of the

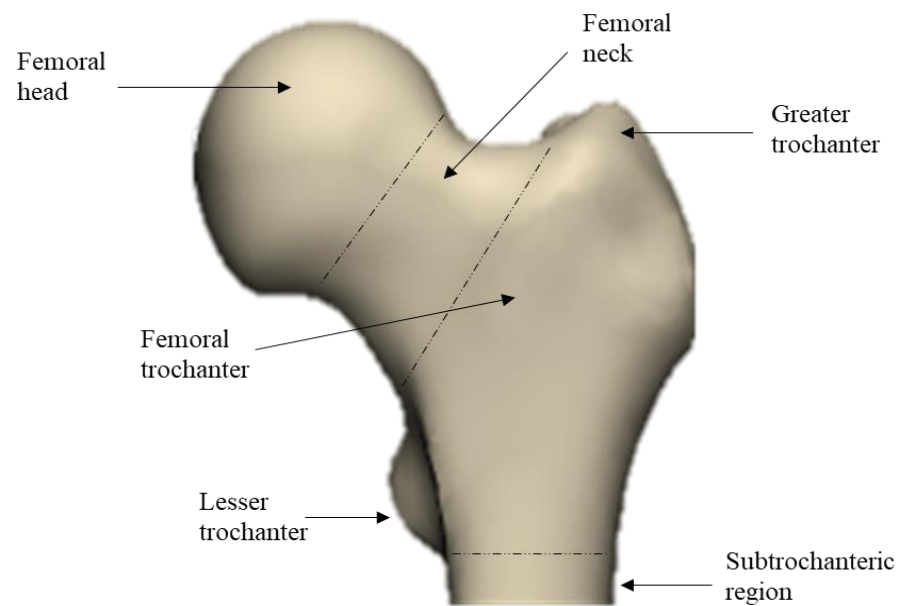


**Figure 1.1: The Anterior View of the Proximal Femur.**

The overall purpose of the proximal femur is the hip articulation, transferring load in multiple directions to the strong diaphysis, and also providing a site for muscle attachments. It can be divided into four regions: femoral head, neck, trochanter, and subtrochanteric areas (a part of the femoral diaphysis).

body) and more prominent one is called the greater trochanter and the smaller one on the medial (close to the mid-line of the body) aspect is called the lesser trochanter. The trochanteric region performs as an important muscle attachment site. The subtrochanteric area is defined as part of the femoral diaphysis that is situated approximately below the lesser trochanter and is the bridge between the femoral trochanter and the rest of the femoral shaft [27].

### **1.3 Factors Affecting the Hip Fracture Risk and Current Evaluation Methods**

---

The factors affecting the risk of sustaining a hip fracture in older adults can be classified into three categories of 1) bone strength, 2) fall probability, and 3) fall impact force.

The strength of the proximal femur depends on its material properties, which can be evaluated by the average BMD measured in a DXA scan. However, it should be noted that only 70% of bone consists of mineral content and the rest is organic materials and water [28]. Hence, considering only the BMD as a representation of the material properties can be a simplifying assumption. In addition to the material properties, the quality of the material (*e.g.* trabecular quality, and presence of microdamage) [29,30], the distribution of the bone density [31], and the geometry of the bone [32] are other contributing factors to the structural integrity of the proximal femur.

The probability of sustaining a fall depends on many personal and clinical factors. Some of these factors rely on how much a patient is prone to be in a high risk situation (*e.g.* level of activity, and equipment assisted walking ) [33], and the others are related to the

patient's balance maintenance (*e.g.* age, cognitive issues, comorbidities, and reflexes) [34]. Therefore, in addition to the strength status of the bone, personal and clinical factors play an important role, too.

The last category of factors that contribute to the hip fracture risk is the force that is experienced during a fall, since an acute fracture (not a fatigue fracture) is sustained only when the experienced force exceeds the strength of the bone [28]. The amount of force during a fall depends on hip impact velocity, soft tissue damping, and the effective mass during the impact [35]. Most of these factors rely on the anthropometric measurement of the person. For example, a taller person most likely experiences a higher impact velocity, and a person with a higher body mass index most likely benefits more from the soft tissue energy damping during an impact onto the hip (*i.e.* more mass for their height, therefore thicker soft tissue over the hip). Both height and weight, as well as body composition, influence the effective mass during the impact. Also, studies have shown that the condition in which the fall is initiated, the direction of the fall, and reflexes to avoid the fall would affect impact velocity and effective mass as well [35].

Considering many elements are affecting the risk of sustaining a hip fracture, it is worth noting that the main focus of this thesis is to predict the fracture risk based on the frameworks consisting of factors that affect the structural integrity of the proximal femur with regards to the feasibility of implementing them in clinical practice. However, in some studies, additional aspects (*e.g.* age, BMI, and sex) have been added to the prediction model as well.

## 1.4 Mathematical and Statistical Analyses

---

Various statistical and mathematical analyses have been used in this field and hence are reviewed herein.

### 1.4.1 Principal Component Analysis

Principal Component Analysis (PCA) is a mathematical technique to reduce the dimensionality of large and complex datasets while preserving as much variability as possible or needed [36]. This method is mostly used as an approach to summarize the main characteristics of a dataset and also to make predictive models. Typically, by doing PCA the data are transformed into a new coordinate system where the largest variance can be found along the first axis of the new coordinate system (first principal component), and the next largest variance is found along the second axis (second principal component), etc. [37]. The proportion of variance explained by each principal component is equal to the eigenvalue of that principal component (eigenvector).

Conceptually, PCA can be considered as fitting an  $m$ -dimensional ellipsoid to the data with each axis of the ellipsoid being a principal component. If a specific axis is very small, that axis could be eliminated resulting in the loss of a small portion of the data [37].

The fundamental concept of PCA involves having a dataset (matrix  $X$ ) consisting of ‘ $p$ ’ columns as variables and ‘ $n$ ’ rows as observations (each observation has  $p$  variables). This permits a linear combination of the matrix columns to be found that has the maximum variance [36], which can be calculated through eigenvalue decomposition of the covariance

matrix of the original data. Some of the main advantages of PCA are reduced complexity, lack of redundancy in the data (given the orthogonal components), and reduction in noise (since only the main variations are considered, and small variation by the noise are ignored). However, the main disadvantage of PCA is that even an obvious feature could be disregarded if not present in the training set; therefore, having the right training set can have a significant impact on the results [38].

### **1.4.2 Logistic Regression Analysis**

Logistic regression analysis in statistics is used to model the probability of certain outcomes. A binary logistic model has dependent variables with two possible outcomes (*e.g.* fractured vs. non-fractured), labeled as zero and one. In this model, the logarithm of odds ( $p/(1-p)$ , where  $p$  is the probability), is a linear function of independent variables that could either be binary or continuous. The calculated probability is between zero and one, and the function that transforms the logarithm of odd to the probability is called the logistic function [39].

Some of the advantages of logistic regression analysis are that the input does not require any scaling, the output is well-calibrated predicted probabilities, it does not require too many computational resources, it is easy to implement, and efficient to train [40]. The main disadvantages of this method include not being able to solve non-linear problems and being vulnerable to overfitting, which is the overreaction of the predictive model to small fluctuations in the training data. This might happen when there are too many variables

relative to the number of observations; however, using cross-validation can help to avoid overfitting [41].

### **1.4.3 Leave-one-out Cross-Validation**

Cross-validation is a statistical method that is used to evaluate how a predictive model performs in practice, and its main goal is to assess the model's ability to predict the outcome for new data that were not used in creating it. Cross-validation uses two datasets: first, the training set in which the known data are trained to predict the output, and second, a testing set that uses the trained function created in the training set to predict the output [42].

The leave-one-out cross-validation is a particular form of cross-validation that involves using one observation in the testing set and 'n-1' (n is the number of observations) observations in the training set. To predict the outcome for each observation, the model has to iterate 'n' times (Figure 1.2). When using the leave-one-out cross-validation, there is less bias and also no randomness of choosing a testing set and training set from the observations [41], which makes this method highly desirable. However, this method is computationally expensive (time and power), especially if the dataset is very big.

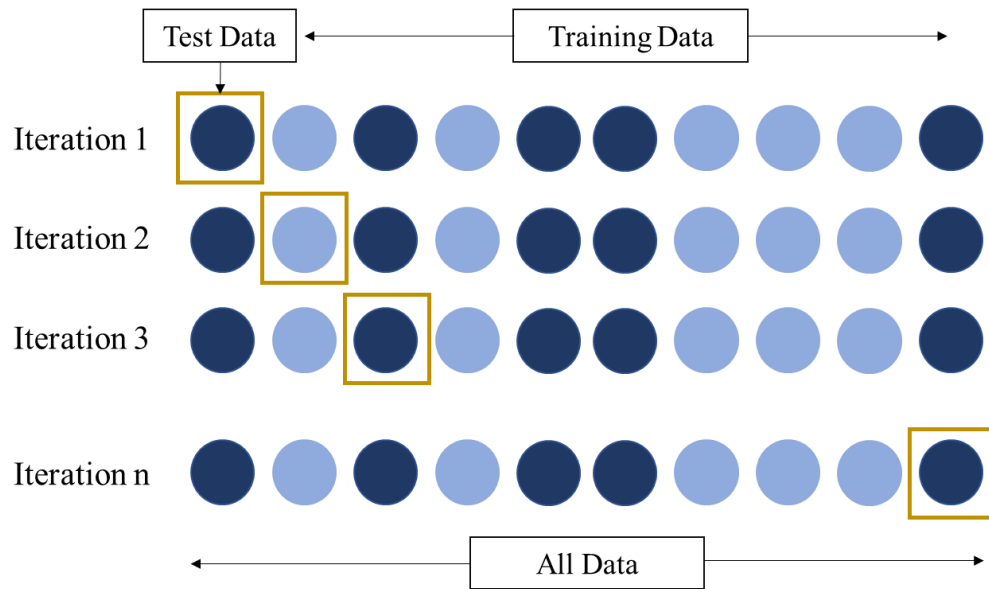


**Figure 1.2: Diagram of Leave-one-out Cross-Validation.**

In each iteration, one observation is the test data and the rest of the observations are the training data, the test error rate is the average of all  $n$  errors, the light and dark blue represent different types of data (*e.g.* fractured and non-fractures subjects).

#### **1.4.4 Receiver Operating Characteristic Curve**

The Receiver Operating Characteristic (ROC) curve is a widely used [43–46] graphical plot that demonstrates the diagnostic ability of different predictors based on various thresholds, and it is created by plotting the true positive rate against the false positive rate. The true positive rate is also called sensitivity, and the false positive rate can be calculated as ‘1-specificity’ [47]. The area under the ROC curve is the probability that a predictor ranks a randomly chosen positive higher than a randomly chosen negative, or in other words, classifies a higher risk over a lower risk subject correctly [47]. Therefore, the higher the area under the curve, the stronger a model is in its diagnostic ability.

One of the main advantages of using the ROC curve is that it allows choosing an optimum threshold based on the desired trade-off between sensitivity and specificity, also the curve makes the comparison of various diagnostic tests graphically simple. However, in the case of limited sample size, the plot might look very jagged.

#### **1.5 Texture Analysis**

---

Texture analysis of radiographic images is a tool to assess the architecture of trabecular bone, and provides insight into the bone quality instead of bone quantity [48]. Several methods of texture analysis exist to estimate the trabecula structure indices from a 2D image [49]. The basis of most of these methods (*e.g.* homogeneity index (HI), trabecular bone score (TBS)) is on calculating the gray-level co-occurrence matrices (GLCM). The GLCM is a matrix defined over an image that represents the co-occurred (pixels of the

same value) grayscale values in a certain direction and offset, and is used to define the texture of an image.

Homogeneity index is a function that uses the GLCM and represents the spatial distribution of gray levels in a picture [48]. When applying HI to a trabecular bone image, it acts as an indication of the trabecular connectivity, where a higher HI is correlated with higher trabecular connectivity. A modified HI was used in a clinical study [30] to investigate its ability to predict femoral neck fractures, and their results showed that the modified HI was a better predictor of the fracture risk than BMD alone.

Trabecular bone score (TBS) is another measure of bone texture correlated with bone microstructure, and it relies on acquiring information from the measurement of the statistical properties of image pixels. The logic behind calculating TBS is that in a 2D image of bone with high trabecular density, it is more likely to have a large number of pixel value variations of small amplitude. On the other hand, when the density of the trabeculae is low and the bone is porous, the 2D image is more likely to have a low number of variations of high amplitude [49].

Generally, a low TBS is associated with a porous and not well-structured bone, whereas an elevated TBS represents a well-structured trabecula architecture [50]. TBS is positively correlated with trabecular connectivity density, bone volume fraction, and trabecula numbers. It is also negatively correlated with trabecular separation indices. It is worth mentioning that TBS association with trabecular thickness is not yet determined, since in some studies it showed a negative correlation *e.g.* [51], whereas in another study

it showed a positive correlation [52]. In practice, TBS is typically calculated from a standard lumbar spine DXA image, using commercially available software [53].

## **1.6 Direct Measurement of Geometry and BMD Distribution**

---

To consider the effect of geometry from a 2D image either the direct measurement of geometrical features or recreating the model of the proximal femur (either 2D or 3D) based on a DXA image has been used. The direct measurement of BMD distribution has not been investigated frequently and BMD distribution was usually investigated along with the geometry (*e.g.* in Hip Structural Analysis).

### **1.6.1 Direct Measure of Geometry**

Some studies have investigated the relationship between the geometry of the femur and the types of hip fractures [54–56], while in other similar ones the association of the hip fracture with different geometry traits such as neck-shaft angle (NSA), hip axis length (HAL), and femoral length width (FNW) in subjects with hip fractures and a control group have been explored (Table 1.1). Although these studies provide very useful information, not all of them are in agreement with each other. The strength of a complex shape like the proximal femur depends on its entire geometry and cannot be limited to some simplified geometrical traits. To capture all contributing factors a powerful tool in catching high dimensional variability is needed.

**Table 1.1: Summary of Research Studies of Hip Geometry in Fracture vs. Control Groups.**

The table is adapted from [57], NSA: neck-shaft angle, HAL: hip axis length, FNW: femoral neck width, N/A: not available or not measured.

Study	Number of subjects		Geometric Feature – Fracture vs. Control		
	Fracture	Control	NSA	HAL	FNW
Gnudi <i>et al.</i> [55]	181	366	Increase	Increase	Not significant
Bergot <i>et al.</i> [58]	49	98	Not significant	Increase	N/A
Partanen <i>et al.</i> [59]	70	40	Increase	Not significant	Not significant
Alonso <i>et al.</i> [60]	411	545	Increase	Not significant	Increase
Gnudi <i>et al.</i> [61]	111	329	Increase	Increase	Increase
Michelotti and Clark [62]	43	119	N/A	Not significant	Increase
Center <i>et al.</i> [63]	36	224	N/A	Not significant	N/A
Boonen <i>et al.</i> [64]	135	75	N/A	Increase	N/A
Faulkner <i>et al.</i> [32]	64	134	Not significant	Increase	Not significant

### **1.6.2 Hip Structural Analysis**

Hip structural analysis (HSA) is a measure of structural properties of proximal femurs. These properties are a combination of geometrical and mechanical characteristics of the bone at various cross-sections [65]. More specifically, HSA accounts for the outer and inner diameter of the bone, cross-sectional area (excluding the bone marrow and pores), estimated cortical thickness, cross-sectional moment of inertia, section modulus (second moment of area divided by the maximum diameter at that cross-section), buckling ratio (ratio of the outer diameter to the cortical thickness), neck-shaft angle, and hip axis length. These measurements are done at three locations of the narrowest point of the femoral neck, trochanteric region, and femoral shaft [66–68].

Some studies have investigated the average measures of HSA in fractured and non-fractured groups, or have assessed if HSA can enhance hip fracture risk prediction [68–70]. The results of these studies mostly showed that there was a significant difference between the fractured and non-fractured groups [69]; however, not all variables added discriminative value to hip fracture risk prediction [68]. The International Society of Clinical Densitometry (ISCD) published a position statement in 2015 that HSA should not be used to assess hip fracture risk with an exception for femur axis length [71].

### **1.7 Model Reconstruction**

---

One method to investigate the effects of geometry and BMD distribution on hip fracture risk is to reconstruct the 2D or 3D shape of the proximal femur from a DXA scan.

In 2D model reconstruction, the results are mostly used to measure specific traits or investigate the correlation between its variables (from the reconstruction procedure) and the fracture risk. In 3D model reconstruction, in addition to these applications, the estimated model could be used as an input for FEA.

Most of the studies that propose a technique to reconstruct the shape and BMD distribution of the femur are based on a two-stage procedure, in which a template shape of the femur is created based on available 2D or 3D models, and stage two is about deforming the template shape to match the data from any new 2D image. These methods can be categorized based on their different approaches in creating the template shape, techniques of altering the template shape to match the 2D image, consideration of BMD distribution, and type of 2D image used.

### **1.7.1 Recreating the 2D Model**

Baker-LePain *et al.* [72] used a Statistical Shape Modeling (SSM) algorithm proposed by Cootes and colleagues [73] on the X-ray radiographs of hips in a population of clinical subjects with and without hip fractures. To make the template model, landmarks were assigned on the contour of the femur in the training set and after aligning the points, the average of the landmarks was calculated to find the template shape. Principal Component Analysis was then used to find the main modes of variation in the shape of the femur. To describe the shape of any new femur, the template model was adjusted by the main modes of variation to minimize the difference between the estimated geometry and the real geometry of the bone.

The results of this study showed that by using SSM and logistic regression analysis, the area under the ROC curve to predict the risk of a hip fracture was improved significantly; however, it is not clear if they used cross-validation or any other statistical method to make independent predictions. This study only included the effect of geometry in fracture risk and did not investigate BMD distribution, and also an X-ray image in addition to the DXA image was used for the analysis.

Goodyear *et. al* [44], adopted Statistical Shape and Appearance Modeling (SSAM) to account for both the effects of geometry and BMD distribution of the proximal femur in hip fracture risk. They used an open-source software (Active Appearance Modelling Toolkit Software Manchester University, UK) to create SSAM, and then compared the modes of variation between two groups of subjects who had sustained a hip fracture and who had not. Subsequently, they performed a stepwise logistic regression analysis to only include the variable in the risk assessment that showed a significant effect on the outcome. Their results demonstrated that using only some specific modes in addition to the BMD could increase the area under the ROC curve compared to using the BMD alone. However, using stepwise regression is criticized due to the test bias, and also including fewer independent variables in the model than the total number of variables in an effort to make the fit look better.

### **1.7.2 Recreating the 3D Model Based on a Template Model**

In 2009, Langton *et al.* [74] developed a method to estimate the 3D shape of the proximal femur from the anterior-posterior projection of CT scans (to be used as the 2D

image). First, three different maps from CT scan images were derived for each of the bones in the training set: 1) the ‘offset’ map, defined as the number of voxels from a pre-determined plane to the first bone voxel in that column, 2) the ‘depth’ map, defined as the number of voxels between the first and the last bone voxel along the specific column, and 3) the ‘BMD’ map, defined as the integrated BMD content along a particular direction divided by the area under calculation. Therefore, the shape of each femur could be described by the offset and depth maps, considering they represented the femur contour in the frontal plane and how much thickness it had in various locations, and the BMD map was used as a 2D image.

The process of creating the template shape from these three maps had five stages. First, landmarks were assigned to the 2D image (BMD map), so that they accounted for the visible shape features of the femur. Then, general Procrustes analysis (GPA) was used to eliminate the effect of translation, rotation, and scaling among different landmarks’ coordinates in the 2D BMD images. In stage three, the mean of each specific landmark among the training sets was calculated to obtain the average landmarks’ coordinates, and then in stage four, the offset and depth maps of each femur in the training sets were warped to the average landmarks’ coordinates. Finally, the pixel-by-pixel average of the offset and depth images were calculated, and the 3D shape represented by these maps was considered as the template model. After these steps, the template shape (3D grid) was ready to be altered to match any new image.

To match the 3D shape to a new 2D image, first, the landmarks were assigned to the 2D image, and GPA was applied for alignment and scaling purposes, and then the average 3D grid was warped to the landmarks' positions by thin-plate splines (TPS, an interpolation technique). The result of this process is a 3D estimation of the shape that would have created the 2D image. One of the main limitations of this method was that it could not capture the right shape if there was any curve with a high angle in the transverse plane, and also, it was only able to estimate the 3D shape of the proximal femur, and did not provide any insight into the BMD distribution.

Vaananen *et al.*[75] used this technique and modified it so it could account for the BMD distribution of the proximal femur to some degree. In their method, the BMD distribution was considered based on the BMD map. This meant that it could address the medial-lateral and superior-inferior variation but could not estimate anterior-posterior variation in the BMD distribution.

In 2012, Vaananen *et al.* [76] proposed another method to create a 3D model of a femur from a 2D BMD image derived from the anterior-posterior projection of CT scan images. Like other methods, this technique started with creating a template model from a training set. Landmarks were assigned to the 3D shapes of the femurs within the training set, and GPA was performed to align and scale the landmarks. Then, the mean values of each landmark's position were calculated, and the CT-based 3D models within the training set were warped to the mean position of the landmarks by TPS. Next, the average of the

voxel-by-voxel content of the warped images was calculated, so that the template model included information both about the geometry and BMD distribution throughout the bone.

To estimate the 3D shape from a 2D DXA image, landmarks were assigned to the estimated DXA image (anterior-posterior projection of the CT scan), and then the 3D template shape was warped to the BMD image's shape by matching to the landmarks' locations. In the end, the 3D volumetric BMD distribution in the warped templated shape was normalized to match the projection of the 3D shape with the BMD image. The advantage of this method was that GPA and TPS were used fully in 3D, so the changes in the anterior-posterior direction were captured better than in previous methods. However, the alteration of the template model was only based on matching the landmark location, and the dependant BMD variations inside the template models could not be integrated into the final model.

### **1.7.3 Recreating the 3D Model Based on Geometrical Parameters**

Thevenot *et al.* [77] proposed a method to derive a 3D model of femur out of a 2D image, with a focus on creating trabecular and cortical bone based on some geometric parameters. The 3D model generation was divided into three steps: 3D shape generation, meshing, and assigning material properties. To create the 3D shape, a set of eight geometric parameters were defined: femoral neck axis length, neck-shaft angle, trochanteric width, femoral head diameter, femoral neck diameter, femoral shaft diameter, femoral shaft cortex, and calcar femoral cortex width. Then, the relationships between these parameters and the femur overall geometry were established based on the information from CT scans

of seven femurs in the training set, and the impact of each parameter on the overall shape was quantified. Next, the outer surface of the model was defined by a series of curves. The femoral head was assumed as a hemisphere, and the femoral neck was divided into ten segments. A relationship was established between each radius and the aforementioned eight geometrical measures. Therefore, for the reconstruction of a 3D shape from a new 2D image, first, the geometric parameters were measured from the 2D image, and then based on the established relationships from the training set, the shape of the femur was estimated, and a smoothed solid was created.

The assignment of mechanical properties was based on the analysis of the trabecular structure from radiograph images. Young's modulus was calculated using the homogeneity index (HI) adjusted by the Hounsfield Units (HU) measured in CT scan images, and the distribution of the material properties through the trabecular bone was based on Principal Tensile and Compressive System (PTS, PCS). Trabecular bone is a supportive connective tissue and its pattern of growth follows the course of stress lines in the bone. During the load transfer from the femoral head to the diaphysis, the femoral neck and part of the trochanteric area experience a bending moment, this would generate tension on the lateral side and compression on the medial side, forming a group of trabecula to bear the load [78]. The group of trabecula on the lateral side that carries the tension is called PTS, and the ones that carry the compressive load are named as PCS [78].

In the study by Thevenot *et al.* [77], the PTS was divided into 20 sub-curves, with the magnitude of Young's modulus increasing toward the femoral head. The same method

was applied to PCS, where it was divided into 10 sub-curves with increasing value of Young's modulus toward the lower neck. The material outside PTS and PCS was assigned mechanical properties depending on its location, *e.g.* shaft, trochanter, femoral head, and neck. For each new model, the localization of the different regions for assigning material properties was based on its 2D radiograph.

Although the reconstruction of the proximal femur geometry seemed logically appropriate (however very labor-intensive), the reconstruction of the BMD distribution was based on the assumption that specific areas of the femur have the same material properties, and therefore the distribution of the BMD in the bone was an oversimplification.

#### **1.7.4 Recreating the 3D Model Based on SSAM**

The statistical models for constructing 3D models based on 2D images are mainly based on active shape [73], and active appearance modeling [79], in which first a template model of an object is created from a large dataset. Then, the new 3D model is constructed by altering the template model by its modes of variation (eigenvectors) in order to maximize the similarity between the projection of the template shape and the 2D image.

Whitmarsh *et al.* [80] proposed a method based on statistical appearance modeling that could derive not only the shape but also the BMD distribution throughout the femur. They used CT scans of femurs in the training set and assessed the accuracy of their technique using DXA images of clinical subjects. The template shape model was built based on the work of Frangi *et al.* [81], which used non-rigid registration of the CT volumes

onto a segmented reference subject with an intensity-based algorithm. After registration, all data were gathered into a single matrix, and principal component analysis (PCA) was applied, which allowed any new shape and density distribution to be described as the template model plus a set of eigenvalues and eigenvectors.

For the reconstruction of a 3D shape from a 2D image, the intensity-based 3D-2D registration of the template model onto the DXA image was performed, whereby an iterative optimization process was applied to maximize the similarity of the DXA image to the digitally reconstructed radiograph (DRR) of the 3D model, which is a simulation of a 2D X-ray image from a CT-scan. The generation of the DRR was based on a ray casting technique [82], in which a ray was cast through the volume in the direction of the projection (perpendicular to the DXA image plane). The density value of each pixel is the integral of density in the 3D model lying in the direction of the casted ray. To maximize the similarity between the DRR and the DXA image, the instance model together with a pose and scaling factor can be found through optimization to minimize the differences between the DRR and the DXA image in terms of femur's contour and the pixels' intensity.

Vaananen *et al.* [83] proposed a new method to derive the 3D model of a femur from a 2D DXA image by using statistical shape and appearance models (SSAM) and feature-based image registration. To create the template shape for SSAMs, first, the landmarks were registered to the 3D CT-based model of the femurs and pelvis within the training set, and GPA and TPS were used to align, scale and warp the models to the mean of the landmarks' position. Next, a template mesh was generated on the mean shape

considering the cortical bone separately from the trabecular and then warped back to the shape of each training bone in two iterations. The BMD value of each warped element was collected after removing GPA. The BMD values for each model in the training set were normalized to its mean and standard deviation. Finally, all geometry (node coordinates) and density information (elements' BMD) were collected into a matrix, and PCA was applied to identify the eigenvectors, so that each new shape could be defined as the summation of the mean shape and linear combination of the eigenvectors.

In this method, the reconstruction of each femur began with registering the DRR over the DXA scan. A genetic algorithm in MATLAB was used to register a combination of translation, rotation, scale, and mode values so that the cost function including the sum of the absolute error between areal BMD of the image, quality of mesh function, and anatomical positioning function would be minimized. In this method, the cortical bone was reconstructed separately, and a threshold was given to the minimum cortical thickness; therefore, there was an overestimation in the amount of cortical bone in the reconstructed model.

## **1.8 Evaluation Techniques**

---

Several methods are used to evaluate new predictive methods, with most of the previous studies using either a cadaveric study or a clinical observational study.

### **1.8.1 Cadaveric Studies**

Performing destructive and non-destructive mechanical testing on post-mortem human specimens or isolated bones provides valuable insight into fracture mechanisms as well as establishing injury criteria. Some of the advantages of this technique are controlled orientation of loading, the feasibility of imaging the bones before testing, controlled loading rate, and a guaranteed fracture, whereas in a clinical population a huge cohort might be needed to find a few people who sustain a fracture. The main focus of validating a fracture risk predictor model with a cadaveric study is to predict the fracture loads by the proposed model and then compared to those measured in the experiment. One of the most important requirements to get relevant data from these kinds of tests is to simulate the conditions under which injury most probably occurs.

The primary direction of falls in older adults in which hip fractures occur is a sideways fall onto the hip [84,85]. Many of the experimental studies that have investigated the risk of hip fracture have conducted quasi-static destructive tests on proximal femurs simulating sideways falls [86–89]. However, in reality, the incidents that lead to a fracture are never quasi-static or have a constant displacement rate, and are more like an impact [90]. Quasi-static tests are easier to implement and can be done by a standard material testing machine, and hence controlling the test conditions can be simpler. Also, numerical modeling of the quasi-static tests is less complicated. On the other hand, during an impact test, there is less control over the test conditions, so it is more elaborate to implement, and

numerical modeling is also more complicated. However, impact testing is a more accurate representation of the conditions in which a fracture happens.

One of the limitations of cadaveric studies in fracture risk prediction models is that further studies are still required to correlate the predicted/measured fracture load with the fracture risk in reality, as there are numerous personal and clinical factors that contribute to the incidence of sustaining a bone fracture. Some of these factors include soft tissue thickness, use of assistive devices, physical activity level, and patients' lifestyle.

### **1.8.2 Clinical Studies**

In contrast to cadaveric studies, studies that are performed on a group of living subjects provide more insights into the risk factors of sustaining a hip fracture. Some of the advantages of clinical studies are considering the effects of aging impairments, muscle activation, soft tissue, real loading direction, and including a variety of people that would be a better representation of the real world.

However, performing clinical studies has more complications in terms of obtaining ethics approval, recruiting the subjects, resources, follow-ups, data acquisition, and data analysis. These studies might also require a long period to find the outcome of interest (*e.g.* only a small fraction of participants may ever sustain an injury). Therefore, various types of clinical studies exist to mitigate the drawbacks.

Case-control studies are a type of observational study in which two groups of subjects differing in the outcome (*e.g.* fracture vs. non-fracture) are selected and compared

based on the supposed contributing factors or exposures (*e.g.* BMD, smoking). This type of study is mostly used when the outcomes of interest are rare, and the factor or exposure of interest is only measured in the cases (subjects who have the condition) and controls (subjects who do not have the condition) [46]. Case-control studies can nest in large cohort studies to use data collected previously in that study (nested case-control study), this way the cost and time of performing a new study can be avoided. In the nested case-control studies, usually, one to four controls (*i.e.* those who did not experience fracture) are selected for each case (*i.e.* those who experienced fracture), and a previous study has shown that using three controls could only result in a small efficiency lost [91].

## **1.9 Study Objectives**

---

The overall goal of this Ph.D. research was to enhance hip fracture risk estimation in older adults to allow early identification of patients at high risk of sustaining a fracture. These patients could benefit from protective and preventive measures to avoid the injury and all the pain, social, and economic burdens that come with it.

Therefore, with a focus on the feasibility of implementing the proposed technique in clinical practice, image processing of DXA scans was investigated in this research and four objectives were identified.

### **1.9.1 Objectives**

Objective 1: To compare the proximal femur's strength in the quasi-static (QS) scenario with the impact (IM) scenario in the simulation of side-ways falls.

Objective 2: To analyze the shape, BMD distribution, and trabecular quality of the proximal femur based on the 2D statistical shape and appearance modeling of isolated cadaveric femurs' DXA scans (tested in Objective 1), and investigate how the combination of different modes and texture analysis is correlated with the strength of the bone.

Objective 3: To investigate the accuracy of 2D image processing of DXA scans in the prediction of an impending fracture in a population of subjects in a five year follow up after the baseline imaging using the Canadian Multicentre Osteoporosis Study (CaMos) database.

Objective 4: To investigate hip fracture risk prediction by analyzing the shape and BMD distribution of the proximal femur based on the 3D statistical shape and appearance modeling of DXA scans, and compare the results with 2D SSAM predictions using a subset of CaMos subjects from Objective 3.

The corresponding hypotheses were:

Hypothesis 1: Femurs' strength in the impact is greater than the quasi-static one and the fracture patterns are different, yet highly correlated with each other.

Hypothesis 2: At least one combination of modes from the statistical shape and appearance modeling can be found that is moderately to highly correlated with the fracture loads from the experiment.

Hypothesis 3: The proposed technique can identify patients at high risk of sustaining a hip fracture more accurately than T-score.

Hypothesis 4: The fracture risk predictions based on 2D are comparable to and not significantly different from 3D predictions.

### **1.10 Structure of the Thesis**

---

This thesis is written in a sandwich format as per the definition of the McMaster University School of Graduate Studies. Chapter 2 outlines comparing the fracture limits of the proximal femur in a sideways fall configuration in two scenarios of constant displacement and impact. Chapter 3 describes implementing 2D statistical shape and appearance modeling and texture analysis of DXA scans of cadaveric specimens to predict the fracture load for those femurs, and compares the results with the experimental ones. Chapter 4 outlines applying 2D statistical shape and appearance modeling to DXA scans of a clinical population from the Canadian Multicentre Osteoporosis Study (CaMos), predicting the hip fracture risk for them, and finally comparing the results with the BMD predictions and fracture history of the subjects. Chapter 5 describes creating and implementing 3D statistical shape and appearance modeling on DXA scans of a clinical population from Canadian Multicentre Osteoporosis Study (CaMos) and predicting the hip fracture risk for them and comparing the results with the 2D statistical shape and appearance modeling predictions. Chapter 6 summarizes the conclusions of this thesis, outlines the limitations of this research as a whole, as well as discusses the future directions and clinical implications of the studies presented in this thesis.

### 1.11 References

- [1] Golob AL, Laya MB. Osteoporosis: Screening, Prevention, and Management. *Med Clin North Am* 2015;99:587–606. <https://doi.org/10.1016/j.mcna.2015.01.010>.
- [2] Watts NB, Bilezikian JP, Camacho PM, Greenspan SL, Harris ST, Hodgson SF, Kleerekoper M, Luckey MM, McClung MR, Pollack RP, Petak SM. American Association of Clinical Endocrinologists Medical Guidelines for Clinical Practice for the diagnosis and treatment of postmenopausal osteoporosis. *Endocr Pract* 2010. <https://doi.org/10.4158/EP.16.S3.1>.
- [3] Abrahamsen B, Van Staa T, Ariely R, Olson M, Cooper C. Excess mortality following hip fracture: A systematic epidemiological review. *Osteoporos Int* 2009. <https://doi.org/10.1007/s00198-009-0920-3>.
- [4] Orive M, Aguirre U, García-Gutiérrez S, Las Hayas C, Bilbao A, González N, Zabala J, Navarro G, Quintana JM. Changes in health-related quality of life and activities of daily living after hip fracture because of a fall in elderly patients: A prospective cohort study. *Int J Clin Pract* 2015. <https://doi.org/10.1111/ijcp.12527>.
- [5] Leibson CL, Tosteson ANA, Gabriel SE, Ransom JE, Melton LJ. Mortality, disability, and nursing home use for persons with and without hip fracture: A population-based study. *J Am Geriatr Soc* 2002. <https://doi.org/10.1046/j.1532-5415.2002.50455.x>.
- [6] Beaupre LA, Binder EF, Cameron ID, Jones CA, Orwig D, Sherrington C, Magaziner J. Maximising functional recovery following hip fracture in frail seniors. *Best Pract Res Clin Rheumatol* 2013. <https://doi.org/10.1016/j.berh.2014.01.001>.
- [7] Tarride JE, Hopkins RB, Leslie WD, Morin S, Adachi JD, Papaioannou A, Bessette L, Brown JP, Goeree R. The burden of illness of osteoporosis in Canada. *Osteoporos Int* 2012. <https://doi.org/10.1007/s00198-012-1931-z>.
- [8] Laing AC, Robinovitch SN. The force attenuation provided by hip protectors depends on impact velocity, pelvic size, and soft tissue stiffness. *J Biomech Eng* 2008;130:061005. <https://doi.org/10.1115/1.2979867>.
- [9] Bhan S, Levine IC, Laing AC. Energy absorption during impact on the proximal femur is

- affected by body mass index and flooring surface. *J Biomech* 2014. <https://doi.org/10.1016/j.jbiomech.2014.04.026>.
- [10] Nikander R, Sievänen H, Heinonen A, Daly RM, Uusi-Rasi K, Kannus P. Targeted exercise against osteoporosis: A systematic review and meta-analysis for optimising bone strength throughout life. *BMC Med* 2010;8. <https://doi.org/10.1186/1741-7015-8-47>.
- [11] Pavone V, Testa G, Giardina SMC, Vescio A, Restivo DA, Sessa G. Pharmacological therapy of osteoporosis: A systematic current review of literature. *Front Pharmacol* 2017. <https://doi.org/10.3389/fphar.2017.00803>.
- [12] Sozen T, Ozisik L, Calik Basaran N. An overview and management of osteoporosis. *Eur J Rheumatol* 2017. <https://doi.org/10.5152/eurjrheum.2016.048>.
- [13] Cosman F, de Beur SJ, LeBoff MS, Lewiecki EM, Tanner B, Randall S, Lindsay R. Clinician's Guide to Prevention and Treatment of Osteoporosis. *Osteoporos Int* 2014. <https://doi.org/10.1007/s00198-014-2794-2>.
- [14] Siris ES, Chen YT, Abbott TA, Barrett-Connor E, Miller PD, Wehren LE, Berger ML. Bone mineral density thresholds for pharmacological intervention to prevent fractures. *Arch Intern Med* 2004. <https://doi.org/10.1001/archinte.164.10.1108>.
- [15] Miller PD, Barlas S, Brenneman SK, Abbott TA, Chen YT, Barrett-Connor E, Siris ES. An approach to identifying osteopenic women at increased short-term risk of fracture. *Arch Intern Med* 2004. <https://doi.org/10.1001/archinte.164.10.1113>.
- [16] Miura M, Nakamura J, Matsuura Y, Wako Y, Suzuki T, Hagiwara S, Orita S, Inage K, Kawarai Y, Sugano M, Nawata K, Ohtori S. Prediction of fracture load and stiffness of the proximal femur by CT-based specimen specific finite element analysis: Cadaveric validation study. *BMC Musculoskelet Disord* 2017. <https://doi.org/10.1186/s12891-017-1898-1>.
- [17] Van Den Munckhof S, Zadpoor AA. How accurately can we predict the fracture load of the proximal femur using finite element models? *Clin Biomech* 2014;29:373–80. <https://doi.org/10.1016/j.clinbiomech.2013.12.018>.
- [18] Bessho M, Ohnishi I, Matsuyama J, Matsumoto T, Imai K, Nakamura K. Prediction of

- strength and strain of the proximal femur by a CT-based finite element method. *J Biomech* 2007;40:1745–53. <https://doi.org/10.1016/j.jbiomech.2006.08.003>.
- [19] Bessho M, Ohnishi I, Matsumoto T, Ohashi S, Matsuyama J, Tobita K, Kaneko M, Nakamura K. Prediction of proximal femur strength using a CT-based nonlinear finite element method: Differences in predicted fracture load and site with changing load and boundary conditions. *Bone* 2009;45:226–31. <https://doi.org/10.1016/j.bone.2009.04.241>.
- [20] Khoo BCC, Brown K, Cann C, Zhu K, Henzell S, Low V, Gustafsson S, Price RI, Prince RL. Comparison of QCT-derived and DXA-derived areal bone mineral density and T scores. *Osteoporos Int* 2009. <https://doi.org/10.1007/s00198-008-0820-y>.
- [21] Dragomir-Daescu D, Op Den Buijs J, McEligot S, Dai Y, Entwistle RC, Salas C, Melton LJ, Bennet KE, Khosla S, Amin S. Robust QCT/FEA models of proximal femur stiffness and fracture load during a sideways fall on the hip. *Ann Biomed Eng* 2011. <https://doi.org/10.1007/s10439-010-0196-y>.
- [22] Poelert S, Valstar E, Weinans H, Zadpoor AA. Patient-specific finite element modeling of bones. *Proc Inst Mech Eng Part H J Eng Med* 2013;227:464–78. <https://doi.org/10.1177/0954411912467884>.
- [23] Yang L, Palermo L, Black DM, Eastell R. Prediction of incident hip fracture with the estimated femoral strength by finite element analysis of DXA scans in the study of osteoporotic fractures. *J Bone Miner Res* 2014;29:2594–600. <https://doi.org/10.1002/jbmr.2291>.
- [24] Tommasini SM, Nasser P, Hu B, Jepsen KJ. Biological co-adaptation of morphological and composition traits contributes to mechanical functionality and skeletal fragility. *J Bone Miner Res* 2008. <https://doi.org/10.1359/jbmr.071014>.
- [25] Metcalfe D. The pathophysiology of osteoporotic hip fracture. *McGill J Med* 2008.
- [26] Toogood PA, Skalak A, Cooperman DR. Proximal femoral anatomy in the normal human population. *Clin Orthop Relat Res* 2009. <https://doi.org/10.1007/s11999-008-0473-3>.
- [27] Jackson C, Tanios M, Ebraheim N. Management of subtrochanteric proximal femur fractures: A review of recent literature. *Adv Orthop* 2018.

- <https://doi.org/10.1155/2018/1326701>.
- [28] Introductory biomechanics: from cells to organisms. *Choice Rev Online* 2007. <https://doi.org/10.5860/choice.45-1476>.
- [29] Burr DB, Forwood MR, Fyhrie DP, Martin RB, Schaffler MB, Turner CH. Bone microdamage and skeletal fragility in osteoporotic and stress fractures. *J Bone Miner Res* 1997. <https://doi.org/10.1359/jbmr.1997.12.1.6>.
- [30] Thevenot J, Hirvasniemi J, Pulkkinen P, Maätta M, Korpelainen R, Saarakkala S, Jamsä T. Assessment of risk of femoral neck fracture with radiographic texture parameters: A Retrospective study. *Radiology* 2014. <https://doi.org/10.1148/radiol.14131390>.
- [31] Humbert L, Martelli Y, Fonolla R, Steghofer M, DI Gregorio S, Malouf J, Romera J, Barquero LMDR. 3D-DXA: Assessing the Femoral Shape, the Trabecular Macrostructure and the Cortex in 3D from DXA images. *IEEE Trans Med Imaging* 2017;36:27–39. <https://doi.org/10.1109/TMI.2016.2593346>.
- [32] Faulkner KG, Cummings SR, Black D, Palermo L, Glüer C -C, Genant HK. Simple measurement of femoral geometry predicts hip fracture: The study of osteoporotic fractures. *J Bone Miner Res* 1993. <https://doi.org/10.1002/jbmr.5650081008>.
- [33] Robinovitch SN, Feldman F, Yang Y, Schonnop R, Leung PM, Sarraf T, Sims-Gould J, Loughi M. Video capture of the circumstances of falls in elderly people residing in long-term care: An observational study. *Lancet* 2013. [https://doi.org/10.1016/S0140-6736\(12\)61263-X](https://doi.org/10.1016/S0140-6736(12)61263-X).
- [34] Levy LA. Falls in Older People: Risk Factors and Strategies for Prevention. *J Am Podiatr Med Assoc* 2002. <https://doi.org/10.7547/87507315-92-6-371>.
- [35] Nasiri Sarvi M, Luo Y. Sideways fall-induced impact force and its effect on hip fracture risk: a review. *Osteoporos Int* 2017. <https://doi.org/10.1007/s00198-017-4138-5>.
- [36] Jolliffe IT, Cadima J. Principal component analysis: A review and recent developments. *Philos Trans R Soc A Math Phys Eng Sci* 2016. <https://doi.org/10.1098/rsta.2015.0202>.
- [37] Maurits N, Ćurčić-Blake B. Math for scientists: Refreshing the essentials. 2017. <https://doi.org/10.1007/978-3-319-57354-0>.

- [38] Karamizadeh S, Abdullah SM, Manaf AA, Zamani M, Hooman A. An Overview of Principal Component Analysis. *J Signal Inf Process* 2013. <https://doi.org/10.4236/jsip.2013.43b031>.
- [39] Tolles J, Meurer WJ. Logistic regression: Relating patient characteristics to outcomes. *JAMA - J Am Med Assoc* 2016. <https://doi.org/10.1001/jama.2016.7653>.
- [40] Sperandei S. Understanding logistic regression analysis. *Biochem Medica* 2014. <https://doi.org/10.11613/BM.2014.003>.
- [41] Cawley GC, Talbot NLC. On over-fitting in model selection and subsequent selection bias in performance evaluation. *J Mach Learn Res* 2010.
- [42] Vehtari A, Gelman A, Gabry J. Practical Bayesian model evaluation using leave-one-out cross-validation and WAIC. *Stat Comput* 2017. <https://doi.org/10.1007/s11222-016-9696-4>.
- [43] Orwoll ES, Marshall LM, Nielson CM, Cummings SR, Lapidus J, Cauley JA, Ensrud K, Lane N, Hoffmann PR, Kopperdahl DL, Keaveny TM. Finite element analysis of the proximal femur and hip fracture risk in older men. *J Bone Miner Res* 2009. <https://doi.org/10.1359/jbmr.081201>.
- [44] Goodyear SR, Barr RJ, McCloskey E, Alesci S, Aspden RM, Reid DM, Gregory JS. Can we improve the prediction of hip fracture by assessing bone structure using shape and appearance modelling? *Bone* 2013;53:188–93. <https://doi.org/10.1016/j.bone.2012.11.042>.
- [45] Gregory JS, Stewart A, Undrill PE, Reid DM, Aspden RM. Identification of hip fracture patients from radiographs using fourier analysis of the trabecular structure: A cross-sectional study. *BMC Med Imaging* 2004. <https://doi.org/10.1186/1471-2342-4-4>.
- [46] Bredbenner TL, Mason RL, Havill LM, Orwoll ES, Nicolella DP. Fracture risk predictions based on statistical shape and density modeling of the proximal femur. *J Bone Miner Res* 2014. <https://doi.org/10.1002/jbmr.2241>.
- [47] Fawcett T. An introduction to ROC analysis. *Pattern Recognit Lett* 2006. <https://doi.org/10.1016/j.patrec.2005.10.010>.
- [48] Thevenot J, Hirvasniemi J, Finnilä M, Pulkkinen P, Kuhn V, Link T, Eckstein F, Jämsä T,

- Saarakkala S. Trabecular homogeneity index derived from plain radiograph to evaluate bone quality. *J Bone Miner Res* 2013;28:2584–91. <https://doi.org/10.1002/jbmr.1987>.
- [49] Silva BC, Leslie WD, Resch H, Lamy O, Lesnyak O, Binkley N, McCloskey E V., Kanis JA, Bilezikian JP. Trabecular bone score: A noninvasive analytical method based upon the DXA image. *J Bone Miner Res* 2014;29:518–30. <https://doi.org/10.1002/jbmr.2176>.
- [50] Silva BC, Bilezikian JP. Trabecular bone score: perspectives of an imaging technology coming of age TT - Escore de osso trabecular: perspectivas de um método de imagem em aprimoramento. *Arq Bras Endocrinol Metab* 2014.
- [51] Hans D, Barthe N, Boutroy S, Pothuau L, Winzenrieth R, Krieg MA. Correlations Between Trabecular Bone Score, Measured Using Anteroposterior Dual-Energy X-Ray Absorptiometry Acquisition, and 3-Dimensional Parameters of Bone Microarchitecture: An Experimental Study on Human Cadaver Vertebrae. *J Clin Densitom* 2011. <https://doi.org/10.1016/j.jocd.2011.05.005>.
- [52] Pothuau L, Carceller P, Hans D. Correlations between grey-level variations in 2D projection images (TBS) and 3D microarchitecture: Applications in the study of human trabecular bone microarchitecture. *Bone* 2008;42:775–87. <https://doi.org/10.1016/j.bone.2007.11.018>.
- [53] Martineau P, Leslie WD. Trabecular bone score (TBS): Method and applications. *Bone* 2017. <https://doi.org/10.1016/j.bone.2017.01.035>.
- [54] Kazemi SM, Qoreishy M, Keipourfard A, Sajjadi MM, Shokraneh S. Effects of hip geometry on fracture patterns of proximal femur. *Arch Bone Jt Surg* 2016. <https://doi.org/10.22038/abjs.2016.6993>.
- [55] Gnudi S, Ripamonti C, Lisi L, Fini M, Giardino R, Giavaresi G. Proximal femur geometry to detect and distinguish femoral neck fractures from trochanteric fractures in postmenopausal women. *Osteoporos Int* 2002. <https://doi.org/10.1007/s198-002-8340-2>.
- [56] Pulkkinen P, Partanen J, Jalovaara P, Jämsä T. BMD T-score discriminates trochanteric fractures from unfractured controls, whereas geometry discriminates cervical fracture cases from unfractured controls of similar BMD. *Osteoporos Int* 2010. <https://doi.org/10.1007/s00198-009-1070-3>.

- [57] Brownbill RA, Ilich JZ. Hip geometry and its role in fracture: what do we know so far? *Curr Osteoporos Rep* 2003. <https://doi.org/10.1007/s11914-003-0005-8>.
- [58] Bergot C, Bousson V, Meunier A, Laval-Jeantet M, Laredo JD. Hip fracture risk and proximal femur geometry from DXA scans. *Osteoporos Int* 2002. <https://doi.org/10.1007/s001980200071>.
- [59] Partanen J, Jämsä T, Jalovaara P. Influence of the upper femur and pelvic geometry on the risk and type of hip fractures. *J Bone Miner Res* 2001. <https://doi.org/10.1359/jbmr.2001.16.8.1540>.
- [60] Nishino K, Sato Y, Ikeuchi K. Eigen-texture method: Appearance compression based on 3D model. *Proc IEEE Comput Soc Conf Comput Vis Pattern Recognit* 1999. [https://doi.org/10.1007/978-1-4615-0797-0\\_5](https://doi.org/10.1007/978-1-4615-0797-0_5).
- [61] Gnudi S, Ripamonti C, Gualtieri G, Malavolta N. Geometry of proximal femur in the prediction of hip fracture in osteoporotic women. *Br J Radiol* 1999. <https://doi.org/10.1259/bjr.72.860.10624337>.
- [62] Michelotti J, Clark JM. Femoral neck length and hip fracture risk. *J Bone Miner Res* 1999. <https://doi.org/10.1359/jbmr.1999.14.10.1714>.
- [63] Center JR, Nguyen T V., Pocock NA, Noakes KA, Kelly PJ, Eisman JA, Sambrook PN. Femoral neck axis length, height loss and risk of hip fracture in males and females. *Osteoporos Int* 1998. <https://doi.org/10.1007/s001980050051>.
- [64] Boonen S, Koutri R, Dequeker J, Aerssens J, Lowet G, Nijs J, Verbeke G, Lesaffre E, Geusens P. Measurement of femoral geometry in type I and type II osteoporosis: Differences in hip axis length consistent with heterogeneity in the pathogenesis of osteoporotic fractures. *J Bone Miner Res* 1995. <https://doi.org/10.1002/jbmr.5650101210>.
- [65] Beck TJ. Extending DXA beyond bone mineral density: Understanding hip structure analysis. *Curr Osteoporos Rep* 2007. <https://doi.org/10.1007/s11914-007-0002-4>.
- [66] Ackerman KE, Pierce L, Guereca G, Slattery M, Lee H, Goldstein M, Misra M. Hip structural analysis in adolescent and young adult oligoamenorrheic and eumenorrheic athletes and nonathletes. *J Clin Endocrinol Metab* 2013. <https://doi.org/10.1210/jc.2013->

1006.

- [67] Lou Bonnick S. HSA: Beyond BMD with DXA. *Bone* 2007. <https://doi.org/10.1016/j.bone.2007.03.007>.
- [68] LaCroix AZ, Beck TJ, Cauley JA, Lewis CE, Bassford T, Jackson R, Wu G, Chen Z. Hip structural geometry and incidence of hip fracture in postmenopausal women: What does it add to conventional bone mineral density? *Osteoporos Int* 2010. <https://doi.org/10.1007/s00198-009-1056-1>.
- [69] Ha Y-C, Yoo J-I, Yoo J, Park KS. Effects of Hip Structure Analysis Variables on Hip Fracture: A Propensity Score Matching Study. *J Clin Med* 2019. <https://doi.org/10.3390/jcm8101507>.
- [70] Kaptoge S, Beck TJ, Reeve J, Stone KL, Hillier TA, Cauley JA, Cummings SR. Prediction of incident hip fracture risk by femur geometry variables measured by hip structural analysis in the study of osteoporotic fractures. *J Bone Miner Res* 2008. <https://doi.org/10.1359/jbmr.080802>.
- [71] Broy SB, Cauley JA, Lewiecki ME, Schousboe JT, Shepherd JA, Leslie WD. Fracture Risk Prediction by Non-BMD DXA Measures: The 2015 ISCD Official Positions Part 1: Hip Geometry. *J Clin Densitom* 2015. <https://doi.org/10.1016/j.jocd.2015.06.005>.
- [72] Baker-Lepain JC, Luker KR, Lynch JA, Parimi N, Nevitt MC, Lane NE. Active shape modeling of the hip in the prediction of incident hip fracture. *J Bone Miner Res* 2011. <https://doi.org/10.1002/jbmr.254>.
- [73] Cootes TF, Taylor CJ, Cooper DH, Graham J. Active shape models - their training and application. *Comput Vis Image Underst* 1995. <https://doi.org/10.1006/cviu.1995.1004>.
- [74] Langton CM, Pisharody S, Keyak JH. Generation of a 3D proximal femur shape from a single projection 2D radiographic image. *Osteoporos Int* 2009;20:455–61. <https://doi.org/10.1007/s00198-008-0665-4>.
- [75] Väänänen SP, Isaksson H, Julkunen P, Sirola J, Kröger H, Jurvelin JS. Assessment of the 3-D shape and mechanics of the proximal femur using a shape template and a bone mineral density image. *Biomech Model Mechanobiol* 2011;10:529–38.

- <https://doi.org/10.1007/s10237-010-0253-3>.
- [76] Väänänen SP, Jurvelin JS, Isaksson H. Estimation of 3D shape, internal density and mechanics of proximal femur by combining bone mineral density images with shape and density templates. *Biomech Model Mechanobiol* 2012;11:791–800. <https://doi.org/10.1007/s10237-011-0352-9>.
- [77] Thevenot JÔ, Koivumäki J, Kuhn V, Eckstein F, Jämsä T. A novel methodology for generating 3D finite element models of the hip from 2D radiographs. *J Biomech* 2014;47:438–44. <https://doi.org/10.1016/j.jbiomech.2013.11.004>.
- [78] Rudman KE, Aspden RM, Meakin JR. Compression or tension? The stress distribution in the proximal femur. *Biomed Eng Online* 2006. <https://doi.org/10.1186/1475-925X-5-12>.
- [79] Cooles TF, Edwards GJ, Taylor CJ. Active appearance models. *IEEE Trans Pattern Anal Mach Intell* 2001. <https://doi.org/10.1109/34.927467>.
- [80] Whitmarsh T, Humbert L, De Craene M, Del Rio Barquero LM, Frangi AF. Reconstructing the 3D shape and bone mineral density distribution of the proximal femur from dual-energy x-ray absorptiometry. *IEEE Trans Med Imaging* 2011;30:2101–14. <https://doi.org/10.1109/TMI.2011.2163074>.
- [81] Frangi AF, Rueckert D, Schnabel JA, Niessen WJ. Automatic construction of multiple-object three-dimensional statistical shape models: Application to cardiac modeling. *IEEE Trans Med Imaging* 2002. <https://doi.org/10.1109/TMI.2002.804426>.
- [82] Burghardt AJ, Kazakia GJ, Link TM, Majumdar S. Automated simulation of areal bone mineral density assessment in the distal radius from high-resolution peripheral quantitative computed tomography. *Osteoporos Int* 2009. <https://doi.org/10.1007/s00198-009-0907-0>.
- [83] Väänänen SP, Grassi L, Flivik G, Jurvelin JS, Isaksson H. Generation of 3D shape, density, cortical thickness and finite element mesh of proximal femur from a DXA image. *Med Image Anal* 2015;24:125–34. <https://doi.org/10.1016/j.media.2015.06.001>.
- [84] Kannus P, Leiponen P, Parkkari J, Palvanen M, Järvinen M. A sideways fall and hip fracture. *Bone* 2006. <https://doi.org/10.1016/j.bone.2006.01.148>.
- [85] Majumder S, Roychowdhury A, Pal S. Simulation of hip fracture in sideways fall using a

- 3D finite element model of pelvis-femur-soft tissue complex with simplified representation of whole body. *Med Eng Phys* 2007. <https://doi.org/10.1016/j.medengphy.2006.11.001>.
- [86] Keyak JH, Rossi SA, Jones KA, Skinner HB. Prediction of femoral fracture load using automated finite element modeling. *J Biomech* 1997. [https://doi.org/10.1016/S0021-9290\(97\)00123-1](https://doi.org/10.1016/S0021-9290(97)00123-1).
- [87] Koivumäki JEM, Thevenot J, Pulkkinen P, Kuhn V, Link TM, Eckstein F, Jämsä T. Ct-based finite element models can be used to estimate experimentally measured failure loads in the proximal femur. *Bone* 2012;50:824–9. <https://doi.org/10.1016/j.bone.2012.01.012>.
- [88] Boehm HF, Horng A, Notohamiprodjo M, Eckstein F, Burklein D, Panteleon A, Lutz J, Reiser M. Prediction of the fracture load of whole proximal femur specimens by topological analysis of the mineral distribution in DXA-scan images. *Bone* 2008. <https://doi.org/10.1016/j.bone.2008.07.244>.
- [89] Cheng XG, Lowet G, Boonen S, Nicholson PHF, Brys P, Nijs J, Dequeker J. Assessment of the strength of proximal femur in vitro: Relationship to femoral bone mineral density and femoral geometry. *Bone* 1997. [https://doi.org/10.1016/S8756-3282\(96\)00383-3](https://doi.org/10.1016/S8756-3282(96)00383-3).
- [90] Gilchrist S, Nishiyama KK, de Bakker P, Guy P, Boyd SK, Oxland T, Crompton PA. Proximal femur elastic behaviour is the same in impact and constant displacement rate fall simulation. *J Biomech* 2014. <https://doi.org/10.1016/j.jbiomech.2014.06.040>.
- [91] Cai T, Zheng Y. Evaluating prognostic accuracy of biomarkers in nested case-control studies. *Biostatistics* 2012. <https://doi.org/10.1093/biostatistics/kxr021>.

## **CHAPTER 2 - Comparing the Fracture Limits of The Proximal Femur Under Impact and Quasi-Static Conditions in Simulation of a Sideways Fall**

---

*Overview: In this chapter, the association of the proximal femur fracture load in a simulation of sideways fall in two scenarios of impact, and quasi-static loading rate was investigated to address Objective 1. This chapter has been published in the Journal of the Mechanical Behavior of Biomedical Materials (2020, V103, DOI: 10.1016/j.jmbbm.2019.103593). The proper permission from the copyright holder (Elsevier Ltd.) has been obtained to include the article in this thesis.*



Contents lists available at ScienceDirect

Journal of the Mechanical Behavior of Biomedical Materials

journal homepage: <http://www.elsevier.com/locate/jmbbm>

## Comparing the fracture limits of the proximal femur under impact and quasi-static conditions in simulation of a sideways fall

Fatemeh Jazinizadeh<sup>a</sup>, Hojjat Mohammadi<sup>b</sup>, Cheryl E. Quenneville<sup>a,c,\*</sup>

<sup>a</sup> Department of Mechanical Engineering, McMaster University, Hamilton, ON, Canada

<sup>b</sup> Department of Civil Engineering, McMaster University, Hamilton, ON, Canada

<sup>c</sup> School of Biomedical Engineering, McMaster University, Hamilton, ON, Canada

### ARTICLE INFO

#### Keywords:

Proximal femur  
Fracture risk  
Sideways fall  
Impact loading  
Quasi-static loading  
Rate  
Hip

### ABSTRACT

Sideways falls onto the hip are responsible for a great number of fractures in older adults. One of the possible ways to prevent these fractures is through early identification of people at greatest risk so that preventive measures can be properly implemented. Many numerical techniques that are designed to predict the femur fracture risk are validated through performing quasi-static (QS) mechanical tests on isolated cadaveric femurs, whereas the real hip fracture is a result of an impact (IM) incident. The goal of this study was to compare the fracture limits of the proximal femur under IM and QS conditions in the simulation of a sideways fall to identify any possible relationship between them.

Eight pairs of fresh frozen cadaveric femurs were divided into two groups of QS and IM (left and right randomized). All femurs were scanned with a Hologic DXA scanner and then cut and potted in a cylindrical tube. To measure the stiffness in two conditions of the single-leg stance (SLS) and sideways fall (SWF), non-destructive tests at a QS displacement rate were performed on the two groups. For the destructive tests, the QS group was tested in SWF configuration with the rate of 0.017 mm/s using a material testing machine, and the IM group was tested in the same configuration inside a pneumatic IM device with the projectile target displacement rate of 3 m/s.

One of the IM specimens was excluded due to multiple strikes. The result of this study showed that there were no significant differences in the SLS and SWF stiffnesses between the two groups ( $P = 0.15$  and  $P = 0.64$ , respectively). The destructive test results indicated that there was a significant difference in the fracture loads of the two groups ( $P < 0.00001$ ) with the impact ones being higher; however, they were moderately correlated ( $R^2 = 0.45$ ). Also, the comparison of the fracture location showed a qualitatively good agreement between the two groups.

Using the relationship developed herein, results from another study were extrapolated with errors of less than 12%, showing that meaningful predictions for the impact scenario can be made based on the quasi-static tests. The result of this study suggests that there is a potential to replace IM tests with QS displacement rate tests, and this will provide important information that can be used for future studies evaluating clinical factors related to fracture risk.

### 1. Introduction

Osteoporosis is a generalized skeletal disorder in which a reduction in Bone Mineral Density (BMD) decreases bone strength and can result in an increased risk of fracture. This disease is more common in older adults and is the one of the main reasons for a broken bone among this population. One of the sites commonly affected by osteoporosis is the proximal femur, the fracture of which greatly decreases mobility and

function, as well as being responsible for high health care costs for society (Mears and Kates, 2015). Therefore, it is crucial to prevent fractures from happening through early identification of people at a great risk of sustaining a fracture, who may then use protective measures such as hip protectors (Laing and Robinovitch, 2008), energy attenuating floors (Bhan et al., 2014), targeted exercise (Nikander et al., 2010), and pharmacological interventions (L. Yang et al., 2014).

To realistically estimate a person's fracture risk, one needs to

\* Corresponding author. ABB-C308, McMaster University, 1280 Main St. West, Hamilton, ON, L8S 4L8, Canada.  
E-mail address: [quennev@mcmaster.ca](mailto:quennev@mcmaster.ca) (C.E. Quenneville).

<https://doi.org/10.1016/j.jmbbm.2019.103593>

Received 2 August 2019; Received in revised form 9 December 2019; Accepted 10 December 2019

Available online 13 December 2019

1751-6161/© 2019 Elsevier Ltd. All rights reserved.

understand the fracture mechanism. Many studies have endeavored to create a framework to predict femur fracture risk from a fall. In these studies, the correlation of the fracture load with Finite Element Analysis (FEA) predictions (Dall'Ara et al., 2013; Koivumäki et al., 2012), BMD (Boehm et al., 2008; Leichter et al., 2001), bone's geometry (X. J. Yang et al., 2018), and other factors has been investigated, and typically validated via constant-displacement-rate experiments on cadaveric femur specimens (Gilchrist et al., 2014). However, in reality, the incident that leads to a fracture is rarely quasi-static (QS) or at a constant displacement rate (Gilchrist et al., 2013).

Investigating how a QS constant-displacement-rate experiment might differ from a fall impact (IM) simulation has great importance: if the femur's structural behavior under impact is comparable to a quasi-static test, or at least the relationship between them can be established, experimental impact testing can be replaced with quasi-static ones. It also allows us to extrapolate results from previous studies to conditions more representative of real-life falls.

Bone is well understood to be a viscoelastic material (Carter & Hayes, 1977), and some previous studies have investigated how bone material properties such as elastic modulus and compressive strength depend on the strain rate (Linde et al., 1991; Prot et al., 2016). In addition, the behavior of a whole bone at higher strain rates has been shown to be different from small samples due to the entrapped marrow (Askarinejad et al., 2019; Linde et al., 1991). However, the question remains as to how much this will influence the proximal femur during a sideways fall with an average impact velocity of 3 m/s (Feldman and Robinovitch, 2007; Fleps et al., 2018; van den Kroonenberg et al., 1996). The effect of loading rate on the proximal femur fracture load has been investigated in three previous studies by Courtney et al. (1994), Gilchrist et al. (2014), and Askarinejad et al. (2019). The results of the first study showed that both fracture load and structural stiffness were greater by 20% and 200% with a higher quasi-static displacement rate (displacement rate of 100 mm/s vs. 2 mm/s). In the second study (Gilchrist et al., 2014), three rates of 0.5 mm/s, 100 mm/s, and 3 m/s (IM) were tested and the results showed no significant differences between the stiffness and fracture load in the IM group (displacement rate of 3 m/s) and the QS group with a displacement rate of 0.5 mm/s (QS slow). However, the comparison between the IM group and the QS group with a rate of 100 mm/s (QS fast) showed a significant difference. Finally, in the third study (Askarinejad et al., 2019), while most of the fracture loads in the impact condition were higher than QS ones, no statistically significant difference was observed due to the small sample size and lack of paired specimens. Although bones are expected to have higher fracture loads in impact (Enns-Bray et al., 2018), these three experimental studies (Askarinejad et al., 2019; Courtney et al., 1994; Gilchrist et al., 2014), didn't have a clear and strong consensus on how displacement rate influences proximal femurs structural fracture load, since the results may have been influenced either by the different characteristics of each group (BMD, geometry, age, sex), or lack of statistical power.

Therefore, a new study with paired specimens was proposed to properly quantify any possible effect of loading rate (quasi-static vs impact) on the strength of proximal femurs in a sideways fall configuration and investigate if there is a potential relationship between the IM fracture loads and QS ones. With respect to that, the objectives of this research were to (1) determine how femoral fracture load differs between QS loading and IM loading in the simulation of a sideways fall, and quantify any possible relationship between them, and (2) to determine if the fracture patterns differ between these two scenarios.

## 2. Materials and methods

### 2.1. Specimen preparation

This research was approved by the Hamilton Integrated Research Ethics Board (HiREB). Eight pairs of fresh-frozen human cadaveric femurs (67.4 ± 6.6 years old, four males and four females, Table 1) were

obtained and cleaned of all soft tissues. There were no reported musculoskeletal diseases for the specimens. To obtain the BMD, each femur was scanned with a Hologic DXA scanner (Hologic Discovery A, Hologic, Inc., MA, USA). To simulate the soft tissue during the scan a plastic container filled with water (to a depth of 15 cm) was placed over the specimens (Chappard et al., 2010). Femurs were then cut to a length of 27.5 cm and potted distally in cylindrical tubes with 7.62 cm (3") diameter, using dental cement (Denstone type III, Kulzer, Hanau, Germany) to a depth of 6 cm. Four points were marked on each bone: two on the anterior aspect and two on the lateral aspect, located between 14 and 20 cm from the proximal end (Fig. 1). These were used to create two longitudinal vectors, and then the position of the femur in the pot was adjusted (while the dental cement was still wet) so that vertical laser beams (controlled by a level) would match the identified vectors in both the sagittal and frontal planes. Fixing the femur in the desired positions (internal/external rotation and adduction/abduction) in the SLS and SWF conditions was accomplished by the apparatus that was created to hold the potted specimen. Specimens were kept frozen at -21 °C and were thawed for at least 4 h before testing.

Each specimen was instrumented with three stacked rosette strain gauges (F series, Tokyo Measuring Instruments Laboratory Co., Ltd. Tokyo, Japan). For consistency among samples, geometrical and anatomical landmarks were used to determine the exact location of each landmark for each specimen (Fig. 2).

### 2.2. Mechanical testing

Femurs within each pair were randomly allocated into two groups of IM and QS. To assess whether the two groups could be considered equivalent, the stiffness in two orientations of Single Leg Stance (SLS, defined as 20 degrees of abduction from the vertical axis (Dall'Ara et al., 2013; Keyak, 2000)), and Sideways Fall (SWF, defined as 15 degrees of internal rotation and 10 degrees of adduction (Dragomir-Daescu et al., 2011; Roberts et al., 2010; Wakao et al., 2009)), was measured by loading all femurs for five cycles each to 250 N at a rate of 0.017 mm/s using an Instron material testing machine (Instron 5967, Instron, MA, USA). A custom jig was used to hold the bones in the desired position during testing, and two PMMA (Simplex, Stryker, Michigan, USA) cups were molded for the greater trochanter and femoral head for each specimen to distribute the forces evenly over the region in question in the SWF testing.

Following this, the QS group was preloaded to 250 N and ramp loaded to fracture under simulated Sideways Fall, using the same loading rate as above. A bearing plate beneath the proximal end was used to provide translational degrees of freedom in x and y directions and rotation around the z axis. Also, the distal end was free to rotate around the z and y axes (Fig. 3). The IM tests were delivered by a custom-made pneumatic impacting device (Chakravarty et al., 2017;

Table 1

Summary of specimens' characteristics. Paired specimens were used, with right and left femurs from each donor randomized into the two groups of Impact and Quasi-Static. Each bone was DXA scanned, and no differences found between the specimens allocated to the impact condition and those of the quasi-static condition ( $p = 0.63$ ).

Specimen	Age	Sex	Total BMD mg/cm <sup>2</sup>	
			IM Specimens	QS specimens
1	69	F	803	789
2	70	F	827	821
3	53	F	859	857
4	67	M	970	919
5	73	F	844	759
6	70	M	1105	1101
7	70	M	1009	965
8	62	M	1054	1026
Mean ± SD	67.4 ± 6.6	N/A	933.9 ± 115.2	904.6 ± 120.1

F. Jazinizadeh et al.

Journal of the Mechanical Behavior of Biomedical Materials 103 (2020) 103593

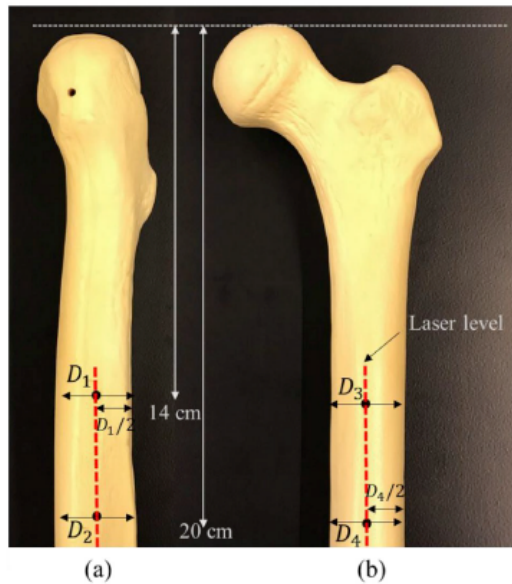


Fig. 1. Illustration of geometrical landmarks that were used to pot the specimens vertically, (a) shows the lateral view and (b) shows the anterior view, the four points (indicated with dots) were connected with lasers to define the vertical alignment in two planes.

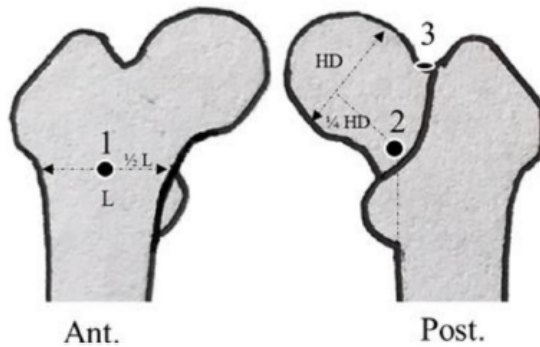


Fig. 2. Location of the strain gauges: (1) the strain gauge on the anterior side of the trochanteric area located on the mid-point of the horizontal line that passes superior border of the lesser trochanter, (2) the strain gauge on the posterior side on the basicervical area at the cross-section of the vertical line that passes the lateral border of the lesser trochanter and the line parallel to the neck axis that passes the  $\frac{1}{4}$  of the femoral head diameter (close to the medial part), and (3) the strain gauge on the superior side of the femoral neck.

Martinez et al., 2018). Briefly, a steel projectile was pushed down an acceleration tube by compressed air to reach the test chamber (Fig. 4). The velocity of the projectile was controlled to deliver an impact velocity of 3 m/s to be representative of the speed of impact during a fall (Feldman and Robinovitch, 2007; Fleps et al., 2018; van den Kroonenberg et al., 1996). A 30 mm layer of vinyl nitrile closed cell foam (with a stiffness of 33.0 kN/m) was placed between the projectile and the load cell to simulate the attenuation provided by soft tissue on the greater trochanter (Laing and Robinovitch, 2008; Nielson et al., 2009). Similarly to the QS tests, rotational degrees of freedom at the distal end were provided in both y and z directions, and rail guides provided

translational freedom in the x-direction. Due to the orientation of the impacting device, translations in the y direction at the proximal end could not be facilitated by bearings, but simply by resting the PMMA cup on a block (Fig. 4).

Specimen four was used as the pilot bone to determine the required mass to break the bones. The first strikes were associated with low masses (4–8 kg), but since no injury was induced to the bone, the projectile mass was then increased to 23 kg. After this increase, specimen four was broken and then the projectile mass remained the same for the rest of the specimens. However, due to the additional impacts it sustained, its failure data were excluded from analysis.

To calculate the maximum displacement rate in the IM group, a laser displacement sensor (IL-300, Keyence, Osaka, Japan) was used to track the displacement of the loading plate. The data of the last 1 ms to reach the peak value were used to calculate the maximum loading rate as well as the displacement rate in the IM group. For the QS group, the displacement rate was constant, and the loading rate was calculated for the last 10 s to reach the peak force.

The signals from the strain gauges were filtered by a low-pass filter with a cut-off value of 50 Hz (Zani et al., 2015). For each strain gauge, the maximum principal strains were calculated. In addition, the data over the 10 s, and 1 ms period to reach this value were used to calculate the strain rates for the QS and IM tests, respectively.

All statistical analyses and comparisons were performed using student t-tests with a significance level of  $\alpha = 0.05$  after checking for the normality of data.

### 3. Results

Comparison of the two groups showed no significant differences in total BMD ( $P = 0.63$ ), (Table 1). Also, neither the QS stiffness measure differed between groups, with SLS averaging  $647 \pm 155$  N/m and  $748 \pm 111$  N/m for the QS and IM, respectively ( $P = 0.15$ ), and SWF averaging  $570 \pm 131$  N/m and  $598 \pm 97$  N/m for the QS and IM groups, respectively ( $P = 0.64$ ).

The average velocity of the projectile in the IM group was  $3.24 \pm 0.08$  m/s, with impact durations of less than 30 ms (Fig. 5). Also, in the QS group (Fig. 6), the duration of the tests from the beginning to the fracture point was an average of  $8.8 \pm 1.6$  min. Displacement and loading rates during the tests were calculated from the displacement sensor and the load cell measurements (Table 2).

The average fracture loads for the QS and IM groups were significantly different, at  $3637 \pm 863$  N and  $7326 \pm 771$  N, respectively ( $p < 0.00001$ ). However, a moderate correlation ( $R^2 = 0.45$ ) was found between the paired specimens (Fig. 7). The following relationship was observed between the fracture loads in the two scenarios of QS and IM from the linear regression:

$$(\text{IM fracture load}) = 0.61^*(\text{QS fracture load}) + 5173$$

The fracture load in the QS group was strongly correlated with BMD ( $R^2 = 0.74$ ), whereas for the IM specimens this correlation decreased to  $R^2 = 0.56$  (Fig. 8). Finally, fracture patterns and locations were noted for each specimen, and for the majority of the pairs were qualitatively very similar for the two fracture conditions (Fig. 9).

Strain data for one of the QS specimens was missing due to operator error (specimen 8). There was a significant difference between the maximum principal strains in the QS and IM for the strain gauges on the posterior side ( $p = 0.03$ ), and the superior side of the neck ( $p = 0.02$ ), but there wasn't a significant difference in the anterior gauges ( $p = 0.53$ ). The Coefficient of Variation (CV) for the femoral neck, posterior, and anterior gauges in the QS were 97%, 50%, and 144%, and in IM they were 83%, 98%, 175%. Strain rates in the IM tests were at least six orders of magnitude higher than QS ones (Table 3).

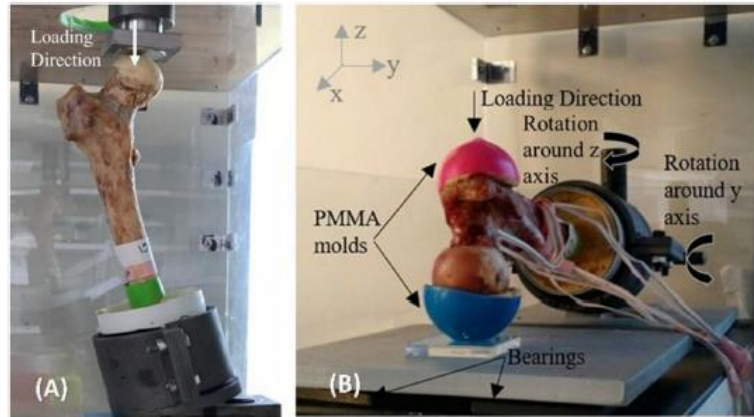


Fig. 3. QS testing setup: (A) Simulation of the SLS to measure the stiffness, and (B) simulation of SWF to measure the stiffness and the fracture load, two PMMA molds at the femoral head and greater trochanter were used to ensure distribution of forces over the bone surface. Bearing plates were used to provide x and y translations and rotation around z at the proximal end, and rotation about the y and z axes was provided at the distal end.

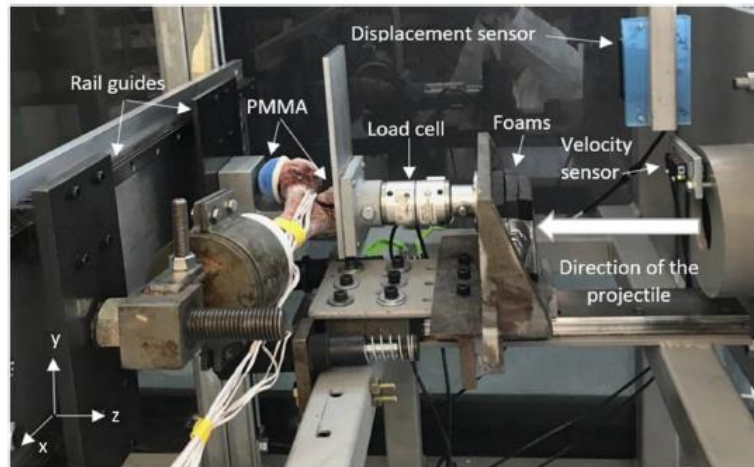


Fig. 4. Impact set up. A rail guide and hinge joints were used to provide the required degrees of freedom at the proximal and distal end, the load cell was located after the foam to enable a more accurate measurement of the force delivered to the bone, a velocity sensor measured the speed of the projectile after being accelerated by the pneumatic device and just before the impact. Also, a laser displacement sensor was used to measure the displacement after the impact.

#### 4. Discussion

Sideways falls onto the hip are responsible for a great number of hip fractures among older adults (Kannus et al., 2006; Parkkari et al., 1999; Wei et al., 2001). One of the most effective methods to prevent these fractures is the early identification of people at greatest risk (Johnell et al., 2005). In addition to BMD measurement, numerical methods such as finite element analysis and image processing are useful tools currently receiving a lot of attention (Bessho et al., 2007; Dall'Ara et al., 2016; Derikx et al., 2011; Duchemin et al., 2008; Keyak, 2001). In most of these studies, to validate their proposed technique an *ex-vivo* experiment on cadaveric human femurs has been performed. However, many of these studies simulated sideways falls in a quasi-static manner, whereas a real fall onto the hip is more likely to be an impact incident. Given the viscoelastic nature of bone, the main goal of the present study was to compare the structural fracture limits of proximal femurs in sideways falls at two displacement rates of quasi-static and impact. The use of

paired specimens to enable a direct comparison between the two groups was a novel approach, and the previously reported velocity of falls onto the hip was simulated for the impact group. In addition, due to the placement of the load cell between the foams (that were simulating the soft tissue) and the specimen, we were able to measure the exact load that was delivered to the bone and caused the fracture.

Comparison of BMD, SLS stiffness and SWF stiffness between the two groups showed that there were no significant differences between the two groups of QS and IM; however, since the specimens in the two groups were pairs this was expected. Therefore, the comparison of the two groups in terms of fracture load and fracture patterns provides extremely valuable information regarding the effect of loading rate and eliminated the confounding factor of varied donors that has historically been present in these types of studies.

Specimen four was used to determine the projectile mass required to cause a fracture, and thus received additional strikes that may have caused microdamage so consequently this specimen was removed from

F. Jazinizadeh et al.

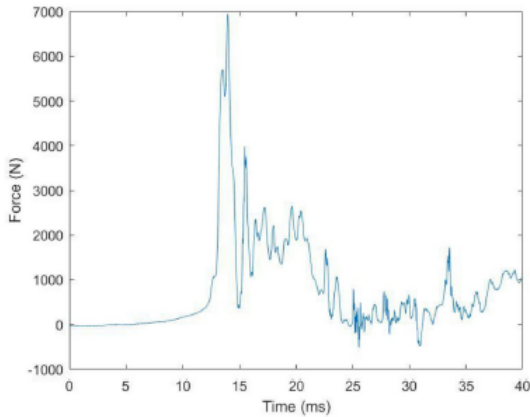


Fig. 5. A typical force-time graph from the impact testing.

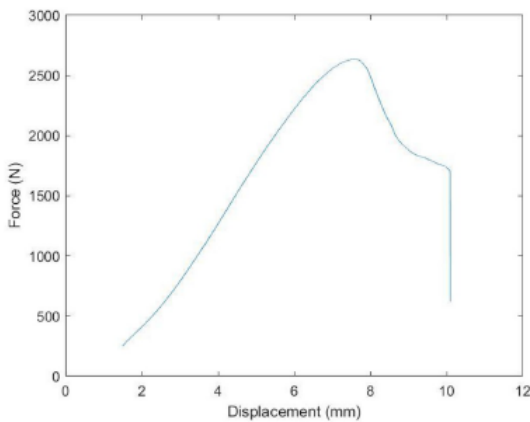


Fig. 6. A typical force-displacement graph from the QS testing, the tests were stopped after a 2000 N force drop.

further fracture and strain analysis. Results showed that there was a significant difference in fracture load ( $P < 0.00001$ ) between the two displacement rates tested, which is unsurprising given the viscoelastic nature of bone and nature of the dynamic loading. The relationship between the fracture loads indicated a moderate correlation ( $R^2 = 0.45$ ). The one pair of specimens that did not follow this trend was specimen 3, where the IM femur had a lower fracture load than the one anticipated by the trendlines found in both the “IM fracture load-QS fracture load”, and “IM fracture load-BMD” graphs. If this specimen were removed from the analysis, a strong coefficient of determination of  $R^2 = 0.97$  for the relationship between the fracture loads in QS and IM displacement rates, and  $R^2 = 0.90$  for the relationship between the IM fracture loads and BMD, would be observed. This suggests that there is the potential to develop a reliable relationship between the two test conditions of IM and

QS, and IM tests (experimentally and numerically) can be replaced by the QS test in the appropriate context, especially in developing fracture risk estimation criteria in cadaveric studies.

In order to examine whether the proposed formula of estimating the IM fracture load from the QS one would be able to predict the results from previous studies, the two pairs of specimens in a previous study (Askarinejad et al., 2019) were chosen and their IM fracture loads were predicted based on the QS ones. For their second and fourth QS specimens, the IM fracture loads were predicted as 7337 N and 7146 N, while the real fracture loads from the experiment were 6288 N and 6661 N, which indicates 7–12% absolute error in the prediction. Considering that the experimental setups were entirely different, a maximum absolute error of 12% means that the proposed formula is able to predict the fracture load well and extrapolation of previous studies results using this approach can make meaningful predictions.

In terms of fracture location and patterns, almost all the specimens in the IM group had more complete fractures than the contralateral ones in the QS group, since the tests in the latter group were terminated after a 2000 N drop in the load (corresponding to initial crack formation). In the IM group, the entire energy of the projectile was delivered to the specimens, and even if the fracture occurred the energy transfer continued, which led to a more substantial and higher number of cracks.

Generally, in both QS and IM groups four main fracture patterns were observed, and each specimen had one or two of these: (1) cracks that propagated through trabecula's secondary compressive group from the inferior medial region toward the trochanteric area, (2) cracks in the middle of the femoral neck, (3) cracks between the superior greater trochanter and lateral side of the trochanteric and subtrochanteric area (which was only seen in the IM group), (4) wedge fractures in the greater trochanter or subtrochanteric area. One of the contributing factors in crack propagation in the proximal femur is the pattern of the trabecula. Fracture types one and two (defined above) were also observed in a previous study (Askarinejad et al., 2019), and were attributed to the

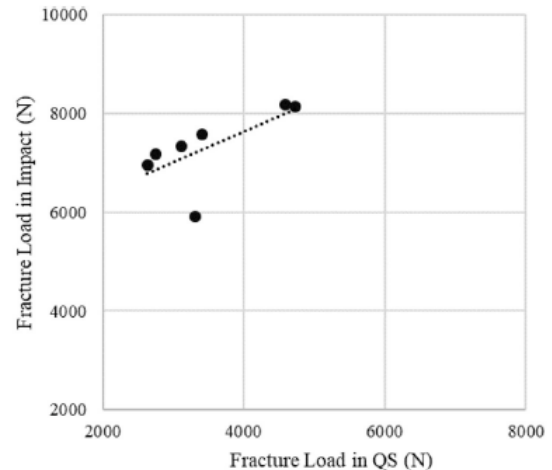
Fig. 7. The relationship between IM and QS fracture loads for the seven pairs of specimens, showing a coefficient of determination of  $R^2 = 0.45$ .

Table 2

Summary of the tests' results. While no differences were found in stiffnesses between groups, the fracture load for the impact condition was significantly larger than that of the quasi-static group.

	Sideways Fall Stiffness (N/m)	Single Leg Stance Stiffness (N/m)	Fracture Load (N)	Displacement Rate (m/s)	Loading Rate (N/m/s)
QS Group	570 ± 131	647 ± 155	3637 ± 863	0.000017	0.002 ± 0.001
IM Group	598 ± 97	748 ± 111	7326 ± 771	1.16 ± 0.58	4634 ± 1774

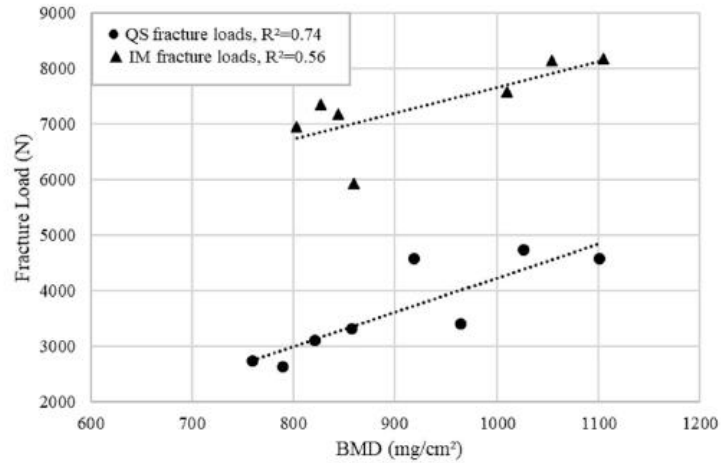


Fig. 8. Fracture load vs. BMD for the two test configurations. The circles show the fracture loads from QS condition, and the triangles represent the IM fracture loads. Impact fracture load for specimen four was not included due to the multiple strikes it sustained as the pilot specimen.

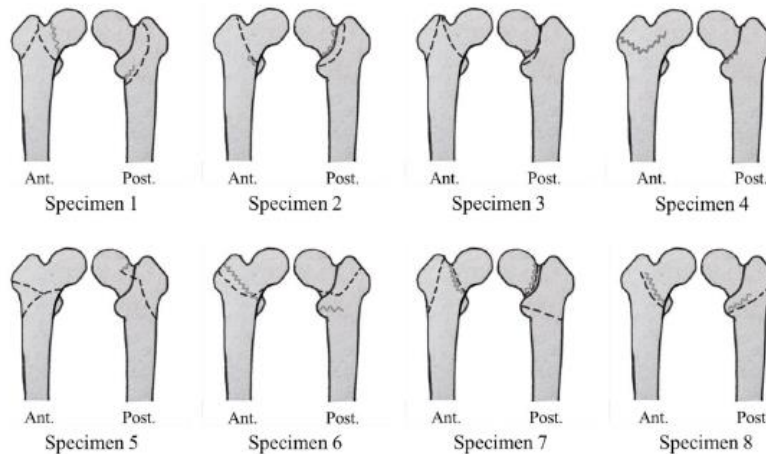


Fig. 9. Fracture patterns in the QS and IM groups in the Anterior (Ant.) and Posterior (Post.) views. The zigzag and dashed lines refer to the fracture patterns in the QS and IM groups, respectively. The IM fracture patterns for specimen four were excluded due to the extra strikes it sustained as a pilot specimen.

Table 3

Maximum principal strain ( $\mu\epsilon$ ), and strain rate ( $\mu\epsilon/ms$ ) measured in the QS (eight specimens) and IM (seven specimens) tests, mean and standard deviation (SD).

		Max Strain ( $\mu\epsilon$ )			Max strain rate ( $\mu\epsilon/ms$ )		
		Gauge 1	Gauge 2	Gauge 3	Gauge 1	Gauge 2	Gauge 3
QS testing	mean	4043	2614	4700	0.0039	0.0059	0.0030
	SD	3924	1295	6749	0.0040	0.0069	0.0018
IM testing	mean	25586	37629	8871	9532	13798	2706
	SD	21295	36705	15535	9480	14727	5130

delamination of the secondary compressive trabecula and low energy crack propagation due to the less connected trabecula in the Ward's triangle, respectively. Overall, the fracture patterns were comparable to similar studies (Ariza et al., 2015; Askarinejad et al., 2019; Villette and Phillips, 2018) and while most of the fractures matched clinically relevant fractures based on the Orthopaedic Trauma Association (OTA) fracture classification (Meinberg et al., 2018), some of the fracture patterns might have been influenced by the specimen's individual shape

and BMD properties as well as specific loading and boundary conditions (minor misalignments or motion) during the testing.

In specimens two and seven in the QS group that sustained a complete fracture, the fracture lines on the posterior side were the same as the contralateral ones in the impact group. So, considering that in the QS tests the force did not completely return to zero after the peak point, the crack locations can be assumed to be almost the same in the two groups, indicating that while the viscoelastic behavior of the proximal femur

Table 4

Comparison of the relevant studies. Three other previous studies have examined the effect of loading rate on fracture threshold in the proximal femur, with differences in methods and findings.

Study	Minimum rate tested	Maximum rate tested	Findings	Advantages
Courtney et al. (1994)	2 mm/s	0.1 m/s	With the higher displacement rate the fracture load was increased	Use of paired specimens
Gilchrist et al. (2014)	2 mm/s 100 mm/s	3 m/s	No significant difference was observed With the higher displacement rate the fracture load was decreased	Use of the sideways fall displacement rate for the impact
Askarinejad et al. (2019)	0.067 mm/s	4 m/s	No significant difference was observed, however most of the IM fracture load tended to be higher than QS ones The fracture patterns were qualitatively the same	Using a displacement rate close to the value of sideways fall for the impact Having two pairs in the specimens Wider range of displacement rates
Present study	0.017 mm/s	3.24 m/s	With the higher displacement rate the fracture load was increased A moderate correlation was found for the fracture forces between the two scenarios The fracture patterns were qualitatively the same	Use of eight paired specimens Use of the sideways fall displacement rate placing the load cell after the compliant foam to measure the actual impact force Wider range of displacement rates

affects the fracture load in a sideways fall, it doesn't greatly affect the location of failure of the proximal femur.

Regarding the displacement rate in the IM scenario, it is worth noting that the velocity of 3 m/s is the speed by which the body (hip) has been reported to hit the ground, and due to the soft tissue energy attenuation, the real displacement rate that is delivered to the bone is less than that. In the present impact setup, the projectile made initial contact with a speed of  $3.24 \pm 0.05$  m/s, and then this speed reduced to  $1.16 \pm 0.58$  m/s as a result of using foams for soft tissue simulation. A similar reduction in the displacement rates could also be observed in a previous work (Gilchrist et al., 2014).

In this study, the simulated sideways fall impact condition was compared to quasi-static loading with the displacement rate of 0.0017 mm/s, with the rationale that these represent the extremities of testing of proximal femur fracture loads, and if there is a correlation between these extremities, it's likely that other quasi-static tests in between would be correlated with the dynamic testing as well. However, to examine what really happens at intermediate rates, more paired specimen testing would be required. It is likely that some of quasi-static tests at the lower displacement rates (e.g. study by Askarinejad et al., 2019) would be similar to the present ones, but at some point, the strain rate effects would start to dominate, and alter the fracture load.

The strain gauge data showed that most of the principal strains measured in the IM group tended to be higher than the corresponding ones in the QS group, which was expected due to the greater number of cracks on the surface in the IM group; however, it should be noted that there was high variability in the strain data, and because of that no statistically significant difference between the strains at the anterior trochanteric area was found. The coefficient of variation for measured strains in QS and IM ranged between 50%-144% and 83%-175% respectively. This high variability was because the specific strain measured by each gauge depended on the pattern of crack propagation around it, and the specific geometry and BMD characteristic of that bone, which makes developing a generalized strain curve challenging. Therefore, the strain data would be more beneficial for developing and validating subject-specific FE models.

The strain rates immediately prior to the fracture in the IM group ranged from 0.05 to  $38$  s<sup>-1</sup>. Having strain rates above  $10$  s<sup>-1</sup> (10,000 µε/ms) indicated that in the sideways fall configuration both viscoelastic and hydraulic effects contributed to the strength of the bone (Linde et al., 1991), and this should be an important consideration for the further numerical simulations in the appropriate context.

Other previous studies have examined the effect of displacement rate on femoral fracture load, with conflicting results. In one previous study (Courtney et al., 1994), an increase in fracture force was observed (Table 4), which agrees with the present results; however, it should be

noted that this study was limited to rates of up to 100 mm/s. In another previous study (Gilchrist et al., 2014), speeds up to 3 m/s were tested and compared with two QS rates of 100 mm/s and 2 mm/s, and their results showed that the yield forces in the IM group were significantly lower than QS group with the rate of 100 mm/s. However, there was no significant difference between the IM group and the QS group with the rate of 2 mm/s. These differences may be attributed to the use of unpaired specimens, and potentially BMD and geometric factors dominating the results as discussed in that study as well. In the last study (Askarinejad et al., 2019), despite having two pairs in their specimens (out of ten femurs), and although the IM fracture loads tended to be higher than QS ones, no significant differences were observed between the fracture loads in the two conditions, which may be attributable to a lack of statistical power (Table 4).

One of the limitations of the current study was that for the impact condition the loading was applied horizontally (z direction) due to the design of the pneumatic impact device, requiring the vertical degree of freedom (y direction) to be constrained against gravity. This is the one boundary condition that differed from the QS setup, where both in plane (x,y) linear degrees of freedom were unconstrained. It is possible that this additional constraint increased the reaction force; however, no substantial movement was observed in the anterior-posterior direction during QS tests, thus suggesting that any such effect was likely relatively minor. The limited number of specimens (16) was another limitation of this study; however, similar studies in our lab (Chakravarty et al., 2017; Martinez et al., 2018) with six pairs of samples have shown that using the paired specimens greatly reduces the variabilities between the two groups and can detect the changes of interest properly.

This study is unique in that it related the structural behavior and fracture limits of the proximal femur in the QS displacement rate (as used in the validation of many previous studies assessing hip fracture risk) and the impact one (as happens in reality). It is the first study to the authors' knowledge that directly compares the results of *ex-vivo* sideways fall destructive tests using only paired specimens for two relevant scenarios of quasi-static and impact displacement rates, which eliminates many potentially confounding factors such as BMD and geometry when using unpaired samples. Also, extrapolating results from other studies with less than 12% error showed that meaningful predictions for the impact scenario can be made based on the quasi-static tests. This study will provide important information that can be used for future studies evaluating clinical factors related to fracture risk.

#### Declaration of competing interest

There are no financial or personal relationships that could inappropriately influence this work, and there is no conflict of interest.

### CRedit authorship contribution statement

**Fatemeh Jazinizadeh:** Conceptualization, Data curation, Formal analysis, Investigation, Methodology, Supervision, Validation, Visualization, Writing - original draft, Writing - review & editing. **Hojjat Mohammadi:** Investigation, Writing - review & editing. **Cheryl E. Quenneville:** Conceptualization, Funding acquisition, Methodology, Project administration, Resources, Supervision, Writing - review & editing.

### Acknowledgments

This work was supported by the Labarge Optimal Aging Initiative. Also, the authors would like to thank Chantal Saab for help in DXA scanning of the specimens.

### Appendix A. Supplementary data

Supplementary data to this article can be found online at <https://doi.org/10.1016/j.jmbm.2019.103593>.

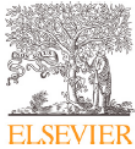
### References

- Ariza, O., Gilchrist, S., Widmer, R.P., Guy, P., Ferguson, S.J., Crompton, P.A., Helgason, B., 2015. Comparison of explicit finite element and mechanical simulation of the proximal femur during dynamic drop-tower testing. *J. Biomech.* 48 (2), 224–232. <https://doi.org/10.1016/j.jbiomech.2014.11.042>.
- Askarinejad, S., Johnson, J.E., Rahbar, N., Troy, K.L., 2019. Effects of loading rate on the of mechanical behavior of the femur in falling condition. *J. Mech. Behav. Biomed. Mater.* 96, 269–278. <https://doi.org/10.1016/j.jmbm.2019.04.038>.
- Besho, M., Ohnishi, I., Matsuyama, J., Matsumoto, T., Imai, K., Nakamura, K., 2007. Prediction of strength and strain of the proximal femur by a CT-based finite element method. *J. Biomech.* 40 (8), 1745–1753.
- Bhan, S., Levine, I.C., Laing, A.C., 2014. Energy absorption during impact on the proximal femur is affected by body mass index and flooring surface. *J. Biomech.* 47 (10), 2391–2397. <https://doi.org/10.1016/j.jbiomech.2014.04.026>.
- Boehm, H.F., Homg, A., Notohamiprodjo, M., Eckstein, F., Burklein, D., Panteleon, A., Lutz, J., Reiser, M., 2008. Prediction of the fracture load of whole proximal femur specimens by topological analysis of the mineral distribution in DXA-scan images. *Bone* 43 (5), 826–831.
- Carter, D.R., Hayes, W.C., 1977. The compressive behavior of bone as a two-phase porous structure. *J. Bone Jt. Surg.* 59 (7), 954–962.
- Chakravarty, A.B., Martinez, A.A., Quenneville, C.E., 2017. The injury tolerance of the tibia under off-Axis impact loading. *Ann. Biomed. Eng.* 45 (6), 1534–1542.
- Chappard, C., Bousson, V., Bergot, C., Mitton, D., Marchadier, A., Moser, T., Benhamou, C.L., Laredo, J.D., 2010. Prediction of femoral fracture load: cross-sectional study of texture analysis and geometric measurements on plain radiographs versus bone mineral density. *Radiology* 255 (2), 536–543. <https://doi.org/10.1148/radiol.10090232>.
- Courtney, A.C., Wachtel, E.F., Myers, E.R., Hayes, W.C., 1994. Effects of loading rate on strength of the proximal femur. *Calcif. Tissue Int.* 55 (1), 53–58.
- Dall'Ara, E., Eastell, R., Viceconti, M., Pahr, D., Yang, L., 2016. Experimental validation of DXA-based finite element models for prediction of femoral strength. *J. Mech. Behav. Biomed. Mater.* 63 (Oct), 17–25.
- Dall'Ara, E., Luisier, B., Schmidt, R., Kainberger, F., Zysset, P., Pahr, D., 2013. A nonlinear QCT-based finite element model validation study for the human femur tested in two configurations in vitro. *Bone* 52 (1), 27–38.
- Derix, L.C., Vis, R., Meinders, T., Verdonschot, N., Tanck, E., 2011. Implementation of asymmetric yielding in case-specific finite element models improves the prediction of femoral fractures. *Comput. Methods Biomech. Biomed. Eng.* 14 (2), 183–193.
- Dragomir-Daescu, D., Op Den Buijs, J., McEligot, S., Dai, Y., Entwistle, R.C., Salas, C., Melton III, L.J., Bennet, K.E., Khoola, S., Amin, S., 2011. Robust QCT/FEA models of proximal femur stiffness and fracture load during a sideways fall on the hip. *Ann. Biomed. Eng.* 39 (2) <https://doi.org/10.1007/s10439-01010196-y>.
- Duchemin, L., Mitton, D., Jolivet, E., Bousson, V., Laredo, J., Skalli, W., 2008. An anatomical subject-specific FE-model for hip fracture load prediction. *Comput. Methods Progr. Biomed.* 11 (2), 105–111.
- Enns-Bray, W.S., Ferguson, S.J., Helgason, B., 2018. Strain rate dependency of bovine trabecular bone under impact loading at sideways fall velocity. *J. Biomech.* 75, 46–52. <https://doi.org/10.1016/j.jbiomech.2018.04.042>.
- Feldman, F., Robinovitch, S.N., 2007. Reducing hip fracture risk during sideways falls: evidence in young adults of the protective effects of impact to the hands and stepping. *J. Biomech.* 40 (12), 2612–2618.
- Flepe, I., Vuille, M., Melnyk, A., Ferguson, S.J., Guy, P., Helgason, B., Crompton, P.A., 2018. A novel sideways fall simulator to study hip fractures ex vivo. *PLoS One* 13 (7), e0201096.
- Gilchrist, S., Guy, P., Crompton, P.A., 2013. Development of an inertia-driven model of sideways fall for detailed study of femur fracture mechanics. *J. Biomech. Eng.* 135 (12), 121001. <https://doi.org/10.1115/1.4025390>.
- Gilchrist, S., Nishiyama, K.K., de Bakker, P., Guy, P., Boyd, S.K., Oxland, T., Crompton, P.A., 2014. Proximal femur elastic behaviour is the same in impact and constant displacement rate fall simulation. *J. Biomech.* 47 (15), 3744–3749.
- Johnell, O., Kanis, J.A., Oden, A., Johansson, H., De Laet, C., Delmas, P., Eisman, J.A., Fujiwara, S., Kroger, H., Mellstrom, D., Meunier, P.J., Melton III, L.J., O'Neill, T., Pols, H., Reeve, J., Silman, A., Tenenhouse, A., 2005. Predictive value of BMD for hip and other fractures. *J. Bone Miner. Res.* 20 (7), 1185–1194.
- Kannus, P., Lepponen, P., Parkkari, J., Palvanen, M., Jarvinen, M., 2006. A sideways fall and hip fracture. *Bone* 39 (2), 383–384.
- Keyak, J.H., 2000. Relationships between femoral fracture loads for two load configurations. *J. Biomech.* 33 (4), 499–502.
- Keyak, J.H., 2001. Improved prediction of proximal femoral fracture load using nonlinear finite element models. *Med. Eng. Phys.* 23 (3), 165–173.
- Koivumäki, J.E., Thevenot, J., Pulkkinen, P., Kuhn, V., Link, T.M., Eckstein, F., Jämsä, T., 2012. Ct-based finite element models can be used to estimate experimentally measured failure loads in the proximal femur. *Bone* 50 (4), 824–829.
- Laing, A.C., Robinovitch, S.N., 2008. The force attenuation provided by hip protectors depends on impact velocity, pelvic size, and soft tissue stiffness. *J. Biomech. Eng.* 130 (6) <https://doi.org/10.1115/1.1112979867>.
- Leichter, I.S., Simkin, A., Neeman, V., Jabochinsky, C., Schoenfeld, D., Foldes, A.J., Liebergall, M., 2001. Optical processing of radiographic trabecular pattern versus bone mineral density of proximal femur as measures of bone strength. *J. Clin. Densitometry* 4 (2), 121–129.
- Linde, F., Norgaard, P., Hvid, I., Odgaard, A., Soballe, K., 1991. Mechanical properties of trabecular bone. Dependency on strain rate. *J. Biomech.* 24 (9), 803–809. [https://doi.org/10.1016/0021-9290\(91\)90305-7](https://doi.org/10.1016/0021-9290(91)90305-7).
- Martinez, A.A., Chakravarty, A.B., Quenneville, C.E., 2018. The effect of impact duration on the axial fracture tolerance of the isolated tibia during automotive and military impacts. *J. Mech. Behav. Biomed. Mater.* 78, 315–320.
- Mears, S.C., Kates, S.L., 2015. A guide to improving the care of patients with fragility fractures, edition 2. *Geriatr. Orthop. Surg. Rehabil.* 6 (2), 58–120. <https://doi.org/10.1177/2151458515572697>.
- Meinberg, E.G., Agel, J., Roberts, C.S., Karam, M.D., Kellam, J.F., 2018. Fracture and dislocation classification compendium-2018. *J. Orthop. Trauma* 32 (Suppl. 1), S1–S170. <https://doi.org/10.1097/BOT.0000000000001063>.
- Nielson, C.M., Bouxsein, M.L., Freitas, S.S., Ensrud, K.E., Orwoll, E.S., Osteoporotic Fractures in Men (MrOS) Research Group, 2009. Trochanteric soft tissue thickness and hip fracture in older men. *J. Clin. Endocrinol. Metab.* 94 (2), 491–496.
- Nikander, R., Sievanen, H., Heinonen, A., Daly, R.M., Uusi-Rasi, K., Kannus, P., 2010. Targeted exercise against osteoporosis: a systematic review and meta-analysis for optimizing bone strength throughout life. *BMC Med.* 8, 47. <https://doi.org/10.1186/1741-7015-8-47>.
- Parkkari, J., Kannus, P., Palvanen, M., Natri, A., Vainio, J., Aho, H., Vuori, I., Jarvinen, M., 1999. Majority of hip fractures occur as a result of a fall and impact on the greater trochanter of the femur: a prospective controlled hip fracture study with 206 consecutive patients. *Calcif. Tissue Int.* 65 (3), 183–187.
- Prot, M., Cloete, T.J., Saletti, D., Laporte, S., 2016. The behavior of cancellous bone from quasi-static to dynamic strain rates with emphasis on the intermediate regime. *J. Biomech.* 49 (7), 1050–1057. <https://doi.org/10.1016/j.jbiomech.2016.02.021>.
- Roberts, B.J., Thrall, E., Muller, J.A., Bouxsein, M.L., 2010. Comparison of hip fracture risk prediction by femoral aBMD to experimentally measured factor of risk. *Bone* 46 (3), 742–746.
- van den Kroonenberg, A.J., Hayes, W.C., McMahon, T.A., 1996. Hip impact velocities and body configurations for voluntary falls from standing height. *J. Biomech.* 29 (6), 807–811.
- Villette, C.C., Phillips, A.T.M., 2018. Rate and age-dependent damage elasticity formulation for efficient hip fracture simulations. *Med. Eng. Phys.* 61, 1–12. <https://doi.org/10.1016/j.medengphy.2018.07.016>.
- Wakao, N., Harada, A., Matsui, Y., Takemura, M., Shimokata, H., Mizuno, M., Ito, M., Matsuyama, Y., Ishiguro, N., 2009. The effect of impact direction on the fracture load of osteoporotic proximal femur. *Med. Eng. Phys.* 31 (9), 1134–1139.
- Wei, T.S., Hu, C.H., Wang, S.H., Hwang, K.L., 2001. Fall characteristics, functional mobility and bone mineral density as risk factors of hip fracture in the community-dwelling ambulatory elderly. *Osteoporos. Int.* 12 (12), 1050–1055.
- Yang, L., Palermo, L., Black, D.M., Eastell, R., 2014. Prediction of incident hip fracture with the estimated femoral strength by finite element analysis of DXA Scans in the study of osteoporotic fractures. *J. Bone Miner. Res.* 29 (12), 2594–2600.
- Yang, X.J., Sang, H.X., Bai, B., Ma, X.Y., Xu, C., Lei, W., Zhang, Y., 2018. Ex vivo evaluation of hip fracture risk by proximal femur geometry and bone mineral density in elderly Chinese women. *Med. Sci. Monit.* 24, 7438–7443. <https://doi.org/10.12659/MSM.910876>.
- Zani, L., Erani, P., Grassi, L., Taddei, F., Cristofolini, L., 2015. Strain distribution in the proximal Human femur during in vitro simulated sideways fall. *J. Biomech.* 48 (10), 2130–2143. <https://doi.org/10.1016/j.jbiomech.2015.02.022>.

## **CHAPTER 3 - Enhancing Hip Fracture Risk Prediction by Statistical Modeling and Texture Analysis on DXA Images**

---

*Overview: In this chapter, 2D SSAM and texture analysis were applied to the DXA scans of the cadaveric femurs to investigate whether these techniques can improve the hip fracture risk estimation to assess Objective 2. This chapter has been published in the Journal of Medical Engineering and Physics (2020, V78, Pages 14-20, DOI: 10.1016/j.medengphy.2020.01.015). The proper permission from the copyright holder (Elsevier Ltd.) has been obtained to include the article in this thesis.*



## Enhancing hip fracture risk prediction by statistical modeling and texture analysis on DXA images



Fatemeh Jazinizadeh<sup>a</sup>, Cheryl E. Quenneville<sup>a,b,\*</sup>

<sup>a</sup>Department of Mechanical Engineering, McMaster University, 1280 Main St. West, Hamilton, Ontario L8S 4L8, Canada

<sup>b</sup>School of Biomedical Engineering, McMaster University, Hamilton, Ontario, Canada

### ARTICLE INFO

#### Article history:

Received 24 September 2019

Revised 14 January 2020

Accepted 26 January 2020

#### Keywords:

Hip fracture risk

DXA scan

Statistical shape and appearance modeling

Bone mineral density

Osteoporosis

### ABSTRACT

Each year in the US more than 300,000 older adults suffer from hip fractures. While protective measures exist, identification of those at greatest risk by DXA scanning has proved inadequate. This study proposed a new technique to enhance hip fracture risk prediction by accounting for many contributing factors to the strength of the proximal femur.

Twenty-two isolated cadaveric femurs were DXA scanned, 16 of which had been mechanically tested to failure. A function consisting of the calculated modes from the statistical shape and appearance modeling (to consider the shape and BMD distribution), homogeneity index (representing trabecular quality), BMD, age and sex of the donor was created in a training set and used to predict the fracture load in a test group. To classify patients as “high risk” or “low risk”, fracture load thresholds were investigated.

Hip fracture load estimation was significantly enhanced using the new technique in comparison to using t-score or BMD alone (average  $R^2$  of 0.68, 0.32, and 0.50, respectively) ( $P < 0.05$ ). Using a fracture cut-off of 3400 N correctly predicted risk in 94% of specimens, a substantial improvement over t-score classification (38%). Ultimately, by identifying patients at high risk more accurately, devastating hip fractures can be prevented through applying protective measures.

© 2020 IPPEM. Published by Elsevier Ltd. All rights reserved.

### 1. Introduction

Osteoporosis is a disease that is characterized by a reduction in bone density, resulting in an increased risk of fragility fractures. The incidence of osteoporosis is likely to grow drastically in the coming years due to the aging population. Hip fractures have a significant impact on mobility and function, and they are not only associated with pain and reduced quality of life for the patients, but also are responsible for high health care costs [1]. As such, it is crucial to prevent these fractures through early diagnosis and by implementing preventive measures such as hip protectors and pharmaceutical interventions.

In clinical practice, diagnosis of osteoporosis and correspondingly hip fracture risk is done based on the assessment of Bone Mineral Density (BMD) using a Dual Energy X-ray Absorptiometry (DXA) scan [2,3]. However, studies suggest that BMD measurement alone is not sufficient to predict an impending hip fracture [3–5], and there is a substantial overlap between the BMD of patients who have suffered a hip fracture and those who have not [6]. Nu-

merical tools such as Finite Element Analysis (FEA) and hip structural analysis have been increasingly used to enhance the prediction of fracture risk in the femur [7–10]. Studies have shown that 3D Quantitative Computed Tomography (QCT)-based, and Magnetic Resonance Imaging (MRI)-guided subject-specific FEA predictions of the proximal femur fracture loads were highly correlated with the measured ones [10–14]; however, due to the cost, high dose of radiation, and inaccessibility, clinical implementation of CT-based FEA is disputed and it is likely that DXA scans will remain as the primary imaging technique in osteoporosis clinics [5]. Therefore, to find more accessible methods that would be compatible with the current clinical gold standard, image processing techniques have recently been used to extract more information from DXA images.

In some recent studies, the effects of trabecular network quality [15–17], geometry [18–20], and BMD distribution [21,22] on the strength of the femur have been investigated. Texture analysis has been used as an indirect measurement of trabecular quality in medical images [23–25]. Due to the complex structure of femurs, characterizing the effect of geometry and BMD distribution on bone fracture risk estimation is complicated. Statistical Shape and Appearance Modeling (SSAM) is an image processing technique that uses Principal Component Analysis (PCA) to reduce dimensionality of contributing variables and has been used to

\* Corresponding author at: Department of Mechanical Engineering, McMaster University, 1280 Main St. West, Hamilton, Ontario L8S 4L8, Canada.

E-mail address: [quennev@mcmaster.ca](mailto:quennev@mcmaster.ca) (C.E. Quenneville).

<https://doi.org/10.1016/j.medengphy.2020.01.015>

1350-4533/© 2020 IPPEM. Published by Elsevier Ltd. All rights reserved.

either create a 3D FE model of a bone [26] or predict fracture risk based on the calculated eigenvalues, also known as modes [27,28]. Studies have also shown that in addition to the known mechanical and material factors, age and sex also play an important role in the probability of sustaining a hip fracture [29,30].

To the best knowledge of the authors, no study has considered all contributing factors together to predict the strength and consequently the fracture risk of an individual's proximal femur. The goals of the present study were to (1) construct a 2D SSAM of the proximal femur based on a training set of DXA scans and evaluate its accuracy in reconstructing the shape and BMD distribution of femurs in a test group, and (2) use the model to predict the fracture load for each femur in the test group and compare it to the measured one from previous experimental tests.

## 2. Materials and methods

This research was approved by the Hamilton Integrated Research Ethics Board (HiREB). Twenty-two (22) fresh-frozen human cadaveric femurs (eight male and 14 female,  $68.5 \pm 13.4$  years old) were cleaned of all soft tissues and scanned with a Hologic DXA scanner (Hologic Discovery A, Hologic, Inc., MA, USA). A water container filled with 15 cm of water was placed over the bone to represent the x-ray attenuation by the soft tissue [31]. Of the 22 femurs, 16 had been tested experimentally to failure under quasi-static conditions simulating a sideways fall [32]. The other six femurs were used for a separate study, and therefore only their scans were available for the current work.

### 2.1. Making the SSAM

To describe the shape and BMD distribution of the proximal femur numerically, fourteen DXA scans were chosen to create a training set, which was used to build an average model, also known as the template model, using MATLAB (R2017b, The MathWorks, Inc., MA, USA). For each subsequent DXA scan, the shape and BMD distribution would then be described based on its variation from the template model (Fig. 2). The training set consisted of eight of the experimentally tested femurs scans (randomly selected) and the six non-tested scans ( $N = 14$ ). To create the template model, a series of anatomical and geometrical landmarks (Fig. 1) on the perimeter of the bone were assigned to each of the scans in the training set. Procrustes Analysis (PA) was used to align the data and remove any effect of translation, rotation, and scaling. The first shape in the training set was used as the reference shape and all other shapes were superimposed to the reference image by (1) translating the center (average of the landmarks) of the shape to the center of the reference shape, (2) scaling the shape so that the root mean square distance (RMSD) of the landmarks from the center of the translated shape was equal to the RMSD of the reference shape, and (3) rotating the shape so that the difference between the shape's landmarks and the landmarks in the reference shape was minimized. The average of each landmark location across the training set was then calculated and used as the mean model. Next, the (x), and (y) coordinates of all landmarks for all DXA scans in the training set were gathered into a matrix and PCA was applied to find the main variations in describing the geometry of the femur.

To find the main variations in BMD distribution, each shape in the training set was warped to the mean model through mapping its landmarks to the mean shape's landmarks. For each warped image, the intensity of the pixels inside the femur's geometry was obtained and normalized to the average and the standard deviation of all pixels for that individual's scan. The average of the normalized BMD values across the training set was calculated as the mean BMD distribution model, and then PCA was applied on the matrix

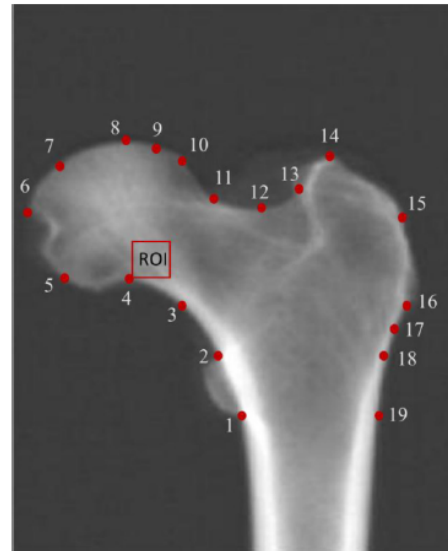


Fig. 1. The location of the landmarks and region of interest (to calculate HI), nineteen landmarks were used, some of which were anatomical (Landmark 1, 2, 4, 6, 8, 10, 12, 14, 16, 18, and 19) and the rest were geometrical (locating at the mid-point of two anatomical landmarks).

containing all normalized pixel intensity vectors in the training set to find the main variations in describing the BMD distribution.

To combine the geometry and the BMD distribution models, the geometry and BMD distribution eigenvalues for the femurs in the training set were put together in a matrix and the average for each mode (eigenvalue) was calculated (average of modes), and subsequently, PCA was applied to the matrix of modes to find the eigenvectors in the combined model.

Homogeneity Index (HI) was used to analyze the trabecular quality in the proximal femurs. The details about the texture analysis and calculating HI can be found in the works of Thevenot et al. [23,25]. The principal compression system, located at the femoral neck (Fig. 1), was used as the Region of Interest (ROI) due to its vulnerability in the sideways fall condition. After selecting the ROI of  $100 \times 100$  pixels, the noise was removed from the image by median filtering and it was rotated to the main orientation of the trabecula. To obtain the Gray Level Co-occurrence Matrix (GLCM), a representation of the co-occurred grayscale values at a certain direction and offset, first the Laplacian of the image perpendicular to the main orientation of the trabecular was calculated, and then the GLCM in the same direction was determined. At the end, the HI was assessed from the GLCM matrix.

### 2.2. Method evaluation

Each new DXA image was described based on the template model plus any variation from it based on the specific eigenvalues of that scan. To do so, first, the same landmarks were assigned to the femur's shape in the DXA scan. Landmarks were aligned with the mean geometry model using PA, and then the femur shape was warped to the template shape and pixel intensities from the warped model were obtained and normalized. The template model was then changed by its mode to match the new image, and by minimizing the difference between the adjusted template model and the landmark locations in the new image. In the next step, the BMD distribution template model was changed to match the BMD

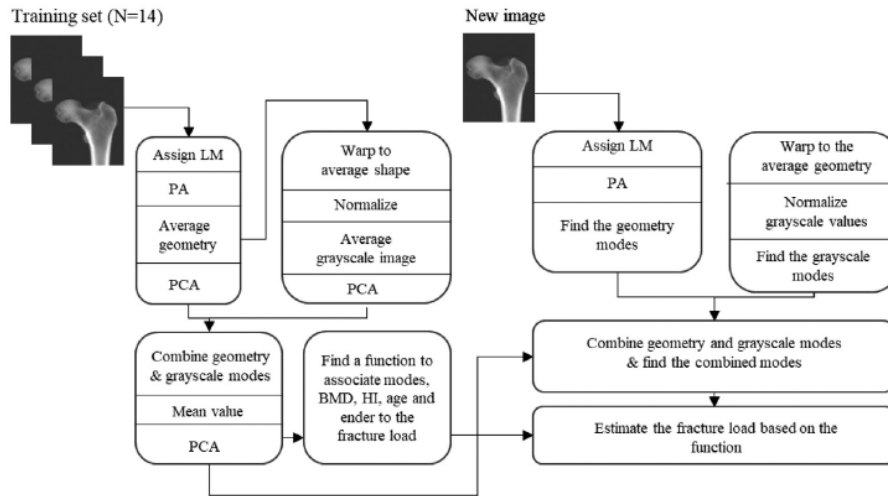


Fig. 2. Flowchart of creating the template model from the training set and adjusting it to describe a new shape in the test group, LM: Landmarks, PA: Procrustes Analysis, PCA: Principal Component Analysis.

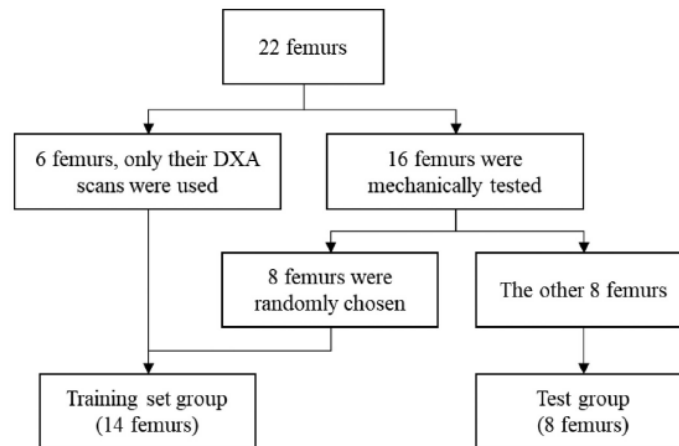


Fig. 3. Flowchart showing training set and test group selection.

map of the image and the BMD modes were calculated. The computed geometry and BMD modes were gathered in a new vector, and the average combined modes were changed to match the new input and the modes for the combined model were determined.

Of the 14 femurs in the training set, only eight of them had fracture force data available and as such this subset was used to determine the coefficients combining the various factors (modes, BMD, HI, age, and sex) through optimization to minimize the difference between the predicted and measured fracture load. After finding the coefficients, the function was used to predict the fracture load in the test group ( $N = 8$ ).

Due to the small number of specimens in the present study, ten training sets were created to make sure that the bones selected in the training set would not affect the results. Each training set consisted of eight randomly selected DXA scans from the "16 mechanically tested group", plus all six DXA scans from the group with only their DXA scans available. The remaining eight femurs

were then assigned to the test group, and their fracture loads were predicted based on the previously described method (Fig. 3). Also, in each test group, the standard clinical metric of total BMD was plotted against the experimental fracture load to create a baseline for comparison with the new method's predictions. The coefficient of determination ( $R^2$ ) was calculated for each of these methods (new technique and BMD vs. the measured fracture load) over the ten test groups, and a student  $t$ -test at a significant level of  $\alpha = 0.05$  was used to identify any differences between them.

In order to be used as a discriminating tool to classify patients as "high risk" or "low risk", two fracture thresholds were tested, at 3000 N and 3400 N. For each specimen, the predicted fracture forces from all test groups were averaged (to minimize the effect of training set selection) and then assigned accordingly. This classification was also performed using the experimentally-measured fracture forces as well as  $t$ -score (where  $-2.5$  was used as the threshold).

**Table 1**  
Specimen characteristics.

Specimen number	Sex	Age	BMD (Mg/cm <sup>2</sup> )	T-score	Fracture load (N)
1	F	57	933	-0.1	3368
2	F	69	789	-1.3	2635
3	F	65	953	0.1	2390
4	F	70	821	-1.0	3114
5	M	61	789	-1.6	2920
6	F	53	857	-0.7	3310
7	M	67	919	-0.8	4582
8	F	73	844	-0.8	2744
9	M	70	1101	0.4	4584
10	M	72	898	-0.9	2703
11	M	47	989	-0.3	4384
12	F	61	724	-1.8	3279
13	M	44	868	-1.1	4433
14	M	70	965	-0.5	3403
15	F	70	661	-2.1	2258
16	M	62	1026	0.1	4731
17	F	94	544	-3.3	N/A
18	F	80	680	-2.1	N/A
19	F	76	559	-3.1	N/A
20	F	99	627	-2.6	N/A
21	F	85	684	-2.1	N/A
22	F	61	745	-1.6	N/A

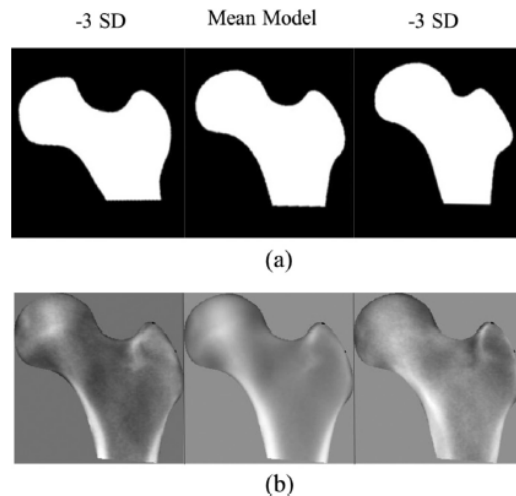


**Fig. 4.** Demonstration of the first geometry modes (on the top), and BMD distribution (on the bottom).

### 3. Results

The average BMD value and fracture loads for the 16 mechanically tested femurs were  $884 \pm 114$  mg/cm<sup>2</sup> and  $3427 \pm 846$  N (Table 1). The average BMD value for the eight non-tested femurs was  $639 \pm 78$  mg/cm<sup>2</sup>. The correlation of determination between the measured fracture loads and BMD and age were  $R^2 = 0.42$  and  $R^2 = 0.20$ , respectively.

Eleven (11) modes of variation were identified to account for more than 95% of variations in describing shape and BMD distribution of the proximal femur, and the first three modes were responsible for more than 60% of the variations. The first mode of geometry described the variations in both the length of the femoral neck as well as its angle with the shaft (Fig. 4a). The first mode for the BMD distribution was responsible for describing how much

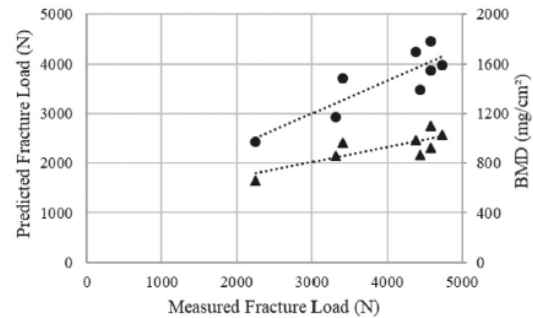


**Fig. 5.** The relationship between BMD and predicted fracture loads with the measured ones from the experimental test for a representative test group, where circles show the new technique's predictions and triangles show the BMD-based predictions.

BMD was distributed centrally vs. near the borders of the proximal femur in the neck, trochanteric and subtrochanteric areas (Fig. 4b).

The errors in reconstruction of the proximal femur shape and BMD distribution (which was measured from the gray value of each pixel) showed an average of 4.25 mm and 0.12% in the gray value, respectively. The lowest error in geometric reconstruction was associated with the geometry of the femoral neck, while the highest error was found in the femoral head and subtrochanteric areas (range: 2.22–6.69 mm). The calculated HI for all specimens ranged between 0.72 and 0.82, with an average of 0.78.

The predicted fracture loads correlated well with the experimental ones (Fig. 5). Depending on which specimens were included in the training set, this achieved an average  $R^2$  of 0.68 (range: 0.55–0.82). In all but one of the training sets, this was superior to the  $R^2$  from BMD measurements alone (average of 0.50, range: 0.21–0.71,  $p = 0.01$ ). Comparing the results with the t-score, in all groups, the predictions from the new method were better correlated than the t-score (average  $R^2$  of 0.32, range: 0.01–0.55).

When the femurs were classified into two groups of high and low fracture risk, with a 3000 N cut-off value, both the new technique and the clinical standard (threshold t-score of  $-2.5$ ) were able to “correctly” classify fracture risks with 62.5% accuracy (verified using the experimental fracture force data). However, when examining the specimens that were incorrectly classified, fracture risk underestimation (where a patient at high risk is incorrectly classified as low risk), occurred in 38% of the clinical standard technique, versus only 19% in the new technique.

Using 3400 N value as the cut-off point led to 94% accuracy in classification of the fracture risk by the new technique, with 0% overestimation and 6% underestimation of the fracture risk, whereas the t-score yielded only 37.5% accuracy in classification of fracture risk (0% fracture risk overestimation and 62.5% underestimation, Fig. 6).

### 4. Discussion

Research has shown that the strength of the proximal femur depends on its shape [33,34], BMD distribution [35], trabecular quality [24], age [36], and sex [29], while the clinical gold standard to estimate fracture risk in older adults only relies on the average measurement of BMD in the proximal femur. As shown in the current study this can cause an error in misidentifying these vulnerable patients at high risk, and more comprehensive techniques are required to better identify patients most in need of protective interventions. To the best of the authors' knowledge, this is the

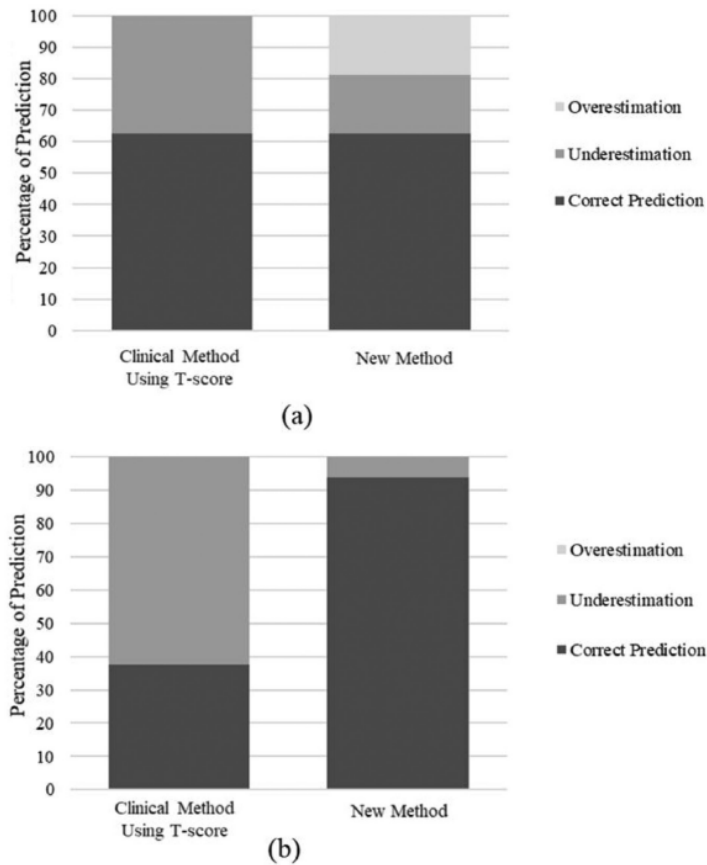


Fig. 6. Comparison of the new method and currently used method in clinical practice in their ability to predict the impending fracture based on the suggested cut-off value of 3000 N (a), and 3400 N (b), fracture risk overestimation refers to treating a patient at low risk of fracture and fracture risk underestimation refers to missing a patient at a high risk.

first study that considers the role of all these contributing factors in fracture risk prediction from a single DXA scan.

The results of this study suggested that by using the new technique both hip fracture load and fracture risk prediction were improved compared to using BMD value and the t-score alone, which was expected due to considering more contributing factors that have an effect on proximal femurs strength. It is worth noting that all these contributing factors were used in a function to estimate the fracture load. So, in the analysis of the results (measured fracture loads vs. estimated fracture loads, and BMD vs. measured fracture load graphs) only linear regression analysis was used and not multiple regression analysis (due to having only one predictor).

For describing the shape and BMD distribution of the proximal femur based on the template model, 95% of the variations were accounted for by having 11 modes. To account for 99% of variations, two more modes would be required, and the results from adding these two modes to the group one analysis did not improve the errors in BMD distribution and shape by more than 5%. So, accounting for 95% of variations was considered sufficient and was used for the rest of the analysis.

To ensure the inclusion of most of the population variations in the proximal femur's features in the template model, the size of the training set should be big enough. This number in similar

previous studies has been between 34 and 111 [26,37]. In the present study, the size of the training set was 22; however, even with the limited training set, significant improvement was found, and better performance is anticipated in the future by increasing the training set.

To decrease the influence of the femurs selected for the training set, ten different training sets were created by randomly choosing from the tested specimens. This approach was used to address the limited size of the training set and to investigate how much variation in the predictions might happen in case of using different template models. It should be noted that six of the scans were constant in all of the training sets, which may have skewed the data in either a positive or negative way.

On average the fracture load of each experimentally-tested specimen was predicted five times (across the ten training sets). The standard deviation of the predictions for each femur ranged from 54 to 333 N, with an average of 183 N. Considering that the average measured fracture load was 3427 N, this corresponds to a 5% coefficient of variation. This suggests that the predicted forces were relatively insensitive to the scans used in the training set. In the only group where the  $R^2$  of the new method predictions was slightly less than the BMD prediction ( $R^2 = 0.55$  vs.  $R^2 = 0.59$ ), the specimens in the training set were from a generally weaker

population. This could have led to a non uniformly distributed training set and affected both the template model and the fracture load prediction function. Moving forward, having a big and comprehensive training set will minimize these effects.

In the predicted vs. measured fracture loads graphs, for the new technique, the average slope and intercept of the linear regression line were  $1.06 \pm 0.20$  and  $512 \pm 307$  across the ten groups. These values in the BMD vs. measured fracture load graphs were much higher ( $5.29 \pm 0.75$ , and  $1265 \pm 667$  respectively). A slope of one in the linear regression means that the predictions are a close representation of reality and any changes in the measured fracture loads will be appropriately reflected in the predicted ones; however, the average intercept of 512 N indicated that there was a systematic error in the new technique that should be addressed.

When assessing a patient, predicting the exact fracture load is likely not as important to a clinician as classifying their fracture risk properly into high and low levels. For this reason, two cut-off values of 3000 N [38] and 3400 N (selected in the present study to investigate an alternate threshold) were used as potential criteria to draw a line between high and low fracture risk. The results showed that when using 3000 N as the cut-off value, the new technique and the clinical practice gold standard of using the t-score of  $-2.5$  predicted the fracture risk with the same accuracy. However, the rate of fracture risk underestimation was higher in the clinical method than the new technique. Underestimation, which falsely classifies a patient as being safe from sustaining a fracture, is a bigger health threat than overestimation, and in this study, all of the high fracture risk specimens were misdiagnosed when using the t-score index (37.5% of the all predictions), whereas the new technique reduced this error to 19%. This agrees with other studies that have indicated that a majority of hip fractures occur in people with non-osteoporotic DXA scans [39–41]. Still, having 19% fracture risk underestimation means that one in five patients will be missed, so there remains room for improvement to reduce the rate of hip fractures through early diagnosis.

When using a new cut-off limit (3400 N), the number of accurate hip fracture risk assessments was as high as 94% with only one misdiagnosis in 16 cases, whereas using t-score suggested that 10 of the subjects were safe while they were actually at high risk of fracture (62.5% of all predictions). This illustrates the sensitivity of classification methods to the thresholds selected; however, in both cases (3000 N and 3400 N thresholds) the rate of fracture risk underestimation was much lower by using the new technique. To determine the optimal limit for fracture risk classification more studies should be conducted on a larger cohort.

This study had some limitations; first, the number of specimens used to build the training set (14 femurs), and test the prediction (eight femurs), was limited; however, by creating ten groups and comparing and averaging the results among them, the influence of specimens used in the training set was reduced. Another limitation of this study was the use of Hologic DXA scans for calculating the HI. Since the DXA scan file from a Hologic scanner does not provide a separate digital image to be used by other software, the images had to be opened by the Hologic software (Hologic APEX v3.4.2. Hologic, Inc., MA, USA) and then the image on the screen was saved and used for further analysis. Therefore, preparing the Hologic scans for processing induced some noise that could have been prevented. In the end, the present work was an *ex-vivo* study, and many contributing factors to a real-life fracture (e.g., trochanteric soft tissue thickness, lifestyle, weight, height, and etc.) were not included. Also, due to the inter and intra technician's inconsistency and variability in patient positioning, DXA scanning of real patients is associated with more sources of errors. Future steps are planned to investigate the capability of this technique to estimate hip fracture risk involving real patients.

In this research, a novel technique to include many of the contributing factors to the proximal femurs' integrity in the estimation of the hip fracture risk was presented and the preliminary results were evaluated by comparing results to the *ex-vivo* mechanical tests on the human cadaveric femur. The results indicated that a significant improvement can be made in fracture risk prediction based on the proposed technique, which could decrease the hip fracture rate through early diagnosis and interventions for the most vulnerable in the population.

#### Declaration of Competing Interest

No conflicts of interest exist. No benefits in any form have been or will be received from a commercial party related directly or indirectly to the subject of this manuscript [40].

#### Acknowledgments

This work was supported by the Labarge Optimal Aging Initiative. The authors would like to thank Chantal Saab for help in DXA scanning of the specimens.

#### References

- Orive M, Aguirre U, García-Gutiérrez S, Las Hayas C, Bilbao A, González N, et al. Changes in health-related quality of life and activities of daily living after hip fracture because of a fall in elderly patients: a prospective cohort study. *Int J Clin Pract* 2015. doi:10.1111/ijcp.12527.
- Golob AL, Laya MB. Osteoporosis: screening, prevention, and management. *Med Clin North Am* 2015;99:587–606. doi:10.1016/j.mcna.2015.01.010.
- Kanis JA. Osteoporosis III: diagnosis of osteoporosis and assessment of fracture risk. *Lancet* 2002. doi:10.1016/S0140-6736(02)08761-5.
- Goodyear SR, Barr RJ, McCloskey E, Alessi S, Aspden RM, Reid DM, et al. Can we improve the prediction of hip fracture by assessing bone structure using shape and appearance modelling? *Bone* 2013;53:188–93. doi:10.1016/j.bone.2012.11.042.
- Yang L, Palermo L, Black DM, Eastell R. Prediction of incident hip fracture with the estimated femoral strength by finite element analysis of dxa scans in the study of osteoporotic fractures. *J Bone Miner Res* 2014;29:2594–600. doi:10.1002/jbmr.2291.
- Gebauer M, Stark O, Vettorazzi E, Grifka J, Püschel K, Arling M, et al. DXA and pQCT predict peritrochanteric and not femoral neck fracture load in a human side-impact fracture model. *J Orthop Res* 2014;32:31–8. doi:10.1002/jor.22478.
- Ha Y-C, Yoo J-I, Yoo J, Park KS. Effects of hip structure analysis variables on hip fracture: a propensity score matching study. *J Clin Med* 2019. doi:10.3390/jcm8101507.
- Mourtada FA, Beck TJ, Hauser DL, Ruff CB, Bao G. Curved beam model of the proximal femur for estimating stress using dual-energy x-ray absorptiometry derived structural geometry. *J Orthop Res* 1996. doi:10.1002/jor.1100140319.
- Terzini M, Aldieri A, Rinaudo L, Osella G, Audenino AL, Bignardi C. Improving the hip fracture risk prediction through 2D finite element models from dxa images: validation against 3D models. *Front Bioeng Biotechnol* 2019. doi:10.3389/fbioe.2019.00220.
- Van Den Munckhof S, Zadpoor AA. How accurately can we predict the fracture load of the proximal femur using finite element models? *Clin Biomech* 2014;29:373–80. doi:10.1016/j.clinbiomech.2013.12.018.
- Dall'Ara E, Luisier B, Schmidt R, Kainberger F, Zysset P, Pahr D. A nonlinear QCT-based finite element model validation study for the human femur tested in two configurations in vitro. *Bone* 2013. doi:10.1016/j.bone.2012.09.006.
- Haider IT, Goldak J, Frei H. Femoral fracture load and fracture pattern is accurately predicted using a gradient-enhanced quasi-brittle finite element model. *Med Eng Phys* 2018. doi:10.1016/j.medengphy.2018.02.008.
- Rajapakse CS, Hotca A, Newman BT, Ramme A, Vira S, Kobe EA, et al. Patient-specific hip fracture strength assessment with microstructural mr imaging-based finite element modeling. *Radiology* 2017. doi:10.1148/radiol.2016160874.
- Rajapakse CS, Chang G. Micro-Finite element analysis of the proximal femur on the basis of high-resolution magnetic resonance images. *Curr Osteoporos Rep* 2018. doi:10.1007/s11914-018-0481-5.
- Lespessailles E, Gadois C, Kousignian I, Neveu JP, Fardellone P, Kolta S, et al. Clinical interest of bone texture analysis in osteoporosis: a case control multicenter study. *Osteoporos Int* 2008. doi:10.1007/s00198-007-0532-8.
- Lu RS, Dennison E, Denison H, Cooper C, Taylor M, Bottema MJ. Texture analysis based on gabor filters improves the estimate of bone fracture risk from dxa images. *Comput Methods Biomech Biomed Eng Imaging Vis* 2018. doi:10.1080/21681163.2016.1271726.
- Thevenot J, Hirvasniemi J, Pulkkinen P, Määttä M, Korpelainen R, Saarakkala S, et al. Assessment of risk of femoral neck fracture with radiographic texture parameters: a retrospective study. *Radiology* 2014. doi:10.1148/radiol.14131390.

- [18] Gnudi S, Ripamonti C, Lisi L, Fini M, Giardino R, Giavaresi G. Proximal femur geometry to detect and distinguish femoral neck fractures from trochanteric fractures in postmenopausal women. *Osteoporos Int* 2002. doi:10.1007/s198-002-8340-2.
- [19] Gnudi S, Ripamonti C, Gualtieri G, Malavolta N. Geometry of proximal femur in the prediction of hip fracture in osteoporotic women. *Br J Radiol* 1999. doi:10.1259/bjr.72.860.10624337.
- [20] Gnudi S, Sitta E, Pignotti E. Prediction of incident hip fracture by femoral neck bone mineral density and neck-shaft angle: a 5-year longitudinal study in post-menopausal females. *Br J Radiol* 2012. doi:10.1259/bjr/57130600.
- [21] Yang L, Burton AC, Bradburn M, Nielson CM, Orwoll ES, Eastell R. Distribution of bone density in the proximal femur and its association with hip fracture risk in older men: the osteoporotic fractures in men (MrOS) study. *J Bone Miner Res* 2012. doi:10.1002/jbmr.1693.
- [22] Yang L, Udall WJM, McCloskey EV, Eastell R. Distribution of bone density and cortical thickness in the proximal femur and their association with hip fracture in postmenopausal women: a quantitative computed tomography study. *Osteoporos Int* 2014. doi:10.1007/s00198-013-2401-y.
- [23] Thevenot J, Hirvasniemi J, Finnilä M, Pulkkinen P, Kuhn V, Link T, et al. Trabecular homogeneity index derived from plain radiograph to evaluate bone quality. *J Bone Miner Res* 2013;28:2584–91. doi:10.1002/jbmr.1987.
- [24] Pothuaud L, Carceller P, Hans D. Correlations between grey-level variations in 2D projection images (TBS) and 3D microarchitecture: applications in the study of human trabecular bone microarchitecture. *Bone* 2008;42:775–87. doi:10.1016/j.bone.2007.11.018.
- [25] Thevenot J, Hirvasniemi J, Pulkkinen P, Määttä M, Korpelainen R, Saarakkala S, et al. Assessment of risk of femoral neck fracture with radiographic texture parameters: a retrospective study. *Radiology* 2014. doi:10.1148/radiol.14131390.
- [26] Väänänen SP, Grassi L, Flivik G, Jurvelin JS, Isaksson H. Generation of 3D shape, density, cortical thickness and finite element mesh of proximal femur from a dxa image. *Med Image Anal* 2015;24:125–34. doi:10.1016/j.media.2015.06.001.
- [27] Whitmarsh T, Fritscher KD, Humbert L, del Rio Barquero LM, Roth T, Kammerlander C, et al. Hip fracture discrimination from dual-energy X-ray absorptiometry by statistical model registration. *Bone* 2012;51:896–901. doi:10.1016/j.bone.2012.08.114.
- [28] Humbert L, Whitmarsh T, Fritscher K, Del Rio Barquero LM, Eckstein F, Link T, et al. Femoral strength prediction using a 3D reconstruction method from dual-energy X-ray absorptiometry. *Proc Int Symp Biomed Imaging* 2012:1451–4. doi:10.1109/ISBI.2012.6235844.
- [29] Lobo E, Marcos G, Santabárbara J, Salvador-Rosés H, Lobo-Escolar L, De la Cámara C, et al. Gender differences in the incidence of and risk factors for hip fracture: a 16-year longitudinal study in a southern european population. *Maturitas* 2017. doi:10.1016/j.maturitas.2016.12.009.
- [30] Marks R. Hip fracture epidemiological trends, outcomes, and risk factors, 1970–2009. *Int J Gen Med* 2010;3:1–17.
- [31] Chappard C, Bousson V, Bergot C, Mitton D, Marchadier A, Moser T, et al. Prediction of femoral fracture load: cross-sectional study of texture analysis and geometric measurements on plain radiographs versus bone mineral density. *Radiology* 2010. doi:10.1148/radiol.10090232.
- [32] Jazinizadeh F, Mohammadi H, Quenneville CE. Comparing the fracture limits of the proximal femur under impact and quasi-static conditions in simulation of a sideways fall. *J Mech Behav Biomed Mater* 2020;103 8 pages. doi:10.1016/j.jmbm.2019.103593.
- [33] Pulkkinen P, Eckstein F, Lochmüller EM, Kuhn V, Jämsä T. Association of geometric factors and failure load level with the distribution of cervical vs. trochanteric hip fractures. *J Bone Miner Res* 2006;21:895–901. doi:10.1359/jbmr.060305.
- [34] Cheng XG, Lowet G, Boonen S, Nicholson PHF, Brys P, Nijs J, et al. Assessment of the strength of proximal femur in vitro: relationship to femoral bone mineral density and femoral geometry. *Bone* 1997. doi:10.1016/S8756-3282(96)00383-3.
- [35] Boehm HF, Horng A, Notohamiprodjo M, Eckstein F, Burklein D, Panteleon A, et al. Prediction of the fracture load of whole proximal femur specimens by topological analysis of the mineral distribution in DXA-scan images. *Bone* 2008. doi:10.1016/j.bone.2008.07.244.
- [36] Ensrud KE. Epidemiology of fracture risk with advancing age. *J Gerontol Ser A Biol Sci Med Sci* 2013. doi:10.1093/gerona/glt092.
- [37] Humbert L, Martelli Y, Fonolla R, Steghofer M, Di Gregorio S, Malouf J, et al. 3D-DXA: assessing the femoral shape, the trabecular macrostructure and the cortex in 3D from dxa images. *IEEE Trans Med Imaging* 2017;36:27–39. doi:10.1109/TMI.2016.2593346.
- [38] Amin S, Kopperdhal DL, Melton LJ, Achenbach SJ, Thorneau TM, Riggs BL, et al. Association of hip strength estimates by finite-element analysis with fractures in women and men. *J Bone Miner Res* 2011. doi:10.1002/jbmr.347.
- [39] Siris ES, Chen YT, Abbott TA, Barrett-Connor E, Miller PD, Wehren LE, et al. Bone mineral density thresholds for pharmacological intervention to prevent fractures. *Arch Intern Med* 2004. doi:10.1001/archinte.164.10.1108.
- [40] Schuit SCE, Van Der Klift M, Weel AEAM, De Laet CEDH, Burger H, Seeman E, et al. Fracture incidence and association with bone mineral density in elderly men and women: the rotterdam study. *Bone* 2004. doi:10.1016/j.bone.2003.10.001.
- [41] Sornay-Rendu E, Munoz F, Garnero P, Duboeuf F, Delmas PD. Identification of osteopenic women at high risk of fracture: the ofely study. *J Bone Miner Res* 2005. doi:10.1359/JBMR.050609.

## **CHAPTER 4 - Advanced 2D Image Processing Technique to Predict Hip Fracture Risk in an Older Population Based on Single DXA Scans**

---

*Overview: To assess Objective 3, 2D SSAM was applied on the DXA scans of a group of subjects from the Canadian Multicentre Osteoporosis Study, that were monitored for at least five years with their fracture history available. This chapter has been published in the Osteoporosis International (2020, DOI: 10.1007/s00198-020-05444-7). the proper permission from the copyright holder (Springer Nature) has been obtained to include the article in this thesis.*

<https://doi.org/10.1007/s00198-020-05444-7>

ORIGINAL ARTICLE



## Advanced 2D image processing technique to predict hip fracture risk in an older population based on single DXA scans

F. Jazinizadeh<sup>1</sup> · J.D. Adachi<sup>2</sup> · C.E. Quenneville<sup>1,3</sup>

Received: 4 March 2020 / Accepted: 29 April 2020

© International Osteoporosis Foundation and National Osteoporosis Foundation 2020

### Abstract

**Summary** A new technique to enhance hip fracture risk prediction in older adults was presented and assessed. The new method dramatically improved prediction at high specificity levels using only a standard clinical diagnostic scan. This has the potential to be implemented in clinical practice to enhance patient fragility diagnosis.

**Introduction** Diagnosis of osteoporosis is based on the measurement of bone mineral density (BMD) using dual-energy X-ray absorptiometry (DXA) scans. However, studies have shown this to be insufficient to accurately predict hip fractures. Therefore, complementary methods are needed to enhance hip fracture risk prediction to identify vulnerable patients.

**Methods** Hip DXA scans were obtained for 192 subjects from the Canadian Multicenter Osteoporosis Study (CaMos), 50 of whom had experienced a hip fracture within 5 years of the scan. 2D statistical shape and appearance modeling was performed to account for the effect of the femur's geometry and BMD distribution on hip fracture risk. Statistical shape modeling (SSM), and statistical appearance modeling (SAM) were also used separately to predict the fracture risk based solely on the femur's geometry and BMD distribution, respectively. Combined with BMD, age, and body mass index (BMI), logistic regression was performed to estimate the fracture risk over the 5-year period.

**Results** Using the new technique, hip fractures were correctly predicted in 78% of cases compared with 36% when using the T-score. The accuracy of the prediction was not greatly reduced when using SSM and SAM (78% and 74% correct, respectively). Various geometric and BMD distribution traits were identified in the fractured and non-fractured groups.

**Conclusion** 2D SSAM can dramatically improve hip fracture prediction at high specificity levels and estimate the year of the impending fracture using standard clinical images. This has the potential to be implemented in clinical practice to estimate hip fracture risk.

**Keywords** DXA scan · Hip fracture risk · Image processing · Statistical shape and appearance modeling

### Introduction

Osteoporosis is a disease in older adults that is characterized by a reduction in bone density and is associated with fragility fractures [1]. With the aging population, the occurrence of

osteoporotic fractures is growing. A previous study has shown that osteoporotic fractures occur more frequently than heart attacks and strokes combined in the USA [2]. These fractures can cause disabilities, mortality, and significant healthcare expenses [3–5]. It is estimated that one in three women and one in 12 men will suffer from a hip fracture in their lifetime [6, 7], and more than 86% of these fractures occur in patients aged 65 or older [4]. Hip fractures in older adults severely affect their mobility, and often reduce independent living, with studies showing that these patients have an elevated risk of admission to assisted living facilities [8]. In addition, there is an increased mortality rate one year after the hip fracture incident [9]. Due to the primary and secondary complications from hip fractures, and with the aging population, it is important to prevent these fractures through early fracture risk assessment, which allows the implementation of protective measures. Currently,

✉ C.E. Quenneville  
quennev@mcmaster.ca

<sup>1</sup> Department of Mechanical Engineering, McMaster University, ABB-C308, 1280 Main St. West, Hamilton, Ontario L8S 4L8, Canada

<sup>2</sup> Department of Medicine, McMaster University, Hamilton, Ontario, Canada

<sup>3</sup> School of Biomedical Engineering, McMaster University, Hamilton, Ontario, Canada

the primary diagnosis of osteoporosis relies on the measurement of the bone mineral density (BMD) derived from a dual-energy X-ray absorptiometry (DXA) scan [10]. The measured BMD is normalized to the mean and standard deviation of the BMD in a young adult reference population to calculate the T-score, and based on the World Health Organization (WHO), a patient with a T-score of  $-2.5$  at the hip or spine is considered to suffer from osteoporosis [11].

Some studies have shown that using DXA scans alone is not sufficient in identifying all patients at risk of a hip fracture, and a large proportion of hip fractures occurs in women with a non-osteoporotic diagnosis based on a DXA scan [12, 13]. Therefore, it's crucial to search for complementary methods to enhance hip fracture risk prediction to identify vulnerable patients.

In addition to the DXA scan, which is an indirect measurement of bone's mechanical properties, numerous other factors have also been identified to have an effect on the patient's fracture risk. These factors (e.g., age, sex, body mass index, history of fracture, smoking, etc.) have been grouped in a widely adapted algorithm known as fracture risk assessment tool (FRAX) [14]. FRAX provides an indication of a person's 10-year risk of fracture probability, with the probability of a major osteoporotic fracture more than 20% considered to be high risk and hence pharmacologic treatment being required [11]. However, studies have shown that FRAX ability to discriminate between women who sustained a major osteoporotic fracture and who did not is suboptimal [15].

Statistical models have been widely used to numerically describe the shape and the pattern of BMD distribution in various bones through reducing the dimensionality of the variables by principal component analysis (PCA) [16–18]. Some studies have used statistical models for the proximal femur to investigate the relationship between these variables (called modes or weighting factors) and hip fracture risk by either estimating the fracture load in a cadaveric study [19] or investigating the occurrence of fractures in a patient study [20, 21]. In most of these studies, a 3D template model was built by averaging the models created from the medical images in a training set, and then the characteristics (shape and BMD distribution) of a new femur from a DXA scan were described based on their variations from the template model. The results of these studies that have implemented 3D statistical modeling suggest that using this technique can improve hip fracture risk prediction. However, while having the 3D model might be a necessity to perform further investigations like 3D finite element analysis (FEA), it's not clear whether 3D statistical models are needed to just explore the association of the modes (weighting factors) with the fracture risk since 2D statistical models can extract similar information from the DXA scan with fewer resources. Also, a previous cadaveric study has shown that 2D statistical shape and appearance modeling (SSAM) can noticeably enhance both the femur's strength

estimation and hip fracture risk prediction compared with the traditional BMD and T-score measurements [22]. In addition to statistical models, texture analysis, e.g., trabecular bone score (TBS) and homogeneity index (HI), which is an indirect measurement of the trabecula quality in microstructure level (trabecular thickness, trabecular spacing, trabecular number, and connectivity) is also another useful method that can be used to enhance hip fracture risk prediction independent of the femur's geometry and BMD distribution [23, 24].

In developing 2D statistical models, the only required system input is the hip DXA scan, while to create 3D statistical models, magnetic resonance imaging (MRI) or computed tomography (CT) scans of the proximal femur are needed to create the template model. Considering that the DXA scans are much more accessible, less expensive, and part of routine osteoporosis assessment, expanding the training set (to include more geometry and BMD distribution features in a population) in the 2D statistical models can be more attainable.

Furthermore, it is not yet well understood how a femur's geometry and its BMD distribution contribute to the predicted fracture risk. Therefore, looking separately at the capacity of each of these factors through statistical shape modeling (SSM) and statistical appearance modeling (SAM), in addition to statistical shape and appearance modeling (SSAM) can lead to valuable findings. This information can direct future studies and clinical implementation paths in the enhancement of hip fracture risk estimation in older adults.

Therefore, the aims of the present study were to (1) develop a 2D statistical model of the femur from clinical DXA scans, (2) investigate if there is a significant difference between different modes of variation in fractured and non-fractured groups, and (3) predict and compare the fracture risk for the patients based on the femur's geometry (SSM), BMD distribution (SAM), and geometry and BMD distribution together (SSAM).

## Methods

### Study population

The Canadian Multicentre Osteoporosis Study (CaMos) is a large prospective study investigating the relationship between the risk factors for osteoporosis and osteoporosis fragility fractures in the Canadian population. It encompasses more than 9400 subjects in nine centers across Canada. All subjects at the baseline had a lumbar spine and hip DXA scan and received a follow-up questionnaire annually. The subjects also had repeated scans in years 3, 5, 10 and 16. The self-report of any fragility fractures was confirmed with medical reports.

For the present study, 50 subjects (37 women,  $78 \pm 8$  years old, and 13 men,  $79 \pm 6$  years old), who sustained a hip fracture and 142 subjects (60 women  $67 \pm 9$  years old, and 82

men,  $67 \pm 10$  years old) who did not sustain a hip fracture in a 5-year period after the baseline, were randomly chosen from the participants who had a hip DXA scan at the baseline with a Hologic DXA scanner (Hologic, Inc., Marlborough, MA). The non-fractured group was chosen from the subset population that was not taking any osteoporosis medications [10]; however, most of the subjects in the fractured group were taking at least one type of medication.

### Image processing

Each hip DXA scan was examined using the three following methods: SAM, SSM, and SSAM. The main algorithm has been previously discussed [22] but will be briefly described here.

A series of landmarks were assigned to each DXA scan on the contour of the femur. By averaging the coordinates of the landmarks across the training set, a template geometry model was created, and then by applying principal component analysis (PCA), the main modes of variation in geometry were calculated (SSM model). Next, each femur's geometry was warped to the template shape, and pixels value were read, normalized, and gathered in a matrix. The average value of each pixel was calculated to create the BMD distribution template model, and then by performing PCA on the matrix containing the pixels' intensities, the main modes of variation in describing the BMD distribution were obtained (SAM model). Subsequently, geometry and BMD distribution models were combined to build the combined shape and appearance model (SSAM). To compute the weight of each mode of variation for each new scan, the same landmarks were assigned to the DXA scan, and then the shape of the femur was warped to the template shape to read the pixels' value. Next, through an optimization procedure to minimize the differences between the estimated geometry and BMD distribution with the actual DXA scan, the weights of the main modes of variation were calculated.

### Fracture risk estimation

The leave one out cross-validation method was used in this study to maximize the number of DXA scans in the training set. Therefore, to evaluate each scan, the other 191 scans were used in the training set, and then the weights of the variation modes were calculated for the scan of interest.

Logistic regression analysis was used to find the probability of sustaining a fracture based on the weights of the variation modes from SSAM, BMD, FRAX, body mass index (BMI), sex, and patients' age. The subjects with more than 50% probability of fracture were assigned to the fractured or high-risk group and the rest were assigned to the non-fractured or low-risk group.

In addition to the SSAM, weight of variation modes from SSM (considering only geometry of the femur) and SAM

(considering only BMD distribution of the femur) were used separately combined with other variables (BMD, BMI, age, sex) to investigate their ability to predict fractures in the subjects as well. Similar to SSAM, the logistic regression was used to predict the fracture risk, and based on the threshold of 50%, subjects were classified in the high- and low-risk groups. These predictions were then compared with the confirmed fractures based on the patients' history.

Also, to investigate the possibility of estimating the year of the fracture, all subjects were classified into three groups depending on the year and occurrence of the fracture, where the subjects who sustained a fracture in less than 2 years were assigned to class one, subjects who sustained a fracture between three and 5 years were assigned to group two, and subjects who did not sustain a fracture in a 5-year period were assigned to class three. For each class, the mean and the standard deviation of the estimated fracture risk (probability of fracture) from combined SSAM were calculated and compared.

A receiver operating characteristic (ROC) curve was generated to plot the rate of true positive prediction against false positive ones at various threshold settings. Therefore, this curve was used to visualize the sensitivity of each method (total hip BMD, total hip T-score, FRAX, SSAM, SSM, SAM) to its specificity. The area under the ROC curve, which illustrates the diagnostic power of each predictor as a scale of 0–1, was used to evaluate the ability of the various methods to classify patients into high and low risk.

To identify the distinctive features in geometry and BMD distribution between the fractured and non-fractured groups, SSAM was applied to all of the DXA scans (all 192 subjects in the training set). Subsequently, the differences between the weight of variation modes in the two groups were identified using a student t test at a significance level of  $\alpha = 0.05$ . The average shape and BMD distribution of the femur in the fractured and non-fractured groups were also investigated for male and female subjects. The neck-shaft angle in the shape image was measured five times in each image (fractured and non-fracture, male and female) and then averaged to account for the repeatability error.

### Results

Twenty-six modes of variation were needed to account for more than 95% of the variations in describing the shape and BMD distribution of femurs from the DXA scans. Modes one and two alone were responsible for more than 69% of the variations (Fig. 1). Comparing the modes between the fractured and non-fractured cases indicated that there was a significant difference between some of the modes (Table 1), and some features such as femoral neck-shaft angle, the outer diameter of the femur at the femoral neck, trochanter and shaft,

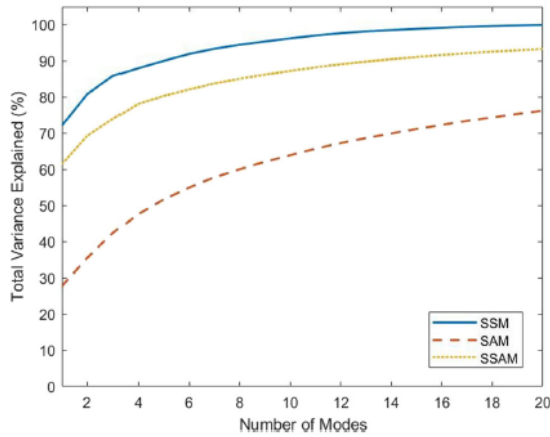


Fig. 1 The percentage of the variances explained by the number of SSAM modes used in the analysis; using 20 modes accounted for more variability in SSM than SAM or SSAM

cortical bone thickness, and BMD concentration in the trochanteric area had a noticeable impact on the vulnerability/strength of the bones (Figs. 2 and 3). The average femoral neck-shaft angle in the fractured and non-fractured groups in female were  $130.0^{\circ} \pm 0.8^{\circ}$  and  $129.0^{\circ} \pm 1.0^{\circ}$ , and in the male were  $129.3^{\circ} \pm 1.0^{\circ}$  and  $128.3^{\circ} \pm 0.6^{\circ}$ , respectively. The femurs in the non-fractured group tended to have a smaller outer diameter, thicker cortical bone in the shaft, and more BMD concentration in the trochanteric area than the fractured group.

FRAX data was only available for 175 subjects, with an average score of  $18.95\% \pm 10.62\%$  for the fractured group and  $6.79\% \pm 3.98\%$  for the non-fractured group. Using various predictors to estimate the hip fracture risk over a 5-year period showed that using combined statistical models (modes from SSAM, BMD, BMI, age, and sex) could improve the identification of the people who are at the highest risk of sustaining a hip fracture by 42% compared with using the T-score alone, and 46% compared with the FRAX (Table 2). Out of the 50 cases of fracture, the T-score of  $-2.5$  as the gold standard of clinical practice was able to correctly identify 18 (36%) fracture cases, and FRAX correctly identified 16 (32%) fracture cases, whereas, FRAX combined with SSAM and BMD

correctly identified 37 (74%) fracture cases, and combined SSAM was able to correctly identify 39 (78%) cases. Among the variables, sex and BMI did not have much of an effect on the number of correct predictions, even when the male and female subjects were investigated separately. However, considering the age of the patients increased the number of correct predictions by three cases (6%). The estimated probabilities of the fracture using combined SSAM for classes one to three were  $0.82 \pm 0.21$ ,  $0.70 \pm 0.42$ , and  $0.10 \pm 0.22$ , respectively.

Predictions of combined statistical shape models (SSM) and combined statistical appearance models (SAM) were also investigated in comparison with the combined statistical shape and appearance models (SSAM), and the results showed that using statistical shape models resulted in an approximately similar number of correct predictions (171 in SSM vs 173 and 169 in SSAM and SAM), with combined SSM correctly identifying 39 (78%) cases of the fractured group, the same as combined SSAM.

The area under the ROC curve (Fig. 4) was calculated as 0.92, 0.93, 0.91, 0.88, 0.89, and 0.90 for the SSAM, SSM, SAM, BMD, T-score, and the FRAX, respectively, with the SSM having the highest value (0.93).

### Discussion

In this study, a new technique to create 2D statistical shape models, statistical appearance models, and statistical shape and appearance models for proximal femurs were introduced and performed on the DXA scans of 192 patients, and the risk of sustaining a hip fracture in the next 5 years for these subjects was estimated. The results of this study are important since they show that while using SSAM to describe the shape and BMD distribution in the proximal femur can enhance fracture risk prediction (compared with using the T-score), the effect of the geometry of the femur alone (from SSM) is as accurate in identifying the high fracture risk cases and is more significant than BMD distribution (from SAM). Also, using the combined 2D SSAM increased the area under the

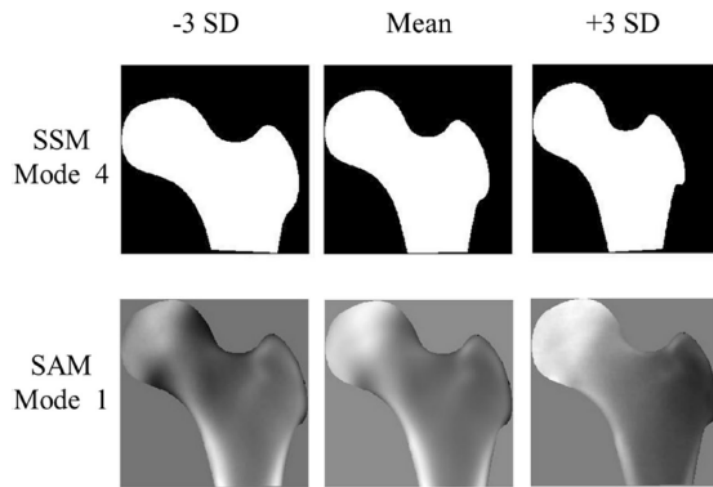
Table 1 Comparing the first ten modes by student t test between the two groups of fractured and non-fractured when using statistical shape modeling (SSM), statistical appearance modeling (SAM), and statistical shape and appearance modeling (SSAM)

p value	Modes									
	1	2	3	4	5	6	7	8	9	10
SSM	0.766	0.856	0.259	0.010*	0.508	0.357	0.510	0.099	0.008*	0.028*
SAM	0.000*	0.002*	0.059	0.205	0.141	0.002*	0.065	0.001*	0.004*	0.997
SSAM	0.774	0.400	0.544	0.001*	0.013*	0.234	0.018*	0.001*	0.000*	0.232

\*Significant difference at  $\alpha = 0.05$

## Osteoporosis Int

**Fig. 2** Graphical illustration of some of the modes that were significantly different between the fractured and non-fractured subjects; negative values in the statistical shape modeling (SSM) mode 4 and positive values in the statistical appearance modeling (SAM) mode 1 corresponded to increased fracture risk



ROC curve by 4% compared with using BMD alone, which means this could help protect thousands of Canadian from devastating injuries, when considering the 21,000–27,000 hip fractures that happen annually in Canada [25]. Considering that in this study only 2D analysis was performed, these findings can further shape the development and implementation of statistical models in clinical practice for hip fracture risk prediction while still using only the standard clinical tool (i.e., no other equipment or extra radiation).

Comparing the modes in the SSM, SAM, and SSAM revealed that some of the modes had significantly different values between the fractured and non-fractured subjects. These modes highlighted some geometric and BMD distribution differences between the two groups. For example, mode four from the SSM was significantly different between the two groups and showed that in the non-fractured cases (that had more positive values), the angle between the femoral neck and shaft tended to be higher and the femoral head diameter, neck diameter, and greater trochanter were narrower. However, two points should be considered when referring to these pictures: first, these shapes illustrate the extreme scenarios of three

standard deviations (SD) from the mean, and as such are not representative of a real-world specimen; secondly, the overall shape of the femur is the summation of all weighted modes, and should not be considered in isolation. Therefore, to address these issues, the average models in the fractured and non-fractured groups were also depicted for males and females separately. The results showed that in the fractured cases, the diameter of the femoral head, neck, and shaft was higher than non-fractured subjects, which is aligned with previous studies [26–30] that have investigated the geometric traits of fractured cases and non-fractured controls. The increased diameter could be attributed to the adaptation mechanism of the body in response to the reduced BMD since the long bones resist bending failure by the second moment of inertia (bigger diameter leads to a higher second moment of inertia) [31]. In these studies [26–30], while the outer diameter of the femur in various areas of the femoral neck, trochanter, and shaft have been shown to increase in the fractured cases, the cortical bone thickness was decreased. The same was observed in the present study and by comparing the BMD distribution figures in the fractured and non-fractured cases

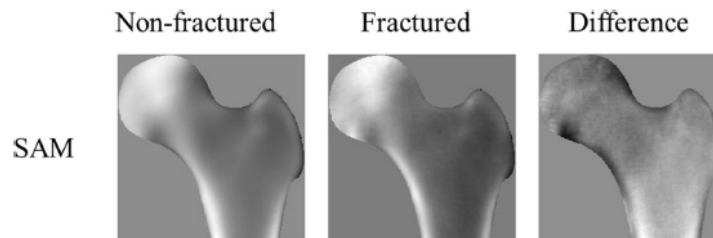


**Fig. 3** The average BMD distribution in the fractured and non-fractured groups for all subjects, as well as the differences between the two groups; the brighter pixels in the difference image, correspond to the higher

densities in the non-fractured subjects, whereas darker pixels correspond to the higher density in the fractured subjects

**Table 2** Summary of the results when using various predictors for hip fracture risk

Predictors	Number of predictions (percentage)				
	Correct fractured	Correct non-fractured	All correct predictions	Fracture risk overprediction	Fracture risk underprediction
T-score	<b>18 (36%)</b>	140 (99%)	158 (82%)	2 (1%)	32 (17%)
FRAX*	<b>16 (32%)</b>	122 (98%)	138 (79%)	3 (2%)	34 (68%)
SSAM+ BMD+ FRAX*	<b>37 (74%)</b>	118 (94%)	155 (89%)	7 (4%)	13 (7%)
SSAM+ T-score+ BMI+ Age+ Sex	<b>39 (78%)</b>	133 (94%)	172 (90%)	9 (5%)	11 (6%)
SSAM+ BMD+ BMI+ Age+ Sex	<b>39 (78%)</b>	134 (94%)	173 (90%)	8 (4%)	11 (6%)
SSAM+ BMD+ BMI+ Age	39 (78%)	134 (94%)	173 (90%)	8 (4%)	11 (6%)
SSAM+ BMD+ BMI+ Sex	37 (74%)	131 (92%)	168 (87%)	11 (6%)	13 (7%)
SSAM+ BMD+ Age+ Sex	40 (80%)	133 (94%)	173 (90%)	9 (5%)	10 (5%)
SSAM+ BMD	36 (72%)	133 (94%)	169 (88%)	9 (5%)	14 (7%)
BMD+ BMI+ Age+ Sex	36 (72%)	129 (91%)	165 (86%)	13 (7%)	14 (7%)

\*FRAX data and subsequent prediction with FRAX was only available for 175 of the subjects

The bold numbers show the number (percentage) of correct predictions by the T-score and the proposed technique

(Fig. 3). Comparing the neck-shaft angle between the fractured and non-fractured groups showed that the subjects in the fractured group tended to have a higher angle; however, there was no statistically significant difference between them. Studies by Gnudi et al. [32, 33] previously reported that the wider femoral neck-shaft angle increases the risk of a femoral neck fracture. However, another study by Ito et al. [34] did not find any significant difference in the femoral neck-shaft angle between the cases of femoral neck fracture and the controls, while the neck-shaft angle affected the risk of trochanteric fractures. These contradictory results could be because of the

effect of other variables that are difficult to eliminate in human participant studies.

Considering the BMD distribution (Fig. 3), the cortical bone thickness in the femoral shaft tended to be higher in the non-fractured groups than fractured ones, which is in agreement with previous studies [35, 36]. It should be noted that the BMD distribution images from SAM were normalized to the mean and standard deviation of each scan, and then they were averaged in the two groups (fractured and non-fractured) and depicted in Fig. 3. Therefore, these pictures purely show that if both fractured and non-fractured groups had an equal BMD, how this BMD would have been distributed. In the non-fractured group, the BMD was concentrated in the femoral shaft cortex and trochanteric area, whereas in the fractured groups the BMD was concentrated in the femoral head areas. In a DXA scan, the area in the femoral head is partially overlapped by the pelvis; therefore it could be concluded that some of the BMD concentration in the femoral head was likely influenced by the pelvis.

In addition to the BMD and weighting modes from the statistical models, other parameters such as BMI, age, and sex were also used in the logistic regression to estimate the hip fracture risk, and the results showed that using sex and BMI did not have a notable effect on the number of correct fracture predictions, whereas age played a more important role. The lack of effect of sex in the fracture risk may be attributed to the fact that it was already reflected in the shape and the BMD of the proximal femur [37, 38]. Regarding the BMI, it is a combination of a patient's weight and height, and its effect on the fracture risk could be controversial: with increasing weight, there will be more forces applied to the body during a fall [39]; however, it's more probable that the soft

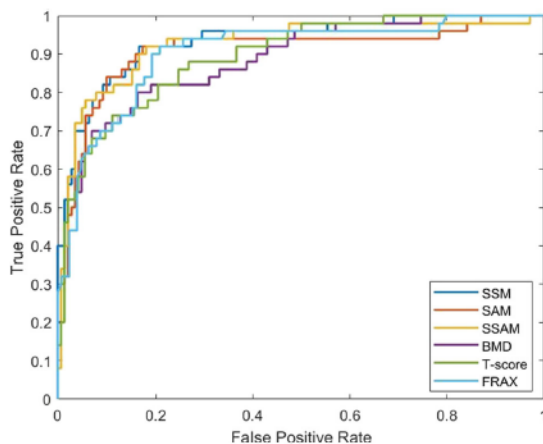


**Fig. 4** Receiver operating characteristic (ROC) curve for the various fracture risk predictors: statistical shape modeling (SSM), statistical appearance modeling (SAM), statistical shape and appearance modeling (SSAM), bone mineral density (BMD), T-score, and FRAX

tissue over the greater trochanter will be thicker and can absorb more energy [40]. Furthermore, if the patient is taller, the energy of the fall can be greater [20], so there will be a greater risk of fracture. A study by Shen et al. [41] showed that higher BMI was associated with less risk of hip fracture in women but not in men, which could be due to the different distribution of body fat in men and women. However, in this study when the fracture risk in men and women were investigated separately, there was still no noticeable difference between the results when not considering the BMI. Therefore, while there might be an optimum value for the BMI to balance the contributing factors to deliver the best results to minimize the fracture risk, it might not be reflected in studies with low sample sizes.

Including age was shown herein to improve the predictive capacity of these models, which may be due to the aging effect not being completely reflected in the other parameters of geometry and BMD distribution. Aging not only affects the bone remodeling process but also influences balance maintenance [42], neurological and musculoskeletal performance [43], and cognitive impairment [43], all of which have an effect on hip fracture risk [44]. Therefore, no matter how accurately one estimates the strength of the proximal femur, the patient's age plays an important role in the risk assessment.

The estimated probability of fracture from combined SSAM showed that the class one (patients who sustained a fracture in less than 2 years) had the highest average probability, above classes two and three. Also, there was a significant difference between the class three average probability of fracture with classes one and two; however, no statistically significant difference was observed between classes one and two. With more investigation and a bigger training set and test group, the approximate year of an impending fracture could possibly be anticipated, and appropriate protective measures and interventions planned accordingly.

In this study, logistic regression was used to find the relationship between the contributing parameters and the fracture risk, and based on the 50% threshold for the probability of fracture, the subjects were classified into high- and low-risk groups. The 50% value herein was an arbitrary divider, and that binary classifications, while easy, reduce the amount of information passed along to clinician and patient. However, one of the limitations of this technique is the number of parameters that can be included in the analysis to avoid non-convergence in the logistic regression. For the SSAM to account for more than 95% of the variations, 26 modes were needed, whereas in the logistic regression, using more than 14 modes led to non-convergence in the regression. It should be noted that these 14 modes were responsible for 90% of variations, which means that some of the relevant information might have been missed in the fracture risk estimation. The same thing happened in the SAM (only considering the BMD distribution); in this case, the 22 modes that could be considered in the logistic regression

were only responsible for 77% of the variations. In applying SSM (only considering the geometry), 14 modes could be included in the analysis and this number of modes was responsible for 98% of the variations, whereas, if 80% of variation was considered (using only two modes), SSM was only able to predict fracture risk with 85% accuracy (164 correct predictions out of 192), which is reduced by 8% (171 correct predictions out of 192). One can conclude that using the geometric data enables us to account for more variations, and this could lead to a better prediction of the fracture risk. In addition, the time and consequently the cost for performing SSM compared with the SSAM and SAM can be significantly lower, and yet can yield comparable results.

In this study, to build the appearance model, all of the pixel intensities were normalized to the mean value, so the appearance model and the shape and appearance model did not include information regarding the absolute BMD value measured by the DXA scan. Therefore, combining the statistical model with the BMD result, which is the primary measure of a bone's mechanical strength, is vital to get more accurate predictions. The area under the ROC curve showed that the combined SSAM model performed better than both the BMD and the T-score as a discrimination tool in diagnosing people at high risk of sustaining a hip fracture. Interestingly, while the maximum improvement for the area under the ROC curve (that was made by the SSM) was 0.05, at a specificity level of 0.80, the new methods were able to increase the sensitivity by around 14%. A closer look at the ROC curve revealed that in the high specificity region (close to the left vertical axis), the proposed techniques led to the much higher sensitivity (true positive, or correct diagnosis of patients at high risk of sustaining hip fracture), and it was only at the lower specificity levels (false positive rate around 50%) that the BMD, T-score, or the FRAX could perform better in the sensitivity.

One of the limitations of this study was that while efforts were made to have the non-fractured cases chosen from the subset of the participants that did not take osteoporosis medication, most of the fractured cases were receiving at least one form of medication. Therefore, it is possible that certain medications might have had an effect on the outcome of the SSAM, and for future studies, the effect of various medications on the outcome of the SSAM would be interesting to investigate.

Adding BMI, age, and sex to the BMD increased the correct fracture prediction by 36%, which is close to the number of correct fracture prediction by the new technique (42%). However, when using combined BMD (BMD, BMI, age, and sex), the percentage of overall correct prediction, including correct fractured and non-fractured cases, placed between the outcome of using T-score alone (82%) and using the combined SSAM model (90%) with 86% overall accuracy. Another way to examine the effectiveness of adding SSAM to the DXA scan was to compare the prediction of SSAM and BMD (without BMI, age, and sex) with the prediction of the

T-score, and one can see that adding SSAM to the measured BMD from the DXA scan increased the number of correct fracture prediction to 72% (which is a 36% improvement) and the overall accuracy to 88%. These numbers show that a significant improvement was made in identifying fractured cases by adding more contributing factors to the BMD (either BMI, age, and sex, or SSAM), and after that, adding more factors only resulted in incremental improvements. Also, some studies have shown that the texture analysis techniques such as TBS, HI, Fourier-based analysis, and multifractal analysis [23, 24, 45] can enhance hip fracture risk independent of the BMD, so future studies combining statistical model and texture analysis are recommended to investigate how more improvement in the hip fracture prediction can be made.

The area under the receiver operating characteristic curve for 2D SSAM in this study was 0.92, which is between the range of 0.84–0.94 reported in previous 3D SSAM studies [20, 21]. Also, a 42% improvement was made in identifying patients at high risk of sustaining a fracture, which is comparable with 45% from a previous 3D SSAM study [21]. This suggests that despite using 2D SSAM (that only used DXA scans in the training set), the fracture risk prediction using this method had comparable results with those of 3D SSAM (that used CT scans in their training set). This is important since it provides significant information for the further development of SSAM in the clinical routine of diagnosis of high fracture risk in older adults without the added computational burden of 3D modeling and radiation of CT scanning.

**Acknowledgments** The authors would like to thank Silvia Dumont and Cluadie Berger for their help in data selection, Dr. Jacques Brown, and Martin Despres for their help in data acquisition, and Jessica Anziano for her help with the data preparation.

**Funding information** This research was supported by Labarge Optimal Aging Initiative under grant number 2016–06 obtained by Dr. Cheryl Quenneville.

**Availability of data and material** Data can be made available upon request.

### Compliance with ethical standards

**Conflicts of interest** Fatemeh Jazinizadeh, Johnathan Adachi, and Cheryl Quenneville declare that they have no conflict of interest.

**Ethical approval** Ethics approval was granted through McGill University and the appropriate ethics review boards for each participating center.

**Informed consent** All participants gave written informed consent.

**Consent for publication** Not applicable.

**Code availability (software application or custom code)** Custom code, not available to the public.

### References

- Klibanski A, Adams-Campbell L, Bassford T, Blair SN, Boden SD, Dickersin K et al (2001) Osteoporosis prevention, diagnosis, and therapy. *J Am Med Assoc* 285:785–795. <https://doi.org/10.1001/jama.285.6.785>
- Watts NB, Bilezikian JP, Camacho PM, Greenspan SL, Harris ST, Hodgson SF, Kleerekoper M, Luckey M, McClung M, Pollack R, Petak S (2010) American Association of Clinical Endocrinologists Medical Guidelines for clinical practice for the diagnosis and treatment of postmenopausal osteoporosis. *Endocr Pract* 16:1–37. <https://doi.org/10.4158/EP.16.S3.1>
- US Department of Health and Human Services. Bone health and osteoporosis: a report of the Surgeon General. US Heal Hum Serv 2004. <https://doi.org/10.2165/00002018-200932030-00004>
- Braithwaite RS, Col NF, Wong JB (2003) Estimating hip fracture morbidity, mortality and costs. *J Am Geriatr Soc* 51:364–370. <https://doi.org/10.1046/j.1532-5415.2003.51110.x>
- Roche JJW, Wenn RT, Sahota O, Moran CG (2005) Effect of comorbidities and postoperative complications on mortality after hip fracture in elderly people: prospective observational cohort study. *Br Med J* 331:1374. <https://doi.org/10.1136/bmj.38643.663843.55>
- Chami G, Jeys L, Freudmann M, Connor L, Siddiqi M (2006) Are osteoporotic fractures being adequately investigated?: a questionnaire of GP & orthopaedic surgeons. *BMC Fam Pract* 7. <https://doi.org/10.1186/1471-2296-7-7>
- Schnell S, Friedman SM, Mendelson DA, Bingham KW, Kates SL (2010) The 1-year mortality of patients treated in a hip fracture program for elders. *Geriatr Orthop Surg Rehabil* 1:6–14. <https://doi.org/10.1177/2151458510378105>
- Leibson CL, Tosteson ANA, Gabriel SE, Ransom JE, Melton LJ (2002) Mortality, disability, and nursing home use for persons with and without hip fracture: a population-based study. *J Am Geriatr Soc* 50:1644–1650. <https://doi.org/10.1046/j.1532-5415.2002.50455.x>
- Melton LJ, Achenbach SJ, Atkinson EJ, Therneau TM, Amin S (2013) Long-term mortality following fractures at different skeletal sites: a population-based cohort study. *Osteoporos Int* 24:1689–1696. <https://doi.org/10.1007/s00198-012-2225-1>
- Sozen T, Ozisik L, Calik BN (2017) An overview and management of osteoporosis. *Eur J Rheumatol* 4:46–56. <https://doi.org/10.5152/eurjrh.2016.048>
- Cosman F, de Beur SJ, LeBoff MS, Lewiecki EM, Tanner B, Randall S, Lindsay R, National Osteoporosis Foundation (2014) Clinician's guide to prevention and treatment of osteoporosis. *Osteoporos Int* 25:2359–2381. <https://doi.org/10.1007/s00198-014-2794-2>
- Siris ES, Chen YT, Abbott TA, Barrett-Connor E, Miller PD, Wehren LE, Berger ML (2004) Bone mineral density thresholds for pharmacological intervention to prevent fractures. *Arch Intern Med* 164:1108–1112. <https://doi.org/10.1001/archinte.164.10.1108>
- Miller PD, Barlas S, Brennen SK, Abbott TA, Chen YT, Barrett-Connor E, Siris ES (2004) An approach to identifying osteopenic women at increased short-term risk of fracture. *Arch Intern Med* 164:1113–1120. <https://doi.org/10.1001/archinte.164.10.1113>
- Kanis JA, Johansson H, Harvey NC, McCloskey EV (2018) A brief history of FRAX. *Arch Osteoporos* 13:118. <https://doi.org/10.1007/s11657-018-0510-0>
- Crandall CJ, Larson J, Cauley JA, Schousboe JT, LaCroix AZ, Robbins JA et al (2019) Do additional clinical risk factors improve the performance of fracture risk assessment tool (FRAX) among postmenopausal women? Findings from the women's health

- initiative observational study and clinical trials. *JBMR Plus* 3: e10239. <https://doi.org/10.1002/jbm4.10239>
16. Lorenz C, Krahnstöver N (2000) Generation of point-based 3D statistical shape models for anatomical objects. *Comput Vis Image Underst* 77:175–191. <https://doi.org/10.1006/cviu.1999.0814>
  17. Väänänen SP, Grassi L, Flivik G, Jurvelin JS, Isaksson H (2015) Generation of 3D shape, density, cortical thickness and finite element mesh of proximal femur from a DXA image. *Med Image Anal* 24:125–134. <https://doi.org/10.1016/j.media.2015.06.001>
  18. Humbert L, Whitmarsh T, De Craene M, Del Rio Barquero LM, Fritscher K, Schubert R, et al. 3D reconstruction of both shape and bone mineral density distribution of the femur from DXA images. 2010 7th IEEE Int Symp Biomed Imaging From Nano to Macro, ISBI 2010 - Proc 2010:456–9. <https://doi.org/10.1109/ISBI.2010.5490310>
  19. Humbert L, Whitmarsh T, Fritscher K, Del Río Barquero LM, Eckstein F, Link T et al (2012) Femoral strength prediction using a 3D reconstruction method from dual-energy X-ray absorptiometry. *Proc - Int Symp Biomed Imaging*:1451–1454. <https://doi.org/10.1109/ISBI.2012.6235844>
  20. Whitmarsh T, Fritscher KD, Humbert L, del Río Barquero LM, Roth T, Kammerlander C, Blauth M, Schubert R, Frangi AF (2012) Hip fracture discrimination from dual-energy X-ray absorptiometry by statistical model registration. *Bone* 51:896–901. <https://doi.org/10.1016/j.bone.2012.08.114>
  21. Bredbenner TL, Mason RL, Havill LM, Orwoll ES, Nicoletta DP (2014) Fracture risk predictions based on statistical shape and density modeling of the proximal femur. *J Bone Miner Res* 29:2090–2100. <https://doi.org/10.1002/jbmr.2241>
  22. Jazinizadeh F, Quenneville CE (2020) Enhancing hip fracture risk prediction by statistical modeling and texture analysis on DXA images. *Med Eng Phys* 78:14–20
  23. Pothuau L, Carceller P, Hans D (2008) Correlations between grey-level variations in 2D projection images (TBS) and 3D microarchitecture: applications in the study of human trabecular bone microarchitecture. *Bone* 42:775–787. <https://doi.org/10.1016/j.bone.2007.11.018>
  24. Thevenot J, Hirvasniemi J, Finnilä M, Pulkkinen P, Kuhn V, Link T, Eckstein F, Jämsä T, Saarakkala S (2013) Trabecular homogeneity index derived from plain radiograph to evaluate bone quality. *J Bone Miner Res* 28:2584–2591. <https://doi.org/10.1002/jbmr.1987>
  25. Leslie WD, O'Donnell S, Lagacé C, Walsh P, Bancej C, Jean S et al (2010) Population-based Canadian hip fracture rates with international comparisons. *Osteoporos Int* 21:1317–1322. <https://doi.org/10.1007/s00198-009-1080-1>
  26. Kaptoge S, Beck TJ, Reeve J, Stone KL, Hillier TA, Cauley JA, Cummings SR (2008) Prediction of incident hip fracture risk by femur geometry variables measured by hip structural analysis in the study of osteoporotic fractures. *J Bone Miner Res* 23:1892–1904. <https://doi.org/10.1359/jbmr.080802>
  27. Ripamonti C, Lisi L, Avella M (2014) Femoral neck shaft angle width is associated with hip-fracture risk in males but not independently of femoral neck bone density. *Br J Radiol* 87:20130358. <https://doi.org/10.1259/bjr.20130358>
  28. Gnudi S, Ripamonti C, Gualtieri G, Malavolta N (1999) Geometry of proximal femur in the prediction of hip fracture in osteoporotic women. *Br J Radiol* 72:729–733. <https://doi.org/10.1259/bjr.72.860.10624337>
  29. Michelotti J, Clark JM (1999) Femoral neck length and hip fracture risk. *J Bone Miner Res* 14:1714–1720. <https://doi.org/10.1359/jbmr.1999.14.10.1714>
  30. Osterhoff G, Morgan EF, Shefelbine SJ, Karim L, McNamara LM, Augat P (2016) Bone mechanical properties and changes with osteoporosis. *Injury* 47:S11–S20. [https://doi.org/10.1016/S0020-1383\(16\)47003-8](https://doi.org/10.1016/S0020-1383(16)47003-8)
  31. Bono CM, Einhorn TA (2003) Overview of osteoporosis: pathophysiology and determinants of bone strength. *Eur Spine J* 12:S90–S96. <https://doi.org/10.1007/s00586-003-0603-2>
  32. Gnudi S, Ripamonti C, Lisi L, Fini M, Giardino R, Giavaresi G (2002) Proximal femur geometry to detect and distinguish femoral neck fractures from trochanteric fractures in postmenopausal women. *Osteoporos Int* 13:69–73. <https://doi.org/10.1007/s198-002-8340-2>
  33. Gnudi S, Sitta E, Pignotti E (2012) Prediction of incident hip fracture by femoral neck bone mineral density and neck-shaft angle: a 5-year longitudinal study in post-menopausal females. *Br J Radiol* 85:e467–e473. <https://doi.org/10.1259/bjr/57130600>
  34. Ito M, Wakao N, Hida T, Matsui Y, Abe Y, Aoyagi K, Uetani M, Harada A (2010) Analysis of hip geometry by clinical CT for the assessment of hip fracture risk in elderly Japanese women. *Bone* 46:453–457. <https://doi.org/10.1016/j.bone.2009.08.059>
  35. Long Y, Leslie WD, Luo Y (2015) Study of DXA-derived lateral-medial cortical bone thickness in assessing hip fracture risk. *Bone Reports* 2:44–51. <https://doi.org/10.1016/j.bonr.2015.02.003>
  36. Ha Y-C, Yoo J-I, Yoo J, Park KS (2019) Effects of hip structure analysis variables on hip fracture: a propensity score matching study. *J Clin Med* 8. <https://doi.org/10.3390/jcm8101507>
  37. Alswat KA (2017) Gender Disparities in Osteoporosis. *J Clin Med Res*. <https://doi.org/10.14740/jocmr2970w>
  38. Looker AC, Beck TJ, Orwoll ES (2001) Does body size account for gender differences in femur bone density and geometry? *J Bone Miner Res* 16:1291–1299. <https://doi.org/10.1359/jbmr.2001.16.7.1291>
  39. Nasiri Sarvi M, Luo Y (2017) Sideways fall-induced impact force and its effect on hip fracture risk: a review. *Osteoporos Int* 28:2759–2780. <https://doi.org/10.1007/s00198-017-4138-5>
  40. Bouxsein ML, Szulc P, Munoz F, Thrall E, Sornay-Rendu E, Delmas PD (2007) Contribution of trochanteric soft tissues to fall force estimates, the factor of risk, and prediction of hip fracture risk. *J Bone Miner Res* 22:825–831. <https://doi.org/10.1359/jbmr.070309>
  41. Shen J, Leslie WD, Nielson CM, Majumdar SR, Morin SN, Orwoll ES (2016) Associations of body mass index with incident fractures and hip structural parameters in a large Canadian cohort. *J Clin Endocrinol Metab* 101:476–484. <https://doi.org/10.1210/jc.2015-3123>
  42. Kulmala J, Sihvonen S, Kallinen M, Alen M, Kiviranta I, Sipilä S (2007) Balance confidence and functional balance in relation to falls in older persons with hip fracture history. *J Geriatr Phys Ther* 30:114–120. <https://doi.org/10.1519/00139143-200712000-00006>
  43. Formiga F, Lopez-Soto A, Duaso E, Ruiz D, Chivite D, Perez-Castejon JM, Navaro M, Pujol R (2008) Characteristics of fall-related hip fractures in community-dwelling elderly patients according to cognitive status. *Aging Clin Exp Res* 20:434–438. <https://doi.org/10.1007/BF03325149>
  44. Marks R (2010) Hip fracture epidemiological trends, outcomes, and risk factors, 1970-2009. *Int J Gen Med*
  45. Vokes TJ, Giger ML, Chinander MR, Karrison TG, Favus MJ, Dixon LB (2006) Radiographic texture analysis of densitometer-generated calcaneus images differentiates postmenopausal women with and without fractures. *Osteoporos Int* 17:1472–1482. <https://doi.org/10.1007/s00198-006-0089-y>

**Publisher's note** Springer Nature remains neutral with regard to jurisdictional claims in published maps and institutional affiliations.

## **CHAPTER 5 - Comparing the Fracture Limits of The Proximal Femur Under Impact and Quasi-Static Conditions in Simulation of a Sideways Fall**

---

*Overview: In this chapter, 3D SSAM was applied to the DXA scans of a group of subjects from the Canadian Multicentre Osteoporosis Study, and the fracture risk predictions were compared to the 2D SSAM and the standard clinical methods to address Objective 4. This chapter has been submitted to the Annals of Biomedical Engineering, and upon acceptance and publication, the proper permission from the copyright holder will be obtained to include the article in this thesis.*

**3D reconstruction of the proximal femur from a DXA scan compared to 2D  
reconstruction for fracture risk prediction in a clinical population**

**Fatemeh Jazinizadeh <sup>a</sup>, Cheryl E. Quenneville <sup>a,b,\*</sup>**

<sup>a</sup> Department of Mechanical Engineering, McMaster University, Hamilton,  
Ontario, Canada

<sup>b</sup> School of Biomedical Engineering, McMaster University, Hamilton, Ontario,  
Canada

\* Corresponding author: Dr. Cheryl Quenneville, ABB-C308, McMaster  
University, 1280 Main St. West, Hamilton, ON L8S 4L8

Phone: (905) 525-9140 x 21797

Email address: [quennev@mcmaster.ca](mailto:quennev@mcmaster.ca)

## 5.1 Abstract

---

Osteoporosis is a disease most common in older adults that can cause fragility fractures in this population. Due to the adverse impacts of hip fractures on patients' lives, it is crucial to enhance the identification of people at high risk through accessible clinical techniques to facilitate the implementation of protective measures.

Due to the accessibility, low cost, and low radiation dose, DXA scans remain the preferred modality for fracture risk prediction, but is limited to 2D. Reconstructing the 3D geometry and BMD distribution of the proximal femur could be beneficial in enhancing hip fracture risk predictions; however, it is associated with a high computational burden and requires a training set of CT scans of the proximal femur. It is also not clear whether it provides a better performance than 2D model analysis.

The DXA scans and CT scans of 16 cadaveric femurs were used to create training sets for the 2D and 3D model reconstruction based on the statistical shape and appearance modeling. Subsequently, these methods were used to predict the risk of sustaining a hip fracture in a clinical population of 150 subjects (including 50 fractured cases) that were monitored for five years in the Canadian Multicentre Osteoporosis (CaMos) study.

The 3D statistical model was able to reconstruct the geometry and bone mineral density distribution of the femurs from a single DXA scan with an average geometry error of 1.6 mm and bone mineral density error of 0.11 g/cm<sup>3</sup>. This technique was able to improve the identification of patients who sustained a hip fracture more accurately than the standard clinical practice of using the T-score (44% improvement). The predictions from

the 2D statistical model did not differ significantly from the 3D ones (76% correct fracture prediction compared to 80% from the 3D technique).

These results indicated that, while 3D model reconstruction might be necessary for further numerical analysis, to enhance hip fracture risk prediction in clinical practice implementing 2D statistical modeling has comparable performance with lower associated computational load and easier implementation.

**Keywords:** hip fracture risk, proximal femur, DXA scanning, 2D statistical modeling, 3D statistical modeling

## 5.2 Introduction

---

Osteoporosis is a disease most common in older adults, which results in low bone mass and micro-architectural deterioration, and can lead to a pathologic bone fracture [1]. The hip (proximal femur) is one of the most common sites affected by osteoporosis, the fracture of which can result in severe morbidity and mortality [2,3]. Patients with an early diagnosis of osteoporosis can benefit from protective measures to prevent these fractures [6,5,4]. Currently, the most common method for the diagnosis of osteoporosis relies on the measurement of bone mineral density (BMD) from a dual-energy X-ray absorptiometry (DXA) scan [1]. However, studies have shown that the DXA scan alone is not sufficient in identifying all patients at high risk of sustaining a hip fracture [8,7].

DXA scans mainly measure the average BMD in certain regions of the bone, from which the mechanical properties of the bone can be inferred; however, the strength of a femur depends on its geometry [10,9], BMD distribution pattern [12,11], and trabecula's quality [14,13] as well. Many studies have tried to incorporate these factors in fracture risk assessments to enhance the identification of patients at a higher risk of sustaining a fracture [15]. Considering the effect of a femur's geometry and BMD distribution can be done in 2D using DXA scans and X-ray radiographs, or in 3D using Computed Tomography (CT) scans and Magnetic Resonance Imaging (MRI) [16]. While 3D imaging provides more insight into the whole geometry and density distribution of the bone, it is not always feasible to use 3D imaging, due to the expense, time, accessibility, and radiation levels. Therefore, it is anticipated that 2D imaging (DXA scans) will remain as the primary method of diagnosing osteoporosis and consequently fracture risk [17].

To enhance hip fracture risk prediction, researchers have performed 2D analysis on medical images (either DXA scan or another X-ray based radiography of hip) and their results have shown that it has noticeable improvements over BMD alone [19,18,16]. Also, to gain the benefits of 3D imaging, other studies have tried to develop 3D structures from 2D scans, using statistical modeling [22,20,21]. This method allows inference of both geometry and architecture of bones in 3D based on a template model that is created from a training set. Reconstruction of the 3D model of the proximal femur based on a 2D DXA image can provide direct measurement of the 3D features that otherwise cannot be evaluated in a 2D image [23]. The generated 3D model can also be used for further numerical analysis such as finite element analysis [24]. Some studies have investigated hip fracture risk by considering the effect of the femur's shape and BMD distribution through 3D statistical models, and their results showed that fracture risk estimation was substantially improved compared to using traditional BMD evaluation [20,25].

While generating 3D models might be a necessity in further numerical analysis, it is not completely clear if recreating the 3D model from a 2D image to only investigate the geometry and BMD distribution pattern in the femur will have an advantage over investigating the geometry and BMD distribution pattern in 2D alone. Since the 2D and 3D model studies to estimate hip fracture risk were performed based on different training sets and testing groups, the potential to do any direct comparison between them is limited. Therefore the aims of this study were 1) to create 3D shape and BMD distribution models of the proximal femur based on DXA scans, 2) investigate the accuracy of the proposed 3D model reconstruction in comparison to CT scans, and 3) apply 2D and 3D model

analysis methods to a clinical population to estimate their hip fracture risk and compare it to their fracture history in a five-year period after the baseline.

### **5.3 Material and Methods**

---

This study had two phases: in phase one, the 2D and 3D analyses were developed using cadaveric specimens (which had 2D and 3D images). In phase two, the techniques were tested and evaluated on a clinical population who had 2D images and fracture history over five years.

Sixteen isolated cadaveric femurs were used for the training sets in this study [26]. Each femur was scanned with a DXA scanner (Hologic Discovery A, Hologic, Inc., Marlborough, MA, USA) and a CT scan machine (GE LightSpeed, GE Healthcare, Chicago, Illinois, USA) with 0.625 mm slice thickness, 0.7 mm in-plane resolution, and 120kV tube voltage, to obtain the geometry and 2D areal and 3D spatial BMD distribution within the bone.

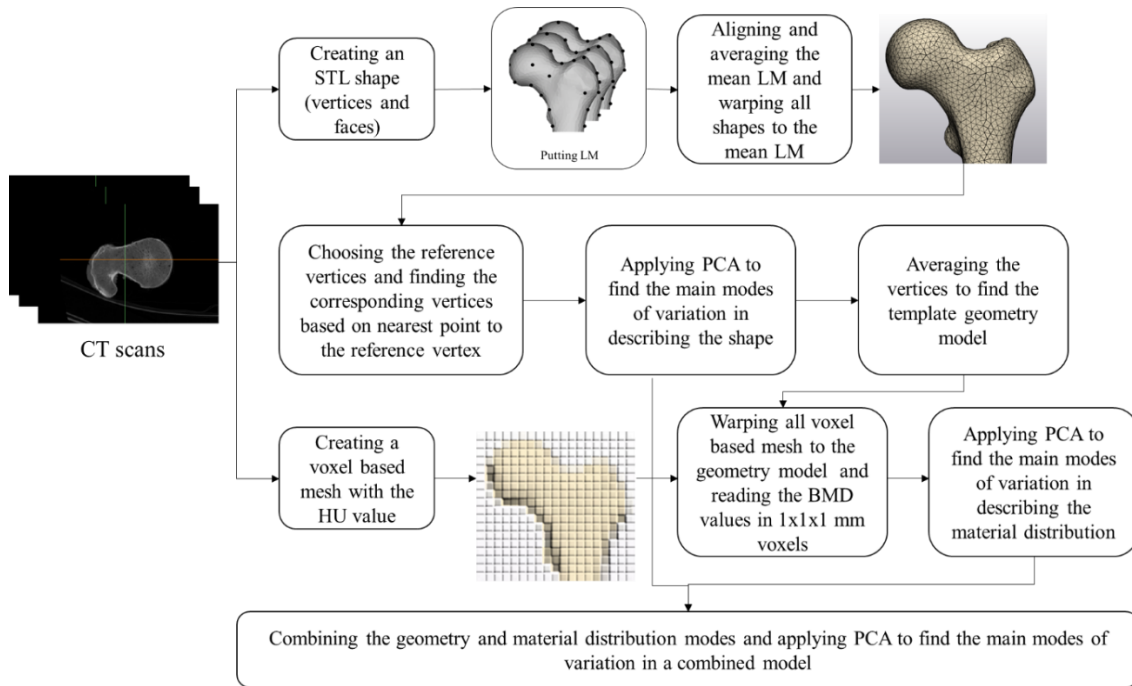
#### **5.3.1 3D Model Reconstruction from DXA Scan**

Image processing was performed using MATLAB Image Processing Toolbox (MATLAB R2019b, MathWorks, Natick, Massachusetts, US). Reconstruction of the model consisted of two stages: 1) creating the BMD and geometry template models, where the 3D template models were created and the main modes of variation in the geometry and BMD distribution in the training set were found, and 2) assessing a new scan, where each new DXA scan can be described by the template model plus some variation from it based on the calculated main modes of variation from the first step. The values of these modes

were estimated through an optimization process to minimize the differences between the calculated model and the real DXA scan.

### **5.3.1.1 Creating the BMD and Geometry Template Models**

To create the 3D SSAM, the CT scans of the cadaveric femurs were used to generate 3D models for the training set (MIMICS 22.0, Materialise NV, Leuven, Belgium). For each scan, an STL file was generated to represent the geometry of the proximal femur and a voxel-based mesh was created to describe the BMD distribution in the bones. Twenty-seven geometric landmarks were assigned to each of the models (Figure 5.1). The landmarks were placed on the exterior surface of the bone and were based on the identifiable anatomical features. After aligning and removing the effect of translation, rotation, and scaling (using General Procrustes Analysis, GPA) the average landmark coordinates were calculated. Then all models were warped to the average landmark coordinates. The minimum number of vertices from the CT scan 3D model creation was 2255 vertices, so these were chosen as the reference vertices and corresponding vertices in other 3D models were selected automatically by a closest point algorithm. The average 3D shape was thus calculated (creating the template geometry model), and then all 3D models as well as the voxel-based mesh were warped to the average model. Hounsfield Unit (HU) values were then captured in 1x1x1 mm voxels for each warped 3D model and normalized to the mean and standard deviation of that model. They were then averaged for all specimens to create the template BMD model. Finally, Principal Component Analysis (PCA) was used on both geometry and BMD data to find the main modes of variation in them, which were then gathered in a matrix and PCA was used again to find the main



**Figure 5.1 Flowchart of Creating the 3D Statistical Shape and Appearance Models.**

From the CT scans of isolated cadaveric femurs an STL file to show the surface geometry and a voxel-based mesh to show the BMD distribution was generated. LM: Landmarks, PCA: Principal Component Analysis, HU: Hounsfield Unit, BMD: Bone Mineral Density.

Modes of variation for SSAM combined.

### **5.3.1.2 Assessing a New Scan**

To create the 3D model of each femur from its DXA scan, 19 landmarks were assigned on the contour of the femur. Next, the geometry template model was adjusted by its main modes of variation to minimize the difference between the DXA scan and anterior-posterior projection of the 3D model (Figure 5.2). After estimating the geometry modes, the femur's shape from the 2D DXA scan was warped to the anterior-posterior projection of the 3D geometry template, and then the gray value of each pixel was captured and normalized to the mean and standard deviation of all pixels for that scan. In the anterior-posterior projection of the 3D template model, the intensity of the voxels (representing the BMD) along the sagittal axis were accumulated to find the each pixel's intensity in the 2D projection, and then the intensity of each pixel was normalized to the mean and standard deviation of all pixels (in the 2D projection).

The 3D BMD template model was changed by its modes, and in each iteration, the anterior-posterior projection of the adjusted template was compared to the warped DXA scan to minimize the differences between the two and eventually finding the BMD modes. In the end, based on the combined geometry and BMD models the combined (SSAM) modes of variations were calculated.

### **5.3.2 Evaluation of the 3D Model Reconstruction**

To evaluate the accuracy of the 3D model reconstruction, the leave-one-out cross-validation technique was used on the 16 cadaveric specimens. So, to create the 3D model

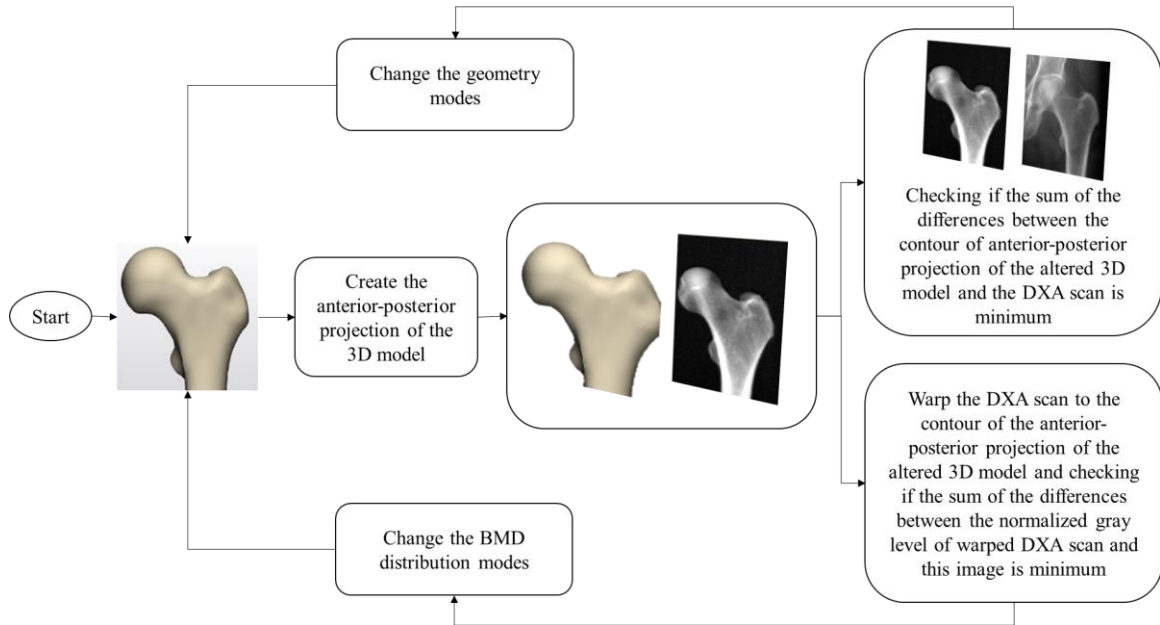


**Figure 5.2 The flowchart of finding the modes for a new DXA scan.**

The modes are found through an optimization process to minimize the difference between the anterior-posterior projection of the template model and the DXA scan.

of each femur from its DXA scan, the CT scans of the other 15 specimens were used in the training set to create the template models and find the main modes of variations. After reconstructing the 3D model for each femur, the created 3D models were compared to the CT-based 3D models. This was evaluated based on the minimum point to surface distance between each vertex from the 3D model reconstruction and the 3D model from the CT scan, as well as the BMD values of the corresponding voxels.

### **5.3.3 Clinical Data**

The subjects used in this study were recruited by the Canadian Multicentre Osteoporosis Study (CaMos). A total of 150 patients' data was used (Table 5.1), 50 of whom sustained a hip fracture within five years of the baseline DXA scan with a Hologic DXA scanner (Hologic, Inc, Marlborough, MA).

#### **5.3.3.1 Predicting the Fracture Risk Based on 3D Model Reconstruction**

In the clinical application, to create the 3D model of each subject's proximal femur from its DXA scan, the training set of 3D models of 16 cadaveric specimens was used, and the weight of each variation mode was calculated based on the algorithm described earlier in section 5.3.1.2 Next, to estimate the fracture risk for each subject ('test group'), the leave-one-out cross-validation was used, where the other 149 subjects ('training set group') were used to create and train the fracture risk prediction function (based on the reported fracture history of the subjects) through logistic regression analysis. The variables used in the functions were the calculated modes, areal BMD, and the mean and standard deviation

**Table 5.1 The summary of patients' characteristics.**

Subjects	Total number	Male	Female	Age (mean±SD)
Fractured	50	13	37	78.3±7.4
Non-fractured	100	57	43	66.2±9.5

Of pixels from the DXA scan. Subjects with an estimated probability of fracture greater than 50% were considered high risk (likely to sustain a hip fracture).

### **5.3.3.2 Predicting the Fracture Risk based on 2D Model Reconstruction**

Details regarding the 2D (i.e. DXA-based) SSAM have been described previously [15]. Briefly, landmarks were assigned to each of the DXA scans and then aligned and averaged to create the geometry template model. Next, each image was warped to the geometry template model and the gray value of each pixel (which is an indication of the areal BMD value) was captured and normalized to the mean and standard deviation of all pixel values (within the same scan). All captured and normalized pixel values within the training set were then averaged to create the template BMD model. Principal Component Analysis (PCA) was used on both models (geometry and BMD) to find the main modes of variation for each and then combined, then PCA was again used to find the main modes of variation in describing the geometry and BMD distribution together. To reconstruct the geometry and BMD distribution of each DXA scan based on the variations in the training set, a series of landmarks on the contour of the femur were assigned to each DXA scan [15]. Then, the template geometry and BMD models were adjusted by the main modes of variation to recreate the DXA scan [15]. To estimate the fracture risk based on the 2D model reconstruction, the leave-one-out cross-validation technique was conducted on the clinical data, as was done on the 3D model reconstructions.

### 5.3.4 Evaluation of the Fracture Risk Predictions

The two new image analysis methods (2D and 3D) were compared to two clinical metrics: total areal BMD and T-score. The total areal BMD from the DXA scans were also investigated using logistic regression analysis and leave-one-out cross-validation in the same way as 2D and 3D SSAM. A threshold of 50% was used to assign each subject to high or low fracture risk. A T-score of -2.5 (the standard threshold for osteoporosis [27]) was also used to divide the subjects into low and high fracture risk groups. In the end, all predictions from 2D SSAM, 3D SSAM, BMD and T-score were compared to the fracture history of the subjects.

To check the diagnostic value of each technique, the Receiver Operating Characteristic (ROC) curve, which plots the true positive rate (sensitivity) versus the false positive rate (1-specificity) based on different thresholds, was plotted and the area under the curve was calculated. To compare the geometry between the average fractured and non-fractured subjects, the mean location of each vertex was calculated for each group. The same was done for the BMD and to graphically illustrate the differences, colored heat maps were created for both.

## 5.4 Results

---

To account for more than 95% of the variation in describing the shape and BMD distribution of the cadaveric femurs nine and 14 modes were needed for 2D and 3D models, respectively. The average point to surface errors in the reconstruction of geometry was  $1.65 \pm 0.58$  mm (range between 0.56-4.22 mm, Figure 5.3), and the maximum error was

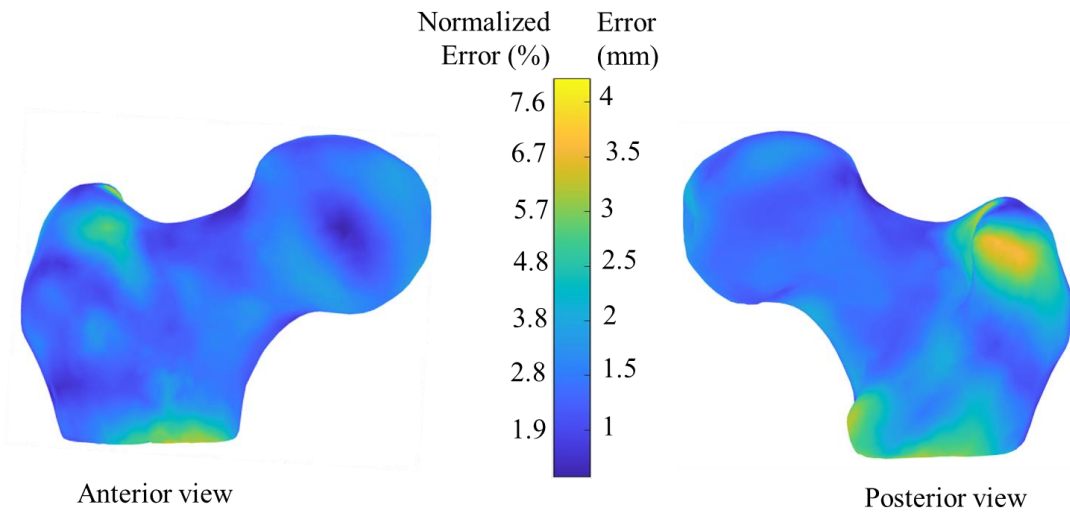


**Figure 5.3 Illustration of the error in reconstruction of the geometry.**

The errors have been normalized to the average of the widest thickness of the femurs in the training set. The maximum error was found at the tip of the greater trochanter.

related to the reconstruction of the greater trochanter. To depict the error proportionally to the geometry of the femur, it was normalized to the average widest anterior-posterior distance of the femurs in the training set (53 mm).

The average BMD reconstruction error for corresponding voxels (1x1x1 mm) was  $0.11 \pm 0.09$  g/cm<sup>3</sup> (range between 0-0.84 g/cm<sup>3</sup>), with the maximum error found in the cortical bone in the medial trochanteric area. The average BMD value from the 3D model reconstruction and the CT scans were illustrated for the mid-frontal plane and mid-transverse plane (Figure 5.4).

In the clinical dataset, 2D SSAM was able to correctly classify 38 (out of 50) fractured cases and 93 (out of 100) non-fractured cases. Using 3D SSAM, the technique was able to correctly classify 40 (out of 50) fractured cases and 92 (out of 100) non-fractured cases. The T-score was able to correctly classify 18 (out of 50) fractured cases and 99 (out of 100) non-fractured cases (Table 2). The areas under the ROC curve for 2D SSAM, 3D SSAM, BMD, and T-score were calculated as 0.92, 0.91, 0.88, and 0.89 respectively, with 2D SSAM having the highest value and BMD having the lowest (Figure 5.5).

The differences between the average 3D shape and BMD distribution model for the fractured and non-fractured subjects were depicted using colored heat maps, and if the average non-fractured vertices were inside the average fractured geometry the distance was considered positive (i.e. non-fractured was smaller), and vice versa (Figure 5.6). Generally,

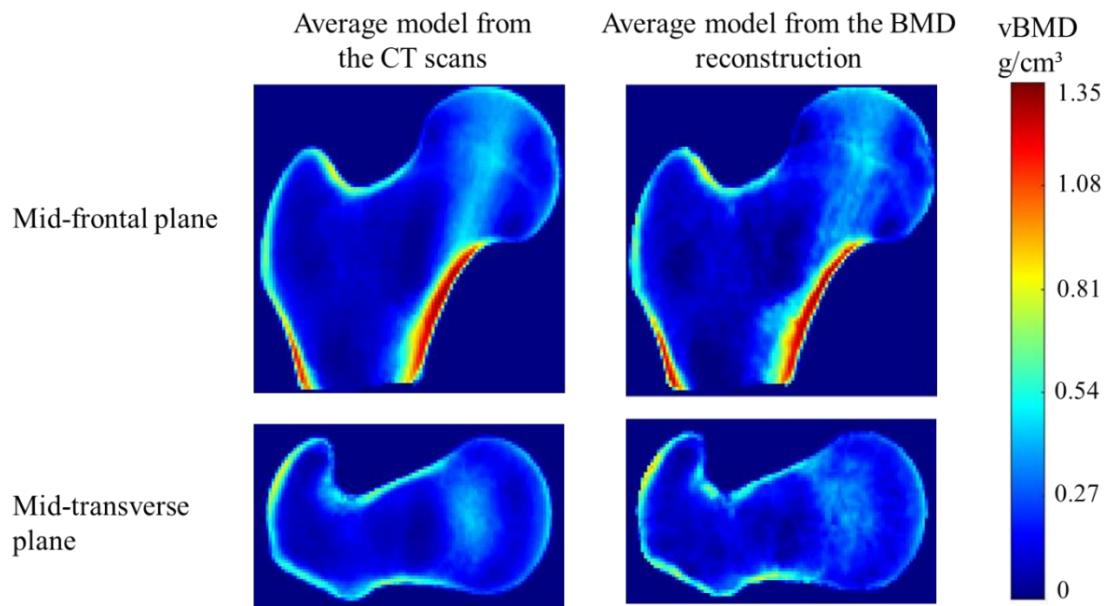


**Figure 5.4 Illustration of the Volumetric BMD (vBMD) in the Average Model from the CT Scans and the Average Model from the BMD Reconstruction in Two Views.**

Top: mid-frontal plane, bottom: mid-transverse plane.

**Table 5.2 A summary of the hip fracture risk prediction results for various classifiers.**

Fracture risk underprediction refers to the subjects that were identified as low risk but sustained a hip fracture and fracture risk overprediction refers to the subjects that were identified as high risk but did not sustain a hip fracture

<b>Predictor</b>	<b>Correct prediction for Fx subjects</b>	<b>Correct prediction for non-Fx subjects</b>	<b>Fracture risk underprediction</b>	<b>Fracture risk overprediction</b>
<b>2D SSAM</b>	38 (76%)	93 (93%)	12 (8%)	8 (5%)
<b>3D SSAM</b>	40 (80%)	92 (92%)	10 (7%)	7 (5%)
<b>BMD</b>	34 (68%)	93 (93%)	16 (11%)	7 (5%)
<b>T-score</b>	18 (36%)	99 (99%)	32 (21%)	1 (1%)

Fx: fractured, non-Fx: non-fractured

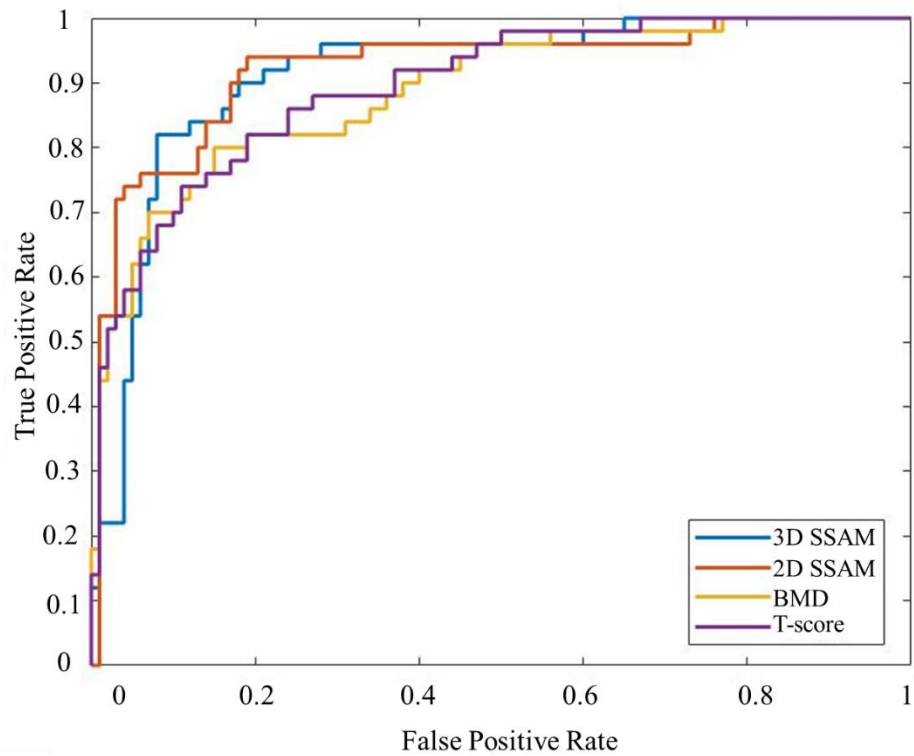


**Figure 5.5 Receiver Operating Characteristic (ROC) Curves for Various Hip Fracture Risk Predictors.**

The area under the curve for 3D and 2D SSAM was slightly higher than BMD and T-score.

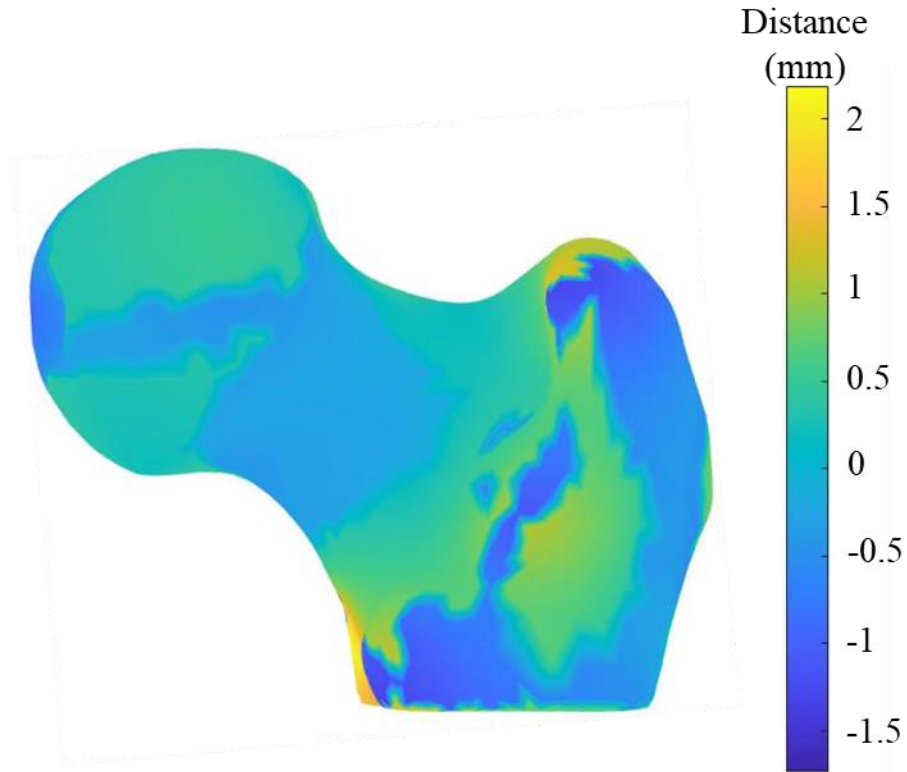


**Figure 5.6 Surface Geometry Variation Between the Mean Fractured and Non-Fractured Subjects.**

The yellow color represents the points where the mean vertices of the non-fracture subjects were inside the mean fractured geometry (i.e. fractured group was larger than non-fractured) and the blue points indicate that the mean vertices of the non-fracture subjects were outside the mean fractured geometry (i.e. the mean fractured geometry was smaller than the non-fractured).

the average proximal femur's geometry for the fractured subjects was larger than the non-fractured one.

For the BMD distribution comparison between the two groups (fractured and non-fractured subjects), the difference between the volumetric BMD of the voxels in the mid-frontal plane was calculated and depicted as a heat map as well, with higher BMD in the non-fractured group having a positive value (Figure 7). The average volumetric BMD map in the mid-frontal plane for the fractured subjects was lower than the non-fractured group, especially in the inner cortex of the trochanteric and subtrochanteric areas.

## **5.5 Discussion**

---

In this research, a novel approach to create a 3D model of the proximal femur from a single 2D DXA scan was introduced, evaluated, and its ability to clinically predict hip fracture risk was assessed in a dataset of patients who were followed for at least five years. The new technique was able to significantly enhance hip fracture prediction in the high risk patients compared to T-score (44% improvement), which means that for the approximately 30,000 hip fractures that happen each year in Canada [28], thousands of patients at high risk could be identified and protected from this injury by using this technique. While applying statistical models can greatly enhance hip fracture risk prediction in patients, we showed that there was no real benefit to adding the 3D reconstruction for injury risk prediction applications, making this easier and faster for clinical implementation. Also, this is the first known study to directly compare 2D vs 3D statistical shape and appearance modeling to predict the hip fracture risk in older adults. This has great importance since

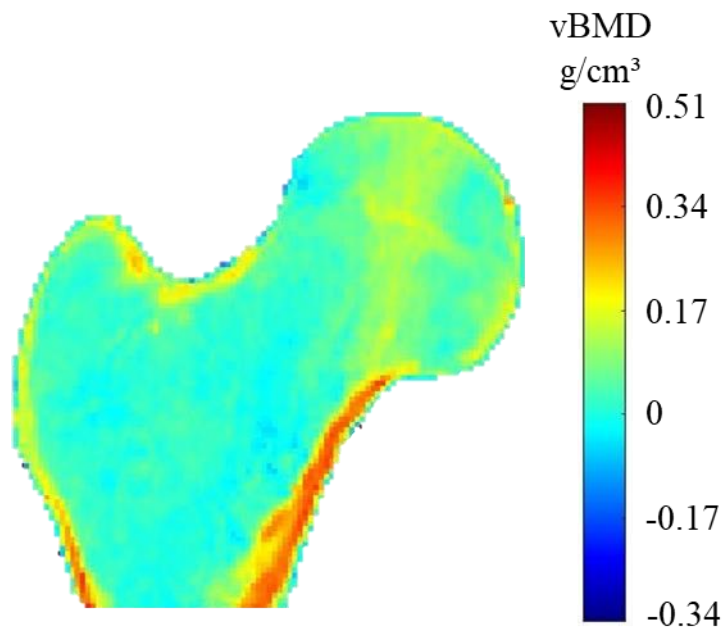


**Figure 5.7 Volumetric BMD Variation in the Mid-Frontal Plane Between the Mean Fractured and Non-Fractured Subjects.**

The red color indicates demonstrates the voxels that have a higher BMD value in the non-fractured subjects than the fractured subjects, and the blue color identifies demonstrates the voxels that have a higher BMD value in the fractured subjects than the fractured ones.

implementing 2D geometry and BMD distribution model reconstruction is associated with less computational burden and is more achievable in clinical practice. These results can shape the future of applying statistical models in clinical practice to predict hip fracture risk.

Two previous studies have reported reconstruction errors in geometry and BMD distribution of similar magnitudes to those in the present study [21,29] (average geometry error of 1.07-1.1 mm, and an average BMD distribution error of 0.07-0.21 g/cm<sup>3</sup>). However, the maximum geometry errors in this study were smaller than those previously reported (5.4 - 9.2 mm previous, vs. 4.2 mm herein).

Comparing the geometry of the proximal femur in the fractured and non-fractured subjects revealed that fractured cases were overall larger than non-fractured ones (Figure 5). This is in agreement with other studies that have investigated the effect of the proximal femur's geometry on hip fracture risk [31,9,32,33,30]. This effect could be attributed to the body's response to a decreased BMD and an effort to resist bending failure by increasing the diameter to increase the second moment of inertia [34]. It is worth noting that that the range of the differences between the fractured and non-fractured geometries was between -1.5 mm to +2 mm, and considering that the average error in the geometry reconstruction was 1.6 mm, some of the difference between the two geometries might have been affected by the inherent error in the reconstruction.

The average voxels' BMD in the mid-frontal plane in the fractured cases were lower than the non-fractured ones (Figure 6). This could be specifically observed in the inner

contour of the cortical bone in the medial region of the trochanteric area, which can be attributed to the thinning of the cortical bone in patients with osteoporosis [35].

The area under the ROC curve for both 2D and 3D were noticeably better than T-score and BMD. When looking at the ROC curve, it can be observed that in the area of high specificity between 50%-95% (close to the left side of the graph, 5%-50% false positive rate) the statistical models were noticeably able to identify more true positive cases (people actually at risk of fracture) than the standard clinical method, which would be more desirable. It also showed that, only in the area of more than 50% false positive rate (close to the right side of the graph), the performance of all the methods were similar, and even in that case the T-score threshold should be modified from the -2.5 that is currently used in clinical practice to improve this.

The area under the ROC curve for another similar 3D study [22] was reported as 0.83 for aBMD plus age, and 0.93 for 3D reconstruction (considering both geometry and BMD distribution) plus aBMD and age. However, two other studies that investigated the 2D analysis have reported 0.16 [19], and 0.03 [18] improvement in area under the ROC curve while considering only the geometry, and geometry plus BMD distribution, respectively. These results suggest that comparing the improvement made by each method should be assessed based on various aspects of its performance, and for evaluation of different techniques a direct comparison based on the same training set and test set should be preferred.

There could be several reasons for the lack of difference between 2D and 3D predictions. The most important one is that it might be possible that there is a correlation between 2D and 3D geometry and BMD distribution features of the proximal femur. In some studies to reconstruct the 3D geometry of the proximal femur [36,37], the main assumption was based on the dependency of 3D features on the 2D ones observed in a 2D image (either DXA scan or other radiograph of the hip). Their results showed that the 3D shape reconstruction of the proximal femur with this assumption had an acceptable average error range, so it could be concluded that the most of the 3D features of proximal femur correspond with its 2D features, and although to describe a shape in 3D, more variables are needed, most of these variables are correlated to ones observed in the 2D image.

In addition to the mechanical properties of the proximal femur, many other factors affect a patients' hip fracture risk. These factors either relate to the patients' characteristics [38] (*e.g.* medication use, fracture history, tobacco use, alcohol consumption), fall mechanics [39] (*e.g.* patients' height, weight, and reflexes), or fall probability [40] (*e.g.* physical activity level, comorbidities, balance and stability, and age). However, in this research, only features related to the proximal femurs' structural strength were investigated. Therefore, a more robust prediction would consider many of these other factors.

One of the limitations of this study was that in the training set, the DXA scans and CT scans of isolated cadaveric femurs were used to make 2D and 3D template models, while for the evaluation of these techniques clinical DXA scans were used. The main difference between the clinical DXA scans and the ones from the isolated femurs was the

effect of the overlapping pelvis over the proximal part of the femoral head, which led to artificially increasing the BMD measure in this area. Also, due to the presence of soft tissues in the clinical DXA scans, they were associated with more noise artifacts. Therefore, since these variabilities weren't captured in the training set, extra error might have been induced in the BMD distribution reconstruction model. However, the effect of these errors was minimized by using the clinical scans in creating the fracture risk estimation function through cross-validation.

This study showed that, while proximal femurs 3D model reconstruction might be necessary for further numerical analysis (*e.g.* finite element analysis and direct measurement of specific 3D traits), it does not add significant value to the hip fracture risk estimation when compared to 2D model reconstruction. This will have a significant impact on how statistical models are adopted by clinical practice. Since implementing 2D techniques is less intensive technically and computationally and uses more accessible and safer imaging modalities (compared to using CT scans) to expand the training set, it has great potential to be implemented in clinical practice as part of standard hip fracture risk estimation in older adults.

### **Acknowledgments**

This research was funded by the Labarge Optimal Aging Initiative. The authors would also like to thank Dr. Jonathan Adachi for his help with CaMos data, Sandra Charbonneau for her help with the CT scanning, and Chantal Saab for her help with DXA scanning of the specimens.

## 5.6 References

- [1] Sozen T., L. Ozisik, N. Calik Basaran, Sozen T., L. Ozisik, N. Calik Basaran. An overview and management of osteoporosis. *Eur J Rheumatol* 2017. <https://doi.org/10.5152/eurjrheum.2016.048>.
- [2] Ip T.P., J. Leung, A.W.C. Kung, Ip T.P., J. Leung, A.W.C. Kung. Management of osteoporosis in patients hospitalized for hip fractures. *Osteoporos Int* 2010. <https://doi.org/10.1007/s00198-010-1398-8>.
- [3] Roche J.J.W., R.T. Wenn, O. Sahota, C.G. Moran, Roche J.J.W., R.T. Wenn, O. Sahota, C.G. Moran. Effect of comorbidities and postoperative complications on mortality after hip fracture in elderly people: Prospective observational cohort study. *Br Med J* 2005. <https://doi.org/10.1136/bmj.38643.663843.55>.
- [4] Woolf A.D., K. Åkesson, Woolf A.D., K. Åkesson. Preventing fractures in elderly people. *Br Med J* 2003. <https://doi.org/10.1136/bmj.327.7406.89>.
- [5] Parker M.J., W.J. Gillespie, L.D. Gillespie, Parker M.J., W.J. Gillespie, L.D. Gillespie. Effectiveness of hip protectors for preventing hip fractures in elderly people: Systematic review. *Br Med J* 2006. <https://doi.org/10.1136/bmj.38753.375324.7C>.
- [6] Lachance C.C., M.P. Jurkowski, A.C. Dymarz, D.C. Mackey, Lachance C.C., M.P. Jurkowski, A.C. Dymarz, D.C. Mackey. Compliant flooring to prevent fall-related injuries: a scoping review protocol. *BMJ Open* 2016. <https://doi.org/10.1136/bmjopen-2016-011757>.
- [7] Siris E.S., Y.T. Chen, T.A. Abbott, E. Barrett-Connor, P.D. Miller, L.E. Wehren, M.L. Berger, Siris E.S., Y.T. Chen, T.A. Abbott, E. Barrett-Connor, P.D. Miller, L.E. Wehren, M.L. Berger. Bone mineral density thresholds for pharmacological intervention to prevent fractures. *Arch Intern Med* 2004. <https://doi.org/10.1001/archinte.164.10.1108>.
- [8] Miller P.D., S. Barlas, S.K. Brenneman, T.A. Abbott, Y.T. Chen, E. Barrett-Connor, E.S. Siris, Miller P.D., S. Barlas, S.K. Brenneman, T.A. Abbott, Y.T. Chen, E. Barrett-Connor, E.S. Siris. An approach to identifying osteopenic women at increased short-term risk of fracture. *Arch Intern Med* 2004. <https://doi.org/10.1001/archinte.164.10.1113>.

- [9] Kaptoge S., T.J. Beck, J. Reeve, K.L. Stone, T.A. Hillier, J.A. Cauley, S.R. Cummings, Kaptoge S., T.J. Beck, J. Reeve, K.L. Stone, T.A. Hillier, J.A. Cauley, S.R. Cummings. Prediction of incident hip fracture risk by femur geometry variables measured by hip structural analysis in the study of osteoporotic fractures. *J Bone Miner Res* 2008. <https://doi.org/10.1359/jbmr.080802>.
- [10] Gregory J.S., R.M. Aspden, Gregory J.S., R.M. Aspden. Femoral geometry as a risk factor for osteoporotic hip fracture in men and women. *Med Eng Phys* 2008. <https://doi.org/10.1016/j.medengphy.2008.09.002>.
- [11] Yang L., A.C. Burton, M. Bradburn, C.M. Nielson, E.S. Orwoll, R. Eastell, Yang L., A.C. Burton, M. Bradburn, C.M. Nielson, E.S. Orwoll, R. Eastell. Distribution of bone density in the proximal femur and its association with hip fracture risk in older men: The osteoporotic fractures in men (MrOS) study. *J Bone Miner Res* 2012. <https://doi.org/10.1002/jbmr.1693>.
- [12] Yang L., W.J.M. Udall, E. V. McCloskey, R. Eastell, Yang L., W.J.M. Udall, E. V. McCloskey, R. Eastell. Distribution of bone density and cortical thickness in the proximal femur and their association with hip fracture in postmenopausal women: A quantitative computed tomography study. *Osteoporos Int* 2014. <https://doi.org/10.1007/s00198-013-2401-y>.
- [13] Thevenot J., J. Hirvasniemi, P. Pulkkinen, M. Määtä, R. Korpelainen, S. Saarakkala, T. Jämsä, Thevenot J., J. Hirvasniemi, P. Pulkkinen, M. Määtä, R. Korpelainen, S. Saarakkala, T. Jämsä. Assessment of Risk of Femoral Neck Fracture with Radiographic Texture Parameters: A Retrospective Study. *Radiology* 2014. <https://doi.org/10.1148/radiol.14131390>.
- [14] Le Corroller T., M. Pithioux, F. Chaari, B. Rosa, S. Parratte, B. Maurel, J.N. Argenson, P. Champsaur, P. Chabrand, Le Corroller T., M. Pithioux, F. Chaari, B. Rosa, S. Parratte, B. Maurel, J.N. Argenson, P. Champsaur, P. Chabrand. Bone texture analysis is correlated with three-dimensional microarchitecture and mechanical properties of trabecular bone in osteoporotic femurs. *J Bone Miner Metab* 2013. <https://doi.org/10.1007/s00774-012-0375-z>.
- [15] Jazinizadeh F., C.E. Quenneville, Jazinizadeh F., C.E. Quenneville. Enhancing hip fracture

- risk prediction by statistical modeling and texture analysis on DXA images. *Med Eng Phys* 2020. <https://doi.org/10.1016/j.medengphy.2020.01.015>.
- [16] Jazinizadeh F., J.D. Adachi, C.E. Quenneville, Jazinizadeh F., J.D. Adachi, C.E. Quenneville. Advanced 2D image processing technique to predict hip fracture risk in an older population based on single DXA scans. *Osteoporos Int* 2020. <https://doi.org/10.1007/s00198-020-05444-7>.
- [17] Yang L., L. Palermo, D.M. Black, R. Eastell, Yang L., L. Palermo, D.M. Black, R. Eastell. Prediction of incident hip fracture with the estimated femoral strength by finite element analysis of DXA scans in the study of osteoporotic fractures. *J Bone Miner Res* 2014;29:2594–600. <https://doi.org/10.1002/jbmr.2291>.
- [18] Goodyear S.R., R.J. Barr, E. McCloskey, S. Alesci, R.M. Aspden, D.M. Reid, J.S. Gregory, Goodyear S.R., R.J. Barr, E. McCloskey, S. Alesci, R.M. Aspden, D.M. Reid, J.S. Gregory. Can we improve the prediction of hip fracture by assessing bone structure using shape and appearance modelling? *Bone* 2013;53:188–93. <https://doi.org/10.1016/j.bone.2012.11.042>.
- [19] Baker-Lepain J.C., K.R. Luker, J.A. Lynch, N. Parimi, M.C. Nevitt, N.E. Lane, Baker-Lepain J.C., K.R. Luker, J.A. Lynch, N. Parimi, M.C. Nevitt, N.E. Lane. Active shape modeling of the hip in the prediction of incident hip fracture. *J Bone Miner Res* 2011. <https://doi.org/10.1002/jbmr.254>.
- [20] Humbert L., T. Whitmarsh, M. De Craene, L.M. Del Río Barquero, K. Fritscher, R. Schubert, F. Eckstein, T. Link, A.F. Frangi, Humbert L., T. Whitmarsh, M. De Craene, L.M. Del Río Barquero, K. Fritscher, R. Schubert, F. Eckstein, T. Link, A.F. Frangi. 3D reconstruction of both shape and bone mineral density distribution of the femur from DXA images. 2010 7th IEEE Int Symp Biomed Imaging From Nano to Macro, ISBI 2010 - Proc 2010:456–9. <https://doi.org/10.1109/ISBI.2010.5490310>.
- [21] Väänänen S.P., L. Grassi, G. Flivik, J.S. Jurvelin, H. Isaksson, Väänänen S.P., L. Grassi, G. Flivik, J.S. Jurvelin, H. Isaksson. Generation of 3D shape, density, cortical thickness and finite element mesh of proximal femur from a DXA image. *Med Image Anal* 2015;24:125–34. <https://doi.org/10.1016/j.media.2015.06.001>.

- [22] Bredbenner T.L., R.L. Mason, L.M. Havill, E.S. Orwoll, D.P. Nicolella, Bredbenner T.L., R.L. Mason, L.M. Havill, E.S. Orwoll, D.P. Nicolella. Fracture risk predictions based on statistical shape and density modeling of the proximal femur. *J Bone Miner Res* 2014. <https://doi.org/10.1002/jbmr.2241>.
- [23] Humbert L., R. Winzenrieth, S. Di Gregorio, T. Thomas, L. Vico, J. Malouf, L.M. del Río Barquero, Humbert L., R. Winzenrieth, S. Di Gregorio, T. Thomas, L. Vico, J. Malouf, L.M. del Río Barquero. 3D Analysis of Cortical and Trabecular Bone From Hip DXA: Precision and Trend Assessment Interval in Postmenopausal Women. *J Clin Densitom* 2019. <https://doi.org/10.1016/j.jocd.2018.05.001>.
- [24] Grassi L., S.P. Väänänen, M. Ristinmaa, J.S. Jurvelin, H. Isaksson, Grassi L., S.P. Väänänen, M. Ristinmaa, J.S. Jurvelin, H. Isaksson. Prediction of femoral strength using 3D finite element models reconstructed from DXA images: validation against experiments. *Biomech Model Mechanobiol* 2017;16:989–1000. <https://doi.org/10.1007/s10237-016-0866-2>.
- [25] Lorenz C., N. Krahnstöver, Lorenz C., N. Krahnstöver. Generation of point-based 3D statistical shape models for anatomical objects. *Comput Vis Image Underst* 2000. <https://doi.org/10.1006/cviu.1999.0814>.
- [26] Jazinizadeh F., H. Mohammadi, C.E. Quenneville, Jazinizadeh F., H. Mohammadi, C.E. Quenneville. Comparing the fracture limits of the proximal femur under impact and quasi-static conditions in simulation of a sideways fall. *J Mech Behav Biomed Mater* 2020;103.
- [27] Cosman F., S.J. de Beur, M.S. LeBoff, E.M. Lewiecki, B. Tanner, S. Randall, R. Lindsay, Cosman F., S.J. de Beur, M.S. LeBoff, E.M. Lewiecki, B. Tanner, S. Randall, R. Lindsay. Clinician’s Guide to Prevention and Treatment of Osteoporosis. *Osteoporos Int* 2014. <https://doi.org/10.1007/s00198-014-2794-2>.
- [28] Leslie W.D., S. O’Donnell, C. Lagacé, P. Walsh, C. Bancej, S. Jean, K. Siminoski, S. Kaiser, D.L. Kendler, S. Jaglal, Leslie W.D., S. O’Donnell, C. Lagacé, P. Walsh, C. Bancej, S. Jean, K. Siminoski, S. Kaiser, D.L. Kendler, S. Jaglal. Population-based Canadian hip fracture rates with international comparisons. *Osteoporos Int* 2010. <https://doi.org/10.1007/s00198-009-1080-1>.
- [29] Whitmarsh T., L. Humbert, M. De Craene, L.M. Del Rio Barquero, A.F. Frangi, Whitmarsh

- T., L. Humbert, M. De Craene, L.M. Del Rio Barquero, A.F. Frangi. Reconstructing the 3D shape and bone mineral density distribution of the proximal femur from dual-energy x-ray absorptiometry. *IEEE Trans Med Imaging* 2011;30:2101–14. <https://doi.org/10.1109/TMI.2011.2163074>.
- [30] Ripamonti C., L. Lisi, M. Avella, Ripamonti C., L. Lisi, M. Avella. Femoral neck shaft angle width is associated with hip-fracture risk in males but not independently of femoral neck bone density. *Br J Radiol* 2014. <https://doi.org/10.1259/bjr.20130358>.
- [31] Gnudi S., C. Ripamonti, G. Gualtieri, N. Malavolta, Gnudi S., C. Ripamonti, G. Gualtieri, N. Malavolta. Geometry of proximal femur in the prediction of hip fracture in osteoporotic women. *Br J Radiol* 1999. <https://doi.org/10.1259/bjr.72.860.10624337>.
- [32] Michelotti J., J.M. Clark, Michelotti J., J.M. Clark. Femoral neck length and hip fracture risk. *J Bone Miner Res* 1999. <https://doi.org/10.1359/jbmr.1999.14.10.1714>.
- [33] Osterhoff G., E.F. Morgan, S.J. Shefelbine, L. Karim, L.M. McNamara, P. Augat, Osterhoff G., E.F. Morgan, S.J. Shefelbine, L. Karim, L.M. McNamara, P. Augat. Bone mechanical properties and changes with osteoporosis. *Injury* 2016. [https://doi.org/10.1016/S0020-1383\(16\)47003-8](https://doi.org/10.1016/S0020-1383(16)47003-8).
- [34] Bono C.M., T.A. Einhorn, Bono C.M., T.A. Einhorn. Overview of osteoporosis: Pathophysiology and determinants of bone strength. *Eur Spine J* 2003. <https://doi.org/10.1007/s00586-003-0603-2>.
- [35] Nguyen B.N.T., H. Hoshino, D. Togawa, Y. Matsuyama, Nguyen B.N.T., H. Hoshino, D. Togawa, Y. Matsuyama. Cortical thickness index of the proximal femur: A radiographic parameter for preliminary assessment of bone mineral density and osteoporosis status in the age 50 years and over population. *CiOS Clin Orthop Surg* 2018. <https://doi.org/10.4055/cios.2018.10.2.149>.
- [36] Schumann S., M. Tannast, L.P. Nolte, G. Zheng, Schumann S., M. Tannast, L.P. Nolte, G. Zheng. Validation of statistical shape model based reconstruction of the proximal femur-A morphology study. *Med Eng Phys* 2010. <https://doi.org/10.1016/j.medengphy.2010.03.010>.
- [37] Thevenot J.Ô., J. Koivumäki, V. Kuhn, F. Eckstein, T. Jämsä, Thevenot J.Ô., J. Koivumäki, V. Kuhn, F. Eckstein, T. Jämsä. A novel methodology for generating 3D finite element

- models of the hip from 2D radiographs. *J Biomech* 2014;47:438–44. <https://doi.org/10.1016/j.jbiomech.2013.11.004>.
- [38] Unnanuntana A., B.P. Gladnick, E. Donnelly, J.M. Lane, Unnanuntana A., B.P. Gladnick, E. Donnelly, J.M. Lane. The assessment of fracture risk. *J Bone Jt Surg - Ser A* 2010. <https://doi.org/10.2106/JBJS.I.00919>.
- [39] Nankaku M., H. Kanzaki, T. Tsuboyama, T. Nakamura, Nankaku M., H. Kanzaki, T. Tsuboyama, T. Nakamura. Evaluation of hip fracture risk in relation to fall direction. *Osteoporos Int* 2005;16:1315–20. <https://doi.org/10.1007/s00198-005-1843-2>.
- [40] Slemenda C., S. Cummings, E. Seeman, P. Lips, D. Black, D.B. Karpf, Slemenda C., S. Cummings, E. Seeman, P. Lips, D. Black, D.B. Karpf. Prevention of hip fractures: Risk factor modification. *Am. J. Med.*, 1997. [https://doi.org/10.1016/s0002-9343\(97\)90028-0](https://doi.org/10.1016/s0002-9343(97)90028-0).

## CHAPTER 6 – General Discussion and Conclusions

---

*Overview: In this chapter, the objectives and hypotheses from chapter one are reviewed, and a summary of the main outcomes of the studies performed in this thesis is provided. The overall strengths and limitations of this work are also discussed. This chapter concludes with the future directions for further investigation, the clinical implications and the significance of the studies presented herein.*

### 6.1 Summary

---

Hip fractures as a result of a sideways fall are a significant cause of morbidity as well as mortality in older adults. Currently, diagnosis of osteoporosis and consequently hip fracture risk is done by measurement of BMD in the proximal femur through DXA scans; however, studies have shown that this method alone is not effective to identify all patients at high risk, and there is an overlap between the BMD of patients who sustained a hip fracture after a fall with those who did not. Therefore, it is crucial to search for complementary methods that can be used in addition to BMD measurement by DXA scan so that more people at high risk of a hip fracture can be identified and benefit from preventive interventions to avoid these devastating injuries. The overall goal of the studies presented in this thesis was to enhance hip fracture risk prediction in older adults through image processing of DXA scans to account for the effects of femur's geometry and BMD distribution in the hip fracture risk assessment.

The first component of this thesis involved performing destructive mechanical testing on isolated cadaveric femurs in two scenarios of quasi-static and impact loading in a simulation of a sideways fall (*i.e.*, Objective 1, Chapter 2). This study was performed to investigate if impact loading (as happens in reality) can be substituted with quasi-static testing (as happens in research) in the evaluation of the frameworks that are generated to assess hip fracture risk prediction. The results of this study showed that (except for one specimen) a strong correlation of determination was found between paired femurs for their fracture loads in impact and in quasi-static loading. Also, using the relationship developed herein between the impact fracture loads and the quasi-static ones, the results from another study were extrapolated with errors of less than 12%, showing that meaningful predictions for the impact scenario can be made based on quasi-static tests. In addition, the comparison of the fracture location showed qualitatively good agreement between the two groups (*i.e.*, Hypothesis 1 accepted).

The results of the experimental study presented in chapter one were then used to evaluate the proposed method in the next chapter (*i.e.*, Objective 2, Chapter 3). Chapter three presented creating and assessing the implementation of 2D statistical shape and appearance modeling (SSAM) of the proximal femur using the DXA scans. The subjects used in this study were isolated cadaveric femurs and the results of the fracture risk prediction were examined based on two methods of fracture load prediction and binary fracture risk classification based on a threshold. This study showed that using 2D SSAM was able to enhance hip fracture risk prediction in high risk subjects more accurately than the T-score alone (*i.e.*, Hypothesis 2 accepted).

To see how the 2D SSAM would translate to a clinical population, chapter four investigated the implementation of this technique on a population of clinical subjects chosen from the Canadian Multicentre Osteoporosis Study (CaMos). Fifty out of the 192 chosen subjects had sustained a hip fracture within a five-year period after the baseline (*i.e.*, Objective 3, Chapter 4). The results comparing fracture risk predictions based on 2D SSAM showed superior identification of people at high risk compared to standard clinical metrics of using T-score and FRAX when considering the fracture history of the subjects (*i.e.*, Hypothesis 3 accepted).

After investigating the ability of 2D SSAM to predict hip fracture risk, to see whether a 3D approach would improve the predictive ability, 3D SSAM was created and assessed in a subset of the subjects from Objective three (*i.e.*, Objective 4, Chapter 5). The reconstruction of the 3D model from the 2D DXA scan showed the same range of errors compared to similar studies, with reducing the magnitude of the maximum error. While 3D SSAM significantly enhanced hip fracture risk prediction for the clinical subjects who sustained a fracture compared to the T-score, the accuracy did not increase noticeably compared to using 2D SSAM (*i.e.*, Hypothesis 4 accepted). This means that while 3D geometry and BMD distribution reconstruction of the proximal femur might be a necessity for further numerical analysis (*e.g.* finite element analysis), for estimating the fracture risk based on considering the effect of a femur's geometry and BMD distribution, performing 2D SSAM in clinical practice appears to be both more feasible and just as accurate as 3D SSAM.

## 6.2 Strengths and Limitations

---

The specific strengths and limitations of each study were discussed in detail in their respective chapters. However, some general ones apply to the whole thesis. In this section, the major strengths and limitations of each study as well as the overall ones are discussed.

One of the strengths of the experimental part of this research was the use of paired specimens to compare and demonstrate a relationship between the fracture load of the proximal femur in impact and quasi-static in simulation of a sideways fall. Paired specimens allowed us to assume equivalence, reducing variability and develop a relationship that could be used to convert results from prior QS tests into predicted IM values. In most of the other similar studies that have investigated hip fracture risk prediction quasi-static tests were used instead of impact ones to quantify the fracture strength. Also, in the few studies that had investigated the differences between impact and quasi-static testing, non-paired specimens were used, which led to a dominant effect of geometry and BMD on the results and limited the statistical power of their findings.

Another strength of this work was that the imaging techniques were evaluated both based on a cadaveric study as well as a clinical group. Cadaveric studies provide valuable information about the strength condition of the bone, as they are guaranteed to fracture and are easy to image; however, clinical studies are superior, since they can provide a more comprehensive insight into the risk factors that affect the occurrence of an injury in reality. Also, clinical studies are a necessity in paving the path for a technique to be implemented in clinical practice.

Another major advantage of this thesis was investigating both 2D and 3D model reconstruction techniques and comparing their ability to predict an individual's hip fracture risk. Interestingly, the results of this work showed that using 2D model reconstruction to consider the effects of geometry and BMD distribution wouldn't noticeably affect the correct identification of patients at high risk of sustaining a hip fracture. To create the training sets for 2D and 3D model reconstructions, DXA scans and CT scans, respectively, of the proximal femurs were required. DXA scans are more accessible, faster, less expensive, and are associated with less dose of radiation compared to CT scans, therefore expanding the training set for 2D model reconstruction in clinical practice is more attainable and desirable.

In this research, real DXA scans were used and not the anterior-posterior projection of the CT scans, as has often been done in previous studies (which may have artificially reduced the error usually induced by the soft tissue and patients positioning). While this is most representative of the clinical scenario, DXA scans are associated with high noise artifact partially due to the presence of soft tissue. Also, the positioning of the subjects during a scan is a major obstacle to consistency. Therefore, while using real DXA scans induces additional error compared to the studies that have evaluated their technique based on the projection of the CT scans, it provides a more realistic assessment of this technique when dealing with real scans in practice.

While this research made many important contributions toward several issues surrounding enhancing hip fracture risk prediction in older adults with a focus on methods that would be feasible to implement in clinical practice, there were also several limitations.

One of the major limitations of this work was the quality of the DXA scans used for the analysis. In this research, subjects (both cadaveric specimens and clinical population subjects) were scanned by a Hologic DXA scanner, hence, the images could only be accessed by the company's software. To eliminate this problem the scans were first opened by the software, and then they were de-analyzed to remove the regions that were selected by the technician, and in the end, a screenshot of the scan was saved for further analysis. This resulted in decreased image quality and consequently losing some valuable information. This information could have had a significant effect on the feasibility of performing further texture analysis on the clinical data. In addition, some of the scans that were used in the clinical studies were 20 years old, and most of those DXA scanners have since been replaced. Therefore, using a more recent baseline for the analysis could help to have a better image quality.

Another limitation of this research was the variability among the subjects, in terms of personal (age, sex, weight, height, alcohol and tobacco use, and level of activity) and clinical (medication, comorbidities, and using protective measures) characteristics. When choosing the subjects, the non-fracture subjects were only selected from the population that was not taking any osteoporosis medication, while in the selection of the fractured subjects this was not considered. Therefore, the potential effect of using certain medications might have been dismissed. Also, the high variability could limit the generation of a comprehensive model to account for all contributing factors, and further studies are required to address that. However, it should be noted that even when considering most of the possible contributing elements, the effect of some factors may still not be possible to

be measured and integrated into a model (*e.g.* effect of microdamage based on the standard clinical imaging).

In this research, reconstruction of the 2D and 3D models was initiated by assigning landmarks to the DXA scans. This assignment was done manually, and hence it could be slightly time-consuming (two minutes for each scan) and also user-dependent. However, the reproducibility of the predictions was investigated to account for the effects of inter- and intra-user dependency. Five subjects (three fractured and two non-fractured) were randomly chosen and three users were asked to assign the landmarks. Also, one user was asked to assign the landmarks three times with at least one week in between each assignment. The results showed that in predicting the fracture risk based on the 2D and 3D model reconstruction, there was no user effect on the binary classification of the fracture risk (Table 6.1, Table 6.2, Table 6.3, and Table 6.4). It can be observed that the standard deviations in most of the predictions are small; however, for some subjects (*e.g.* subject two and three) the ratio of standard deviation over the mean was quite high (maximum of 55%) which indicates the importance of creating a fully automatic platform with minimum user-interference.

### **6.3 Future Directions**

---

The research conducted in this thesis examined implementing 2D and 3D model reconstruction to investigate the effect of geometry and BMD distribution in hip fracture risk. In addition to hip fracture risk prediction, 2D and 3D model reconstruction from a 2D DXA scan can provide valuable insight into subtle changes in the geometry and BMD

distribution of the proximal femur over time [1–3]. Therefore, future studies can investigate using these techniques to monitor the changes that might occur along a period of time or during a specific treatment.

One of the focuses on this research was on generating a technique that could be easily implemented in clinical practice. Therefore, automating and creating a user-friendly platform is a necessary next step towards this goal. Also, for future research, it is recommended to establish a relationship with the DXA scanner manufacturer to get access to the original digital image so that texture analysis of the trabecular bone in the femoral neck and trochanteric area could be included more meaningfully.

Another aspect that should be considered in future studies is evaluating these techniques in large cohort studies to investigate the effect of all contributing factors. A large cohort study could allow matching the control (non-fractured subjects) with the fractured cases to only assess one factor of interest at a time independently, and consequently creating a comprehensive framework for predicting an impending fracture. This would form an important component of a more holistic assessment of fracture risk – while femur geometry and material distribution are important factors, there are not the only factors – integrating it into a FRAX-like tool would improve the overall evaluation of fracture risk while considering factors such as balance that aren't captured from a purely mechanical assessment.

**Table 6.1 Inter-user reproducibility of fracture risk based on 2D SSAM**

The probability of sustaining a hip fracture based on the assignment of landmarks by three users in 2D SSAM analysis, Fx: fracture, where 1 indicated a fracture was sustained and 0 indicated no fracture, SD: standard deviation.

<b>Subject</b>	<b>Fx history</b>	<b>User 1</b>	<b>User 2</b>	<b>User 3</b>	<b>Mean</b>	<b>SD</b>
<b>1</b>	1	0.69	0.64	0.76	0.70	0.05
<b>2</b>	1	0.79	0.80	0.81	0.80	0.01
<b>3</b>	1	0.21	0.26	0.23	0.23	0.02
<b>4</b>	0	0.00	0.00	0.00	0.00	0.00
<b>5</b>	0	0.71	0.58	0.68	0.66	0.06

**Table 6.2 Inter-user reproducibility of fracture risk based on 3D SSAM**

The probability of sustaining a hip fracture based on the assignment of landmarks by three users in 3D SSAM analysis, Fx: fracture, where 1 indicated a fracture was sustained and 0 indicated no fracture, SD: standard deviation.

<b>Subject</b>	<b>Fx history</b>	<b>User 1</b>	<b>User 2</b>	<b>User 3</b>	<b>Mean</b>	<b>SD</b>
<b>1</b>	1	0.92	0.90	1	0.94	0.04
<b>2</b>	1	0.00	0.00	0.16	0.05	0.08
<b>3</b>	1	0.21	0.33	0.19	0.24	0.06
<b>4</b>	0	0.00	0.00	0.00	0.00	0.00
<b>5</b>	0	0.00	0.00	0.00	0.00	0.00

**Table 6.3 Intra-user reproducibility of fracture risk based on 2D SSAM**

The probability of sustaining a hip fracture based on assignments of landmarks by one user over three times in 2D SSAM analysis, Fx: fracture, where 1 indicated a fracture was sustained and 0 indicated no fracture, SD: standard deviation.

<b>Subject</b>	<b>Fx history</b>	<b>1<sup>st</sup> time</b>	<b>2<sup>nd</sup> time</b>	<b>3<sup>rd</sup> time</b>	<b>Mean</b>	<b>SD</b>
<b>1</b>	1	0.72	0.64	0.69	0.68	0.03
<b>2</b>	1	0.79	0.85	0.79	0.81	0.03
<b>3</b>	1	0.48	0.21	0.21	0.30	0.13
<b>4</b>	0	0.00	0.00	0.00	0.00	0.00
<b>5</b>	0	0.72	0.61	0.71	0.68	0.05

**Table 6.4 Intra-user reproducibility of fracture risk based on 3D SSAM**

The probability of sustaining a hip fracture based on assignments of landmarks by one user over three times in 3D SSAM analysis, Fx: fracture, where 1 indicated a fracture was sustained and 0 indicated no fracture, SD: standard deviation.

<b>Subject</b>	<b>Fx history</b>	<b>1<sup>st</sup> time</b>	<b>2<sup>nd</sup> time</b>	<b>3<sup>rd</sup> time</b>	<b>Mean</b>	<b>SD</b>
<b>1</b>	1	0.97	0.86	0.92	0.92	0.04
<b>2</b>	1	0.05	0.03	0.00	0.03	0.02
<b>3</b>	1	0.33	0.07	0.20	0.20	0.11
<b>4</b>	0	0.00	0.00	0.00	0.00	0.00
<b>5</b>	0	0.01	0.00	0.00	0.00	0.00

## 6.4 Clinical Significance

---

In conclusion, in this work, two new methods of 2D and 3D model reconstruction have been created and evaluated based on the DXA scans and CT scans of a set of isolated cadaveric femurs. Also, these model reconstructions have been used to consider the effect of the proximal femur's geometry and BMD distribution on hip fracture prediction. These methods were then assessed in two groups of cadaveric and clinical subjects, and the results showed that both techniques were able to substantially enhance the identification of people at high risk of sustaining a hip fracture noticeably.

This research also furthered our understanding of how the geometric and material distribution traits affect the vulnerability of the proximal femur by comparing the features in the subject who sustained and did not sustain a hip fracture. Another significant impact of this research was to demonstrate that the hip fracture prediction based on 2D model reconstruction did not remarkably differ from the 3D model reconstruction, and since the 2D method is associated with a less computational burden and requires less resources, this finding could shape future of implementing statistical models in clinical practice. This means that for the approximately 30,000 hip fractures that happen each year in Canada [4], thousands of patients at high risk could be identified and protected from this injury by using this technique.

## 6.5 References

---

- [1] Campillo-Sánchez F., R. Usategui-Martín, Á. Ruiz -de Temiño, J. Gil, M. Ruiz-Mambrilla, J.M. Fernández-Gómez, A. Dueñas-Laita, J.L. Pérez-Castrillón, Campillo-Sánchez F., R. Usategui-Martín, Á. Ruiz -de Temiño, J. Gil, M. Ruiz-Mambrilla, J.M. Fernández-Gómez, A. Dueñas-Laita, J.L. Pérez-Castrillón. Relationship between Insulin Resistance (HOMA-IR), Trabecular Bone Score (TBS), and Three-Dimensional Dual-Energy X-ray Absorptiometry (3D-DXA) in Non-Diabetic Postmenopausal Women. *J Clin Med* 2020. <https://doi.org/10.3390/jcm9061732>.
- [2] Gracia-Marco L., B. García-Fontana, E. Ubago-Guisado, D. Vlachopoulos, A. García-Martín, M. Muñoz-Torres, Gracia-Marco L., B. García-Fontana, E. Ubago-Guisado, D. Vlachopoulos, A. García-Martín, M. Muñoz-Torres. Analysis of Bone Impairment by 3D DXA Hip Measures in Patients With Primary Hyperparathyroidism: A Pilot Study. *J Clin Endocrinol Metab* 2020. <https://doi.org/10.1210/clinem/dgz060>.
- [3] Ng C.A., L.B. McMillan, B. Beck, L. Humbert, P.R. Ebeling, D. Scott, Ng C.A., L.B. McMillan, B. Beck, L. Humbert, P.R. Ebeling, D. Scott. Associations between physical activity and bone structure in older adults: does the use of self-reported versus objective assessments of physical activity influence the relationship? *Osteoporos Int* 2020. <https://doi.org/10.1007/s00198-019-05208-y>.
- [4] Leslie W.D., S. O'Donnell, C. Lagacé, P. Walsh, C. Bancej, S. Jean, K. Siminoski, S. Kaiser, D.L. Kendler, S. Jaglal, Leslie W.D., S. O'Donnell, C. Lagacé, P. Walsh, C. Bancej, S. Jean, K. Siminoski, S. Kaiser, D.L. Kendler, S. Jaglal. Population-based Canadian hip fracture rates with international comparisons. *Osteoporos Int* 2010. <https://doi.org/10.1007/s00198-009-1080-1>.

## APPENDIX A – Glossary of the Medical Terms

---

*Overview: this appendix contains a list of the medical terms used through this thesis to provide assistance to the readers who are not familiar with this terminology.*

**Anatomical position:** Body upright, with the face and palms forward and the upper limbs placed at the sides.

**Anterior:** Situated towards the front of the body when in anatomical position.

**Articulation:** The contact junction between two bones.

**Cadaveric:** Of, or pertaining to, a dead body preserved for anatomical study.

**Cancellous Bone:** A spongy, lattice-like structure of bone. Synonymous with trabecular bone.

**Contralateral:** Pertaining to the other side of the body (i.e., left-right).

**Cortical Bone:** A dense bone structure. Synonymous with compact bone.

**Diaphysis:** The shaft of a long bone, a tube made of cortical bone.

**Distal:** Further from the point of reference; away from the midline of the body.

**Femur:** The large bone in the upper leg, extending from the pelvis to the knee.

**FRAX:** A diagnostic tool used to evaluate the 10-year probability of bone fracture risk

**Frontal:** The plane parallel to the long axis of the body separating the body into front and back portions.

**Inferior:** Away from the head; lower

**Joint:** The location at which two bones make contact, permits relative movement.

**Lateral:** A position further away from the midline of the body.

**Marrow:** The soft tissue filling the cavities of bones.

**Medial:** A position closer to the midline of the body.

**Posterior:** Located towards the back of the body.

**Proximal:** Closer to the point of reference; towards the center of the body.

**Sagittal:** The plane parallel to the long axis of the body separating the body into left and right portions.

**Superior:** Toward the head end of the body; upper

**Trabecular:** See cancellous bone.

**Transverse:** Placed crosswise, at a right angle to the long axis of a part.

**T-score:** How much your bone density is higher or lower than the bone density of a healthy 30-year old adult of the same ethnicity and sex.

